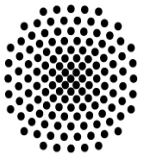

University of Stuttgart
Germany

POLITECNICO
MILANO 1863

SCUOLA DI INGEGNERIA INDUSTRIALE
E DELL'INFORMAZIONE

Numerical Investigation of the Blade Tower Interaction in upwind HAWTs using OpenFOAM

TESI DI LAUREA MAGISTRALE IN
ENERGY ENGINEERING
INGEGNERIA ENERGETICA

Author: **Hashim Hasnain Hadi**

Student ID: 10689433
Advisor: Prof. Luca Cartelezzi
Co-advisor: Dr. Gabriel Axtmann
Academic Year: 2023

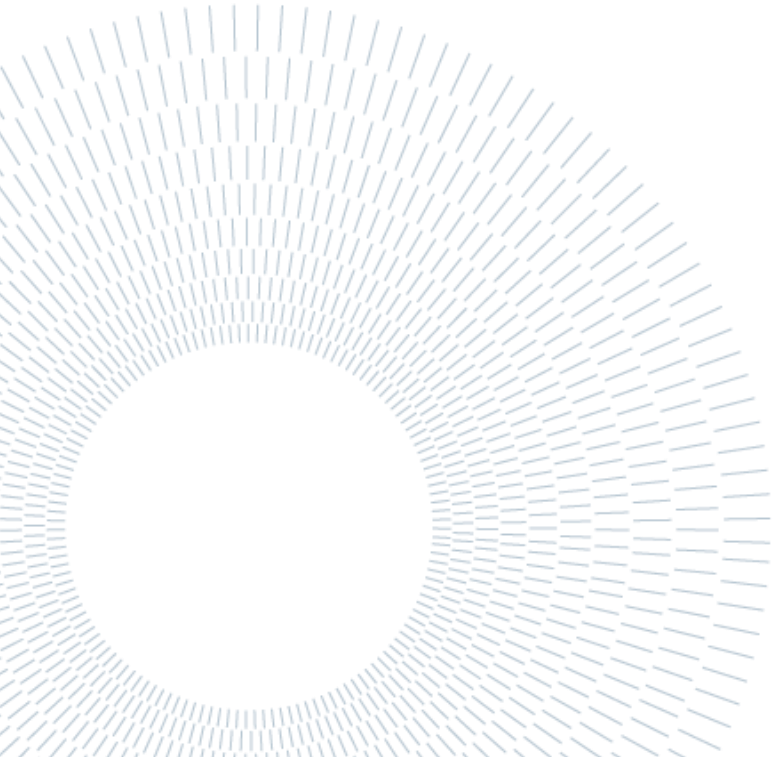

Abstract

This research investigates the tower's and rotor blade's aerodynamic interaction in a wind turbine. The fluctuations of pressure on the surface of the rotor blades and the tower, due to the interaction of the blade and tower, contribute significantly to infrasonic emissions. Further, these fluctuations contribute to fatigue of the wind turbine's structure. Therefore, the effect of various physical influencing variables on pressure fluctuations is studied and evaluated through two-dimensional simulations utilizing OpenFOAM. The 2D configuration is derived from an existing reference wind turbine, using cross-section geometries. Grid is generated using OpenFOAM's blockMesh utility, and mesh motion is achieved utilizing two mesh modifiers, layering, and AMI. Besides the velocity and pressure contours, velocity and pressure fields are also extracted and analyzed for the changes in speed and pressure during blade passage. The impact of the variation of different influencing variables on pressure fluctuations is quantified by introducing a nondimensional comparative variable. It is analyzed that larger tower-airfoil spacing and slower airfoil speed effectively reduce pressure fluctuations on the tower and airfoil surfaces.

Keywords: blade-tower interaction, wind turbine, aerodynamic noise, infrasonic noise, BTI noise, pressure interaction

Abstract in italiano

Questa ricerca studia l'interazione aerodinamica della torre e delle pale del rotore su una turbina eolica. Le fluttuazioni di pressione sulla superficie delle pale del rotore e della torre, dovute all'interazione tra pala e torre, contribuiscono in modo significativo alle emissioni infrasoniche. Inoltre, queste fluttuazioni contribuiscono alla fatica della struttura della turbina eolica. Pertanto, l'effetto di diverse variabili fisiche che influenzano le fluttuazioni di pressione viene studiato e valutato attraverso simulazioni bidimensionali utilizzando OpenFOAM. La configurazione 2D è derivata da una turbina eolica di riferimento esistente, utilizzando le geometrie delle sezioni trasversali. La griglia è generata utilizzando l'utility blockMesh di OpenFOAM e il movimento della maglia è ottenuto utilizzando due modificatori di maglia, layering e AMI. Oltre ai contorni di velocità e pressione, vengono estratti e analizzati anche i campi di velocità e pressione per le variazioni di velocità e pressione durante il passaggio delle pale. L'impatto della variazione di diverse variabili di influenza sulle fluttuazioni di pressione viene quantificato introducendo una variabile comparativa non dimensionale. È stato analizzato che una maggiore distanza tra torre e profilo e una minore velocità del profilo riducono efficacemente le fluttuazioni di pressione sulle superfici della torre e del profilo.

Parole chiave: interazione pala-torre, turbina eolica, rumore aerodinamico, rumore infrasonico, rumore BTI, interazione di pressione.

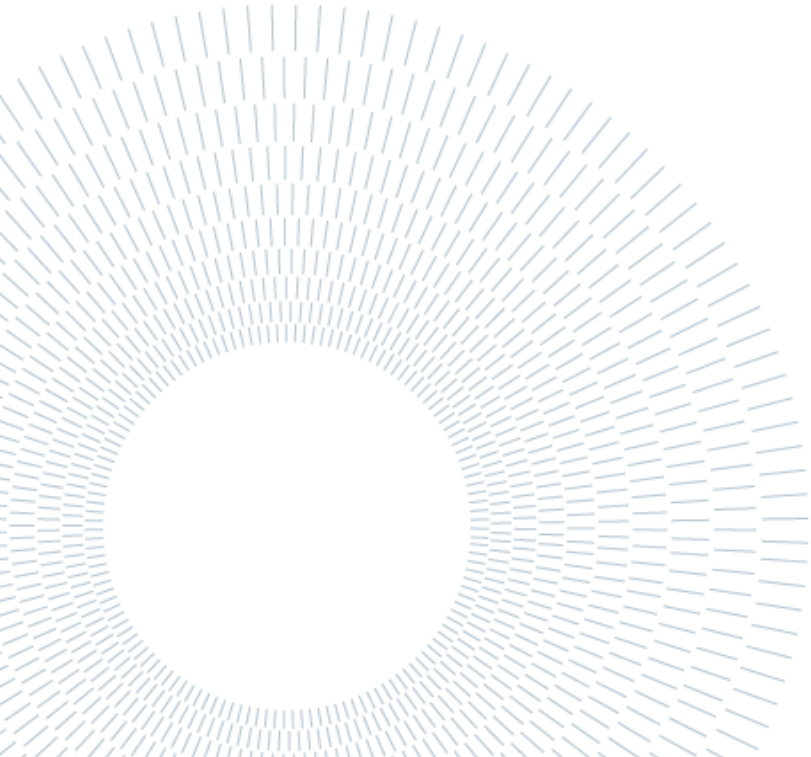

Contents

1 Introduction

1.1. Motivation

Over the past two decades, the global installed wind energy capacity has increased almost 48-fold, from 17.334GW in 2000 to 824.874GW in 2021, according to Renewable Energy Statistics 2021. Similarly, Germany's installed wind capacity has grown 10 times since 2000, peaking at 63.760GW in 2021. The wind power sector accounted for 27% of all renewable electricity worldwide in 2021; for Germany specifically, wind energy contributed 46% [1-2]. As per the Onshore Wind Energy Act of 2022, Germany aims to generate 80% of its power with renewables within the next decade, which will be achieved by doubling the capacity of its onshore wind farms. Only 0.5% of Germany's land area is available for installing onshore wind energy farms, while 0.8% has been allocated. Germany's recent wind energy legislation stipulates that 2% of the country's land should be used for onshore wind turbines [3]. Wind farms are being built near inhabited areas because of an increase in energy demand leading to noise pollution, which is particularly troublesome in Germany. Despite wind energy's potential, wind turbines' noise and visual impact hamper its social acceptance.

Being emission-free, highly efficient, and a baseload power source, commercial wind turbines have grown exponentially in capacity and rotor size from 75kW and 17m to 10MW and 170m for the new generation since the early 2000s. In addition to lowering levelized energy costs (USD/kWh), increasing wind turbine size introduces dynamic loads, elastic deflections, inertial dynamics, and fatigue stress, thus requiring consideration of the blade-tower interaction (BTI) [4]. Large turbines generate more low-frequency noise than small turbines, and the difference is statistically significant. When acoustic pressure levels at relevant neighbor distances are considered, the higher low-frequency content becomes even more apparent [5]. Providing that mechanical noise is adequately eliminated, aerodynamic noise from the blades is the dominant noise source. Aerodynamic noise has three sources: low-frequency noise, self-noise produced by airfoils, and turbulence inflow noise [6]. Van den Berg [7] determined that a sizable portion of the low-frequency part of the sound spectrum is attributed to BTI. Intermittent blade-to-tower interference for short periods of time produces periodic and impulsive noise, whose intensity is determined by numerous factors, such as the aerodynamic coupling between blades and towers, viscous effects on blades, turbine, and tower dimensions, and aeroelastic properties of the rotor and

atmospheric turbulence levels [8]. To increase public acceptance of wind power and to comply with noise regulations, wind turbines must be assessed to predict aerodynamic noise and develop noise-reducing design concepts.

As the load on blades and a tower changes, BTI noise is generated, resulting from two related phenomena that co-occur: reduced inflow velocity fields and blade-passage effects. A tower's obstruction reduces the velocity field upwind, thereby altering the angle of attack of the passing blade and causing BTI noise [9]. Blade-passage effects arise from aerodynamic disturbances due to the interaction between the blades and the tower. This aerodynamic disturbance describes how the moving blade displaces air as it passes the tower. An unloaded three-bladed rotor rig studied experimentally and numerically demonstrated that the air surrounding the blade deflects outward radially at the leading edge but converges at the trailing edge. Due to the blade's passage, large pressure pulses have been reported [10].

According to [11], intense BTI noise was associated with downwind wind turbines. High noise levels resulted from large velocity deficits downwind of the tower and tower–blade vortex interactions, which generated higher pressure pulses at the blade pass frequency. Using a scaled wind turbine model, Greene demonstrated that changing the design to have the rotor mounted upwind would substantially reduce the BTI noise level [12]. In upwind directions, the velocity deficit is lesser than downwind, and there is no vortex shedding. Kelley et al. [13] experimented on a full-scale wind turbine and compared upwind and downwind turbine measurements, validating earlier research [12].

Several numerical modeling studies have been conducted on BTI. NASA developed a code to predict low-frequency noise generated by wind turbines in the early 1980s using Lowson's acoustic equation [14]. Using first-order aerodynamic models and potential flow theory, Doolan et al. [15] explained the aerodynamic origin of BTI noise from modern upwind wind turbines. Curle's theory was then applied to show that the blade-tower aerodynamic interaction results in pressure pulses at the blade-pass frequency when acoustic pressure has been applied in the far-field. Madsen [16] applied blade element momentum and potential flow theories to determine the forces generated on the turbine blades, considering tower influence on rotor aerodynamics. For the aeroacoustic modeling of low-frequency noise, the NASA-LeRC code was used. Neither of these studies considered the nonlinear interaction between the tower and blades. Additionally, noise calculations ignored the variation of force on the tower, only considering the force fluctuations on the blades. Using CFD simulations and the Ffowcs-Williams-Hawkings method, low-frequency noise from wind turbines was investigated, excluding the tower as a source of BTI noise [17]. Applying CFD and Curle's acoustic analogy, Yauwenas et al. [18] numerically investigated the blade-

passage noise of a generic model turbine, finding that tower-induced pressure fluctuations contributed significantly to tonal blade-passage noise.

Several numerical studies have been performed using computational fluid dynamics (CFD) on wind turbines with an upwind rotor to investigate the effect of BTI. Hsu and Bazilevs [19] used the sliding mesh method to simulate the rotation of the blades and showed changes to the force acting on the blades due to BTI. A force oscillation at blade-pass frequency was attributed to BTI. Mo et al. [20] observed a similar effect using the sliding mesh method and measuring power output at the blade–pass frequencies. Zahle et al. [21] detected an interaction between the tower and blades when simulating blade rotation based on the dynamic overset grid method. Wang et al. [22] investigated that pressure changes on the tower are induced by BTI, demonstrating its significance.

On the one hand, the numerical studies described above cannot provide insight into noise generation mechanisms, despite successfully capturing BTI effects with the sliding mesh methods. Alternatively, Nelson [17] implemented a permeable integration surface of the Ffowcs-Williams Hawkings acoustic analogy to calculate wind turbine noise without considering the tower. Further research is therefore needed to investigate the different variables influencing BTI noise in wind turbines.

1.2. Research Question

How do different variables influence blade tower interaction noise?

1.3. Objectives and Scope of this Research

This research is focused on studying the aerodynamic interaction of the rotor blades passing by the tower using CFD simulations. To accomplish this, two-dimensional simulations are evaluated using the PimpleFoam flow solver in OpenFOAM.

The geometry of the airfoil (NACA 633418) is optimized through Pointwise and Xfoil softwares, while the mesh generation code has been written using the blockMesh utility in OpenFOAM. Numerical setups are optimized by comparing the results of various time steps and internal iterations. This is done using the curves of the velocities, the lift coefficient, and pressure in the flow field.

Pressure fluctuations are studied by examining the pressure curves above and below the profile position at several points on the profile and tower surface. The tower-profile distance, tower diameter, and profile speed are analyzed to determine how they affect pressure fluctuation. Furthermore, the changes in pressure distribution are analyzed over time.

Using a discrete Fourier analysis, the effect of the influencing variables on the frequency spectrum of the pressure fluctuation is analyzed. Based on this, the shape of the pressure curve is inferred during the tower-profile interaction. The effect of the influence variables on the amplitude of the pressure fluctuation is compared and evaluated using a dimensionless comparative variable. Finally, recommendations are made for reducing wind turbine profiles and tower surfaces' pressure fluctuation.

1.4. Thesis Organization

In chapter 1, motivation, research question, and research objectives are discussed. Chapter 2 outlines the fundamental theories and equations relevant to this research. An overview of all software used in the study is presented in Chapter 3. Chapter 4 discusses the spatial and numerical discretization: mesh generation, computational setup, and convergence study for this research. The results of various case studies are compared in chapter 5, which examines the impact of physical parameters on pressure fluctuations. The conclusion and recommendations for further research are presented in chapter 6. At the end of the thesis, references used during the project are listed.

2 Theoretical Background

This chapter deals with the fundamentals of the cylinder and profile flow, the aerodynamic interaction of a wind turbine's rotor blade and tower, the numerical basics of CFD, and guidelines for grid creation.

2.1. Physics of Fluid Flow

This section includes the basics of flow around the cylinder and profile, which are necessary to understand the aerodynamic interaction of the tower and rotor blade in wind turbines. Whereas section 2.1.3 deals with the interaction separately.

2.1.1. Cylindrical Flow

The flow field of an inflowing cylinder is characterized by a stagnation area around the stagnation point on the front side and flow areas accelerated by the deflection at the flanks. The Reynolds number primarily determines the character of the flow area behind the cylinder.

$$Re_D = \frac{\rho u_\infty D}{\eta} \tag{2.1}$$

The Reynolds number Re_D is related to the diameter D, the density ϱ, the flow velocity u_∞, and the dynamic viscosity η. For $Re_D < 1$, a stationary and rotational-free laminar flow is established, which is shown in figure 2.1.

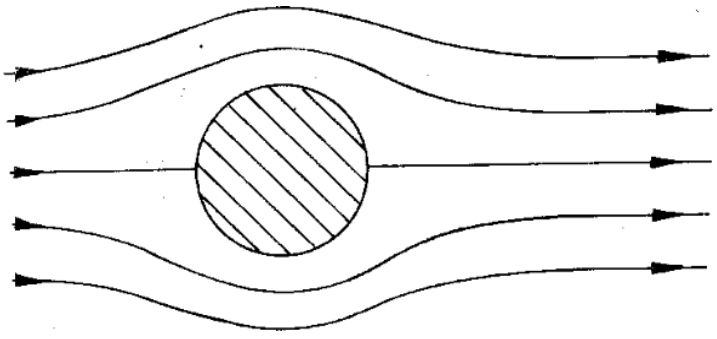

Figure 2.1: Cylinder flow for $Re_D < 1$, stationary, rotation-free, laminar, [23]

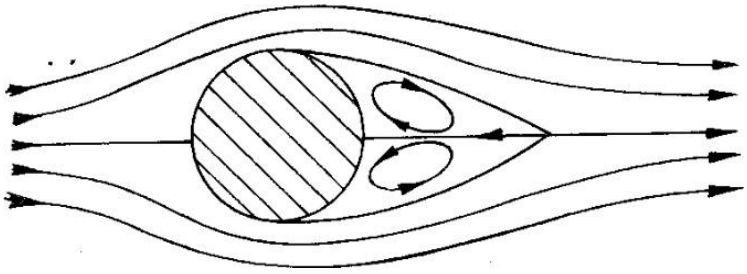

Figure 2.2: Cylinder flow for $Re_d \approx 20$, stationary, torsional, laminar, [23]

At a Reynolds number of Re_D ≈20, two counter-rotating vortices form behind the cylinder (see Figure 2.2), and the flow remains stationary and laminar. From Re ≈100, the after-run of the cylinder becomes unstable, and the flow is, therefore, non-stationary. The left and right vortices are alternately shed with a phase shift of 180°, and the so-called Kármán vortex street is created (Figure 2.3). The shedding frequency f is a function of the Strouhal number Sr_D.

$$Sr_D = \frac{fD}{u_\infty} \tag{2.2}$$

Equations 2.1 and 2.2 can be used to calculate the shedding frequency because the link between Strouhal and Reynolds numbers is understood for cylindrical flow. The ordered, regular shedding of the vortices turns to a chaotic, unpredictable shedding of the vortices with the turbulent transition of the boundary layer. In (Figure 2.4) this happens at Re_D≈ 1000 Reynolds number.

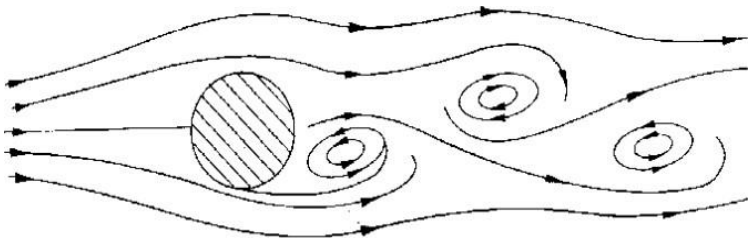

Figure 2.3: Cylinder flow for R_eD ≈100, transient, torsional, laminar, [23].

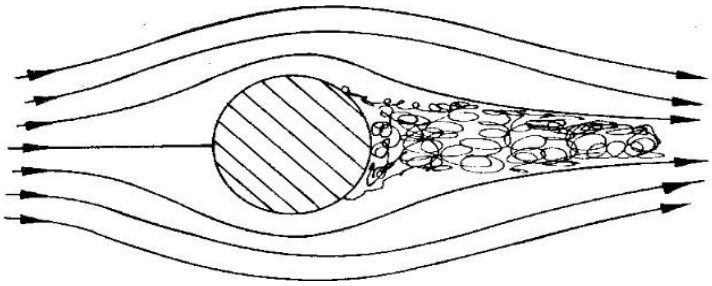

Figure 2.4: Cylinder flow for Re_D≈1000, transient, torsional, turbulent, [23]

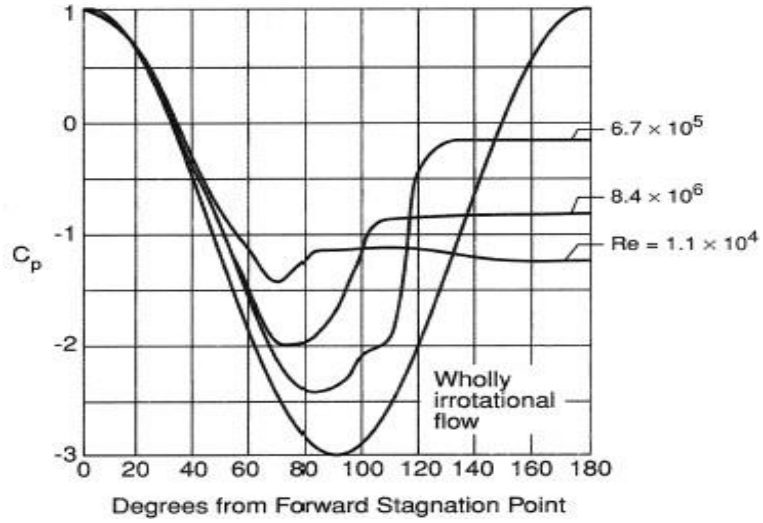

Figure 2.5: Distributions of the pressure coefficient above the azimuth angle θ, [24]

Figure 2.5 shows the pressure coefficient distributions on the cylinder surface as a function of azimuth angle and Reynolds number. In the event of a flow without rotation (a flow that is entirely rotational- free), the distribution is mirror-symmetrical. For all Reynolds values, the stagnation area with $c_p > 0$ for $\theta < 35°$ may be observed clearly. Equation 2.3 states that the input velocity determines the magnitudes of the overpressure at the stagnation point:

$$C_p = \frac{p-p_\infty}{\frac{\rho}{2}u_\infty{}^2} = 1-(\frac{u}{u_\infty})^2 \tag{2.3}$$

This results in the following for the dynamic pressure:

$$p_{trafic\ jam} = \frac{\rho}{2}u_\infty{}^2 \tag{2.4}$$

The magnitude of the maximum over speed that occurs in a rotational-free flow at θ = 90◦ depends on the Reynolds number. According to Equation 2.3, $u_{max} = 2u_\infty$ lies to the rotation-free case.

2.1.2. Flow Profile

2.1.2.1. Geometry

First, some characteristics of profiles that have an influence on the flow around will be described. Figure 2.6 shows a profile with the thickness *d*, the curvature f and the angle of attack α. The profile tendon is the direct connection from nose to trailing edge. If there is an asymmetric curvature of the profile, it differs from the skeletal line. The angle of attack is the angle between the vector of the inflow velocity, here *V*, and of the profile tendon. In addition to the angle of attack, the curvature is responsible for buoyancy [25].

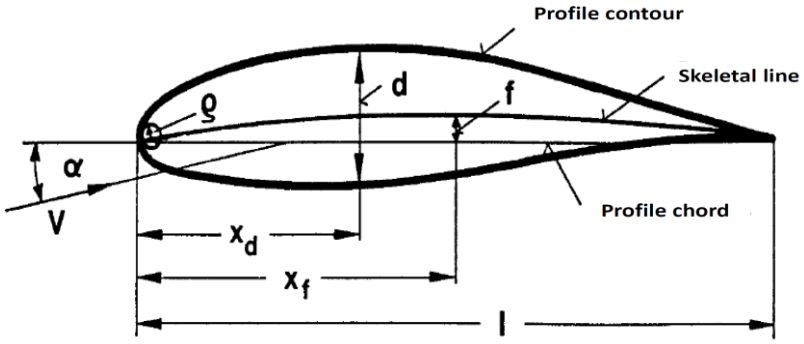

Figure 2.6: Geometry of a curved profile with the angle of attack α

2.1.2.2. Flow diagram

Figure 2.7 illustrates the flow pattern around a smoothly moving profile using streamlines. The stagnation streamline at the nose of the profile can be seen as strongly curved upwards, i.e. the flow is deflected upwards by the profile. On the top of the profile, the streamlines are compacted, which indicates the locally accelerated flow and, thus, the reduced pressure. A reverse effect can be seen at the bottom of the profile. A smooth outflow of the flow can be seen at the profile trailing edge. According to Kutta's drainage condition, the amount and direction of the flow velocity on the suction and pressure side must be the same [26].

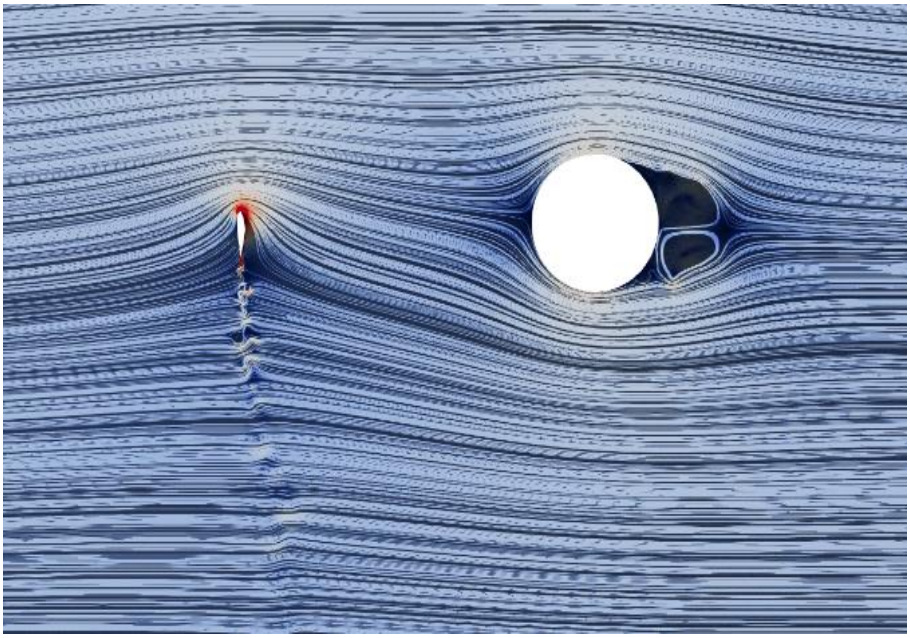

Figure 2.7: Streamlines of a smoothly flowing profile

2.1.2.3. Pressure distribution

In the distribution of the pressure coefficient shown in Figure 2.8, the overpressure and negative pressure areas described above are visible. A suction peak forms on the

suction side of the profile nose due to the locally extremely high flow speed. The area between the suction and pressure side curve corresponds to the buoyancy coefficient [25]. The speed distribution is shown for the same profile for different angles of attack in Figure 2.9.

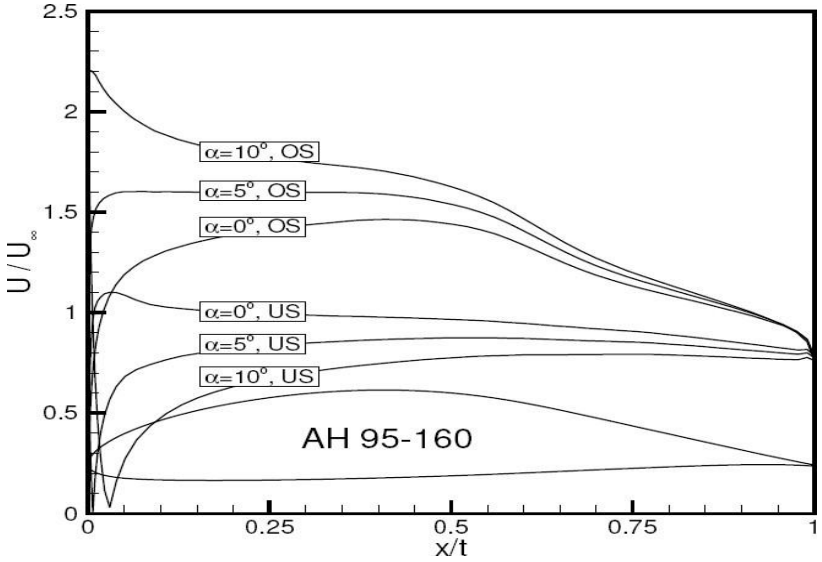

Figure 2.8: Speed distribution of a profile for different angles of attack, [27]

The representation results in compression and displacement of the count in the y-direction. With an increasing angle of attack, the area between the curves of the suction and pressure side of the profile grows, so even if the surface does not correspond to the buoyancy coefficient, these increases. In addition, with an increasing angle of attack, the above-mentioned suction peak is characterized. This plays a significant role in the detachment of the boundary layer, which is dealt with in section 2.1.2.

2.1.2.4. Flow detachment

Detachment refers to a process in the boundary layer of a profile flow in which the flow no longer follows the profile contour. The increase in pressure on the profile suction side shown in Figure 2.8 leads to a delay in the flow, especially in the area close to the wall. If this delay is strong enough, the normal velocity gradient du/dn disappears on the profile surface. This occurs in point S of Figure 2.10.

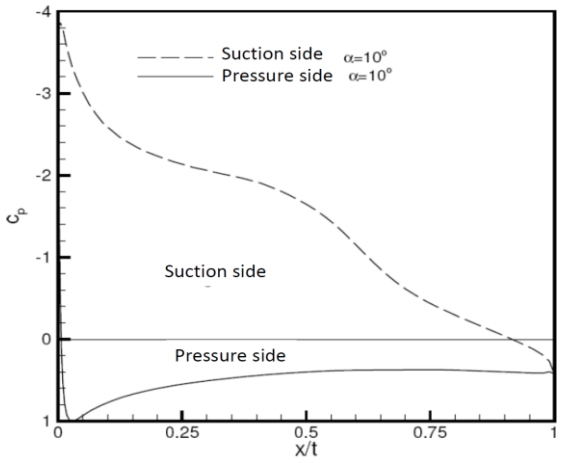

Figure 2.9: Distribution of the pressure coefficient of a profile for $\alpha = 10^{\circ}$, [27]

In the separate area, there is backflow; see point T. If the detached flow is laminar, in most cases, the boundary layer changes at point T and the flow becomes turbulent. Suppose the pressure increase is not too large. In that case, this leads to a re-application of the boundary layer, see point R. Compared to a laminar boundary layer, a turbulent boundary layer reacts more robustly to pressure increases, whereby detachment can be delayed or avoided [25].

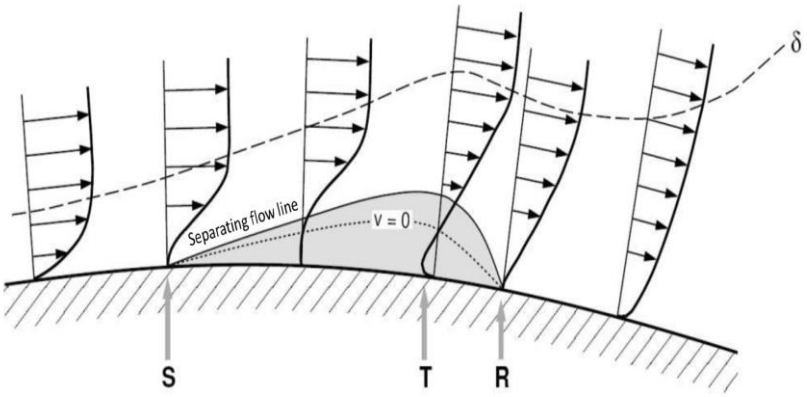

Figure 2.10: By velocity profiles of the flow, laminar detachment bubble illustrated, which is delimited by the separation current line shown, [27]

2.1.3. Aerodynamic interaction of tower and rotor blade in wind turbines

As the primary cause of the pressure changes on the tower and profile surface under investigation, the aerodynamic interaction of the tower and rotor blade is crucial to this work. A wind turbine's rotor blade travels through the reservoir region that forms on the tower's front side as it moves through the tower (see section 2.1.1). In turn, this causes both the angle of attack and the wind velocity on the blade to briefly drop. The rotor blade encounters a decreased buoyancy force because of the decreasing angle of attack and is thus momentarily relieved [28].

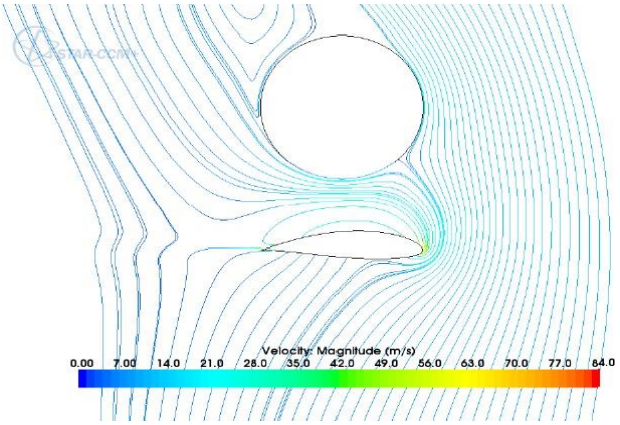

Figure 2.11: Aerodynamic interaction of profile and tower section illustrated by streamlines of a 2D flow simulation. The streamlines are shown relative to the tower for the wind speed u_∞ =7 m/s, [29]

The flow field of a wind turbine simulation in 2D is depicted in Figure 2.11. The streamlines displayed are for the tower, not the profile, thus they are not moved. On the front of the tower, a region of lower velocity can be noticed around the current congested location. It denotes the area of overpressure that was indicated. Nach Gomez, [29], the storage point is temporarily shifted laterally by the effect of the profile. Furthermore, an acceleration of the flow between the tower and the profile can be seen.

2.2. Numerical Basics

This section presents the basics of fluid mechanics and numerical methods used in this work.

2.2.1. Conversation Equation

The conservation equations of fluid mechanics are the basis of the numerical flow simulation on which this work is based.

2.2.1.1. Mass conservation

From the conservation of mass, it follows that for a considered control volume, the mass flow m in and out of the control volume must be the same. This follows:

$$m_1 = m_2 \tag{2.8}$$

The influx of mass into the control volume can be written as

$$m_1 = \iint_A \rho \, \underline{v}.\underline{ds}, \tag{2.9}$$

With the density ρ and the velocity vector $\underline{v}$, as well as the surface integral over the control volume. The change in mass in the control volume is

$$m_2 = -\frac{\partial}{\partial t}\iiint_V \rho \, dV. \tag{2.10}$$

From the Equations 2.8 until 2.10 follows the Integral form the Continuity equation in conservative Form:

$$\frac{\partial}{\partial t}\iiint_V \rho \, dV + \iint_A \rho \, \underline{v}.\underline{ds} = 0 \tag{2.11}$$

2.2.1.2. Conservation of momentum

The application of the context

$$\frac{DI}{Dt} = F \tag{2.12}$$

on a fluid element provides the equations 2.13 and 2.14.

$$\frac{DI}{Dt} = \frac{D}{Dt}\iiint_{v(t)} \rho \underline{v} dV, \tag{2.13}$$

$$F = \underbrace{\iiint_v \rho \underline{f} \, dV}_{\text{Volume force}} + \underbrace{\iint_s \underline{\underline{\sigma}} \, dS}_{\text{surface force}} \tag{2.14}$$

$$\frac{DI}{Dt} = \left.\frac{dI}{dt}\right|_{\underline{r}_b=\text{const.}}' \tag{2.15}$$

With $\underline{r_b}$, the position vector of the particle under consideration and the total differential 2.15

$$\frac{dI}{dt} = \frac{\partial f}{\partial t} + u\frac{\partial f}{\partial x} + v\frac{\partial f}{\partial y} + w\frac{\partial f}{\partial z} \tag{2.16}$$

With the Equations 2.12 until 2.14 results in oneself

$$\frac{D}{Dt}\iiint_v \rho \underline{f} \, dV = \iiint_v \rho \underline{f} dV + \iint_s \underline{\underline{\sigma}} \, dS \, . \tag{2.17}$$

Equation 2.13 can be simplified using the Reynolds transport theorem as follows

$$\frac{DI}{Dt} = \frac{D}{Dt}\iiint_{V(t)} \rho \underline{v} \, dV = \iiint_V \frac{\partial(\rho v)}{\partial t} dV + \iint_s \rho \underline{v} \left(\underline{v}.\underline{n}\right) dS. \tag{2.18}$$

The momentum law in integral form results from equations 2.17 and 2.18

$$\iiint_V \frac{\partial(\rho v)}{\partial t} dV + \iint_s \rho v \underline{(v.n)} dS = \iiint_V \rho \underline{f} \, dV + \iint_s \underline{\underline{\sigma}} \, dS \, . \tag{2.19}$$

With the stress tensor

$$\underline{\underline{\sigma}} = \begin{pmatrix} \sigma_{xx} & \tau_{xy} & \tau_{xz} \\ \tau_{yx} & \sigma_{yy} & \tau_{yz} \\ \tau_{zx} & \tau_{zy} & \sigma_{zz} \end{pmatrix} \tag{2.20}$$

For a Newtonian fluid subject to friction, the typical stresses are:

$$\sigma_{ii} = -p + \eta\left(2\frac{\partial v_i}{\partial x_j} - \tfrac{2}{3} div(\underline{v})\right) + \eta\hat{} div(\underline{v}), \tag{2.21}$$

with the static pressure p and the pressure viscosity $\eta\hat{} = \boldsymbol{\lambda} + \frac{2}{3}\boldsymbol{\eta}$, the tangential stresses can be written as

$$\tau_{ij} = \eta\left(\frac{\partial v_i}{\partial x_j} + \frac{\partial v_j}{\partial x_i}\right) | i \neq j. \tag{2.22}$$

This results in for the stress tensor

$$\underline{\sigma} = \begin{pmatrix} -p + 2\eta\left(\frac{\partial u}{\partial x} - \frac{1}{3}div(\underline{v})\right) & \eta\left(\frac{\partial u}{\partial y} + \frac{\partial v}{\partial x}\right) & \eta\left(\frac{\partial u}{\partial z} + \frac{\partial w}{\partial x}\right) \\ \eta\left(\frac{\partial v}{\partial x} + \frac{\partial u}{\partial y}\right) & -p + 2\eta\left(\frac{\partial v}{\partial y} - \frac{1}{3}div(\underline{v})\right) & \eta\left(\frac{\partial v}{zx} + \frac{\partial w}{\partial y}\right) \\ \eta\left(\frac{\partial w}{\partial x} + \frac{\partial u}{\partial z}\right) & \eta\left(\frac{\partial w}{\partial y} + \frac{\partial v}{\partial z}\right) & -p + 2\eta\left(\frac{\partial w}{\partial z} - \frac{1}{3}div(\underline{v})\right) \end{pmatrix} \tag{2.23}$$

The incompressible Navier-Stokes equations in component notation result from the combination of equations 2.19 and 2.23.

$$\begin{aligned} \frac{\partial u}{\partial t} + u\frac{\partial u}{\partial x} + v\frac{\partial u}{\partial y} + w\frac{\partial u}{\partial z} &= -\frac{1}{\rho}\frac{\partial p}{\partial x} + \nu\left(\frac{\partial^2 u}{\partial x^2} + \frac{\partial^2 u}{\partial y^2} + \frac{\partial^2 u}{\partial z^2}\right) + f_x \\ \frac{\partial v}{\partial t} + u\frac{\partial u}{\partial x} + v\frac{\partial u}{\partial y} + w\frac{\partial u}{\partial z} &= -\frac{1}{\rho}\frac{\partial p}{\partial y} + \nu\left(\frac{\partial^2 v}{\partial x^2} + \frac{\partial^2 v}{\partial y^2} + \frac{\partial^2 v}{\partial z^2}\right) + f_y \\ \frac{\partial w}{\partial t} + u\frac{\partial w}{\partial x} + v\frac{\partial w}{\partial y} + w\frac{\partial w}{\partial z} &= -\frac{1}{\rho}\frac{\partial p}{\partial z} + \nu\left(\frac{\partial^2 w}{\partial x^2} + \frac{\partial^2 w}{\partial y^2} + \frac{\partial^2 w}{\partial z^2}\right) + f_z\,. \end{aligned} \tag{2.24}$$

2.2.1.3. Conservation of Energy

According to the law of energy conservation, a closed system's energy is constant [30]. For enclosed systems whose boundaries are permeable for heat flows and work input, the balance applies.

$$\left\{\begin{matrix}\text{Temporal change of energy} \\ \text{into the system}\end{matrix}\right\} = \left\{\begin{matrix}\text{Heat flow into} \\ \text{the system}\end{matrix}\right\} + \left\{\begin{matrix}\text{Power rendered} \\ \text{to the system}\end{matrix}\right\}$$

For an infinitesimal fluid element, the supplied heat flow follows:

$$Q = \left[\rho q + \frac{\partial}{\partial x}\left(k\frac{\partial T}{\partial x}\right) + \frac{\partial}{\partial y}\left(k\frac{\partial T}{\partial y}\right) + \frac{\partial}{\partial z}\left(k\frac{\partial T}{\partial z}\right)\right] dxdydz \tag{2.26}$$

According to Schlichting, [13], the power supplied can be written as follows:

$$\begin{aligned} W = \Big[-\frac{\partial(up)}{\partial x} - \frac{\partial(vp)}{\partial y} - \frac{\partial(wp)}{\partial z} + \frac{\partial(u\tau_{xx})}{\partial x} + \frac{\partial(u\tau_{yx})}{\partial y} + \frac{\partial(u\tau_{zx})}{\partial z} + \frac{\partial(v\tau_{xy})}{\partial x} + \frac{\partial(v\tau_{yy})}{\partial y} + \frac{\partial(v\tau_{yz})}{\partial z} + \\ \frac{\partial(w\tau_{xz})}{\partial x} + \frac{\partial(w\tau_{yz})}{\partial y} + \frac{\partial(w\tau_{zz})}{\partial z} + \rho\underline{f}.\underline{v}\Big] dxdydz \end{aligned} \tag{2.27}$$

For an infinitesimal fluid element, the change in energy E can be set up as follows:

$$\frac{D}{Dt}E = \rho\frac{D}{Dt\left(e + \frac{|\underline{v}|^2}{2}\right)dxdydz} \tag{2.28}$$

If the elements are combined according to equation 2.25, the energy theorem follows in non-conservative, differential form

$$\begin{aligned} \rho\frac{D}{Dt}\left(e + \frac{|\underline{v}|^2}{2}\right) = \rho q + \frac{\partial}{\partial x}\left(k\frac{\partial T}{\partial x}\right) + \frac{\partial}{\partial y}\left(k\frac{\partial T}{\partial y}\right) + \frac{\partial}{\partial z}\left(k\frac{\partial T}{\partial z}\right) - \frac{\partial(up)}{\partial x} - \frac{\partial(vp)}{\partial y} - \frac{\partial(wp)}{\partial z} + \frac{\partial(u\tau_{xx})}{\partial x} + \\ \frac{\partial(u\tau_{yx})}{\partial y} + \frac{\partial(u\tau_{zx})}{\partial z} + \frac{\partial(v\tau_{xy})}{\partial x} + \frac{\partial(v\tau_{yy})}{\partial y} + \frac{\partial(v\tau_{yz})}{\partial z} + \frac{\partial(w\tau_{xz})}{\partial x} + \frac{\partial(w\tau_{yz})}{\partial y} + \\ \frac{\partial(w\tau_{zz})}{\partial z} + \quad \rho\underline{f}.\underline{v}. \end{aligned} \tag{2.29}$$

2.2.1.4. Combination of the conservation laws

The conservation of mass, momentum and energy together form the Navier Stokes equations. These are in integral, conservative form:

$$\frac{\partial}{\partial t}\iiint_v \underline{W}dV + \iint_s (\underline{F_c} + \underline{F_v})dS = \iiint_v \underline{Q}dV \tag{2.30}$$

With the vector of the conservative variable $\underline{W}$

$$\underline{W} = \begin{pmatrix} \rho \\ \rho u \\ \rho v \\ \rho w \\ \rho E \end{pmatrix} \tag{2.31}$$

The vectors of the conservative and viscous flows, $\underline{F_c}$ & $\underline{F_v}$.

$$\underline{F_c} = \begin{pmatrix} \rho V \\ \rho u V + n_{xp} \\ \rho v V + n_{yp} \\ \rho w V + n_{zp} \\ \rho H V \end{pmatrix} \tag{2.32}$$

With the normal vector $\underline{n}$, the magnitude of the velocity in the normal direction $V = \underline{v}.\underline{n}$, the total heat $H = E + \frac{p}{\rho}$ and the mass-specific energy $E = e + \frac{v^2}{2}$

$$\underline{\mathbf{F}}_{\mathbf{v}} = \begin{pmatrix} 0 \\ n_x\tau_{xx} + n_y\tau_{xy} + n_z\tau_{xz} \\ n_x\tau_{yx} + n_y\tau_{yy} + n_z\tau_{yz} \\ n_x\tau_{zx} + n_y\tau_{zy} + n_z\tau_{zz} \\ n_x\Theta_x + n_y\Theta_y + n_z\Theta_z \end{pmatrix} \tag{2.33}$$

With

$$\Theta_x = u\tau_{xx} + v\tau_{xy} + w\tau_{xz} + k\frac{\partial T}{\partial x}$$
$$\Theta_y = u\tau_{yx} + v\tau_{yy} + w\tau_{yz} + k\frac{\partial T}{\partial y}$$
$$\Theta_x = u\tau_{zx} + v\tau_{zy} + w\tau_{zz} + k\frac{\partial T}{\partial z}$$

According to Bogdanski, [31], the vector of the source terms results in

$$\underline{Q} = \begin{pmatrix} 0 \\ \rho f_x \\ \rho f_y \\ \rho f_z \\ \rho \underline{f}.\underline{v} + \rho \dot{q} \end{pmatrix} \tag{2.34}$$

The thermal equation of state and the caloric equation of state must also be solved in order to complete the system of equations. A function of temperature, density, and the gas constant R, the former gives the pressure. It has a perfect gas-like shape.

$$p = \rho RT \tag{2.35}$$

The caloric equation of state supplies the enthalpy h as a function of the temperature T. This is for an ideal gas

$$dh = c_p dT\ . \tag{2.36}$$

2.2.2. Finite Volume Method

The analysis of a numerical flow simulation served as the foundation for this work. In this scenario, the Navier-Stokes equations are approximately solved on a computational grid that discretizes the computational domain. Using control volumes (3D) or control areas (2D), often known as cells, is one way to solve the equations. Grid points and their connections define these (see Section 2.2.4). The conserved variables in each cell of the finite volume technique are balanced following Section 2.2.1. The fluxes at the cell borders cause the conserved variables in the cells to varying over time. The control volume and differentials numerically approximate the flows at the cell boundaries and the integrals during the balancing. The resulting coupled system of equations is solved iteratively. Termination criteria include, for instance, exceeding a maximum number of iterations or dropping below a limit value for the residual [30].

2.2.3. Turbulence Modeling

To maximize accuracy and reduce processing efforts, various methods of numerical modeling of turbulent flows are employed. Using high-resolution computational grids, the Direct Numerical Simulation, or DNS for short, resolves beautiful, turbulent structures up to the dissipation range. Due to the extraordinarily high computing effort that occurs, the technology is either too costly or time-consuming for the majority of 3D and 2D applications. The RANS and URANS approach, which significantly reduce the grid resolution needed but at the tradeoff of reduced precision and the dissipation of delicate vortex formations, also uses physical turbulence models as an alternative. The turbulence mentioned above models provides the link between Reynolds stresses and fluctuation values, which is necessary to solve the system of equations. Eddy viscosity and Reynolds stress models are the foundation for the semi-empirical models. Unsteady flows are computed using the URANS method (Unsteady Reynolds-Averaged Navier-Stokes). The transient Reynolds-averaged Navier-Stokes equations are combined with turbulence models in this case.

To approximate the turbulence inside the CFD model, unsteady Reynolds averaged Navier Stokes equations (URANS) are used. This simulation is based on the K-SST model of Menter [31] and solves for the turbulent kinetic energy k and the specific turbulent dissipation rate. Using the SST additive, the near-wall regions are modeled with a k-W model, whereas the k-E model is employed to model the free stream.

2.2.4. Pimple Algorithm

In this research, OpenFOAM's pimpleFoam solver is employed, which employs the PIMPLE algorithm. Navier-Stokes equations are solved transiently for incompressible turbulent flow using the PIMPLE algorithm. Figure 2.12 illustrates the PIMPLE algorithm in the paper by Municchi et al. [32]. In addition to the steady-state SIMPLE algorithm, it contains a transient inner pressure corrector loop, also called the PISO algorithm, which checks for convergence based on the number of loop iterations or residuals. In the OpenFOAMWiki, the solvers are discussed more in-depth (SIMPLE algorithm [33], PIMPLE algorithm [34]).

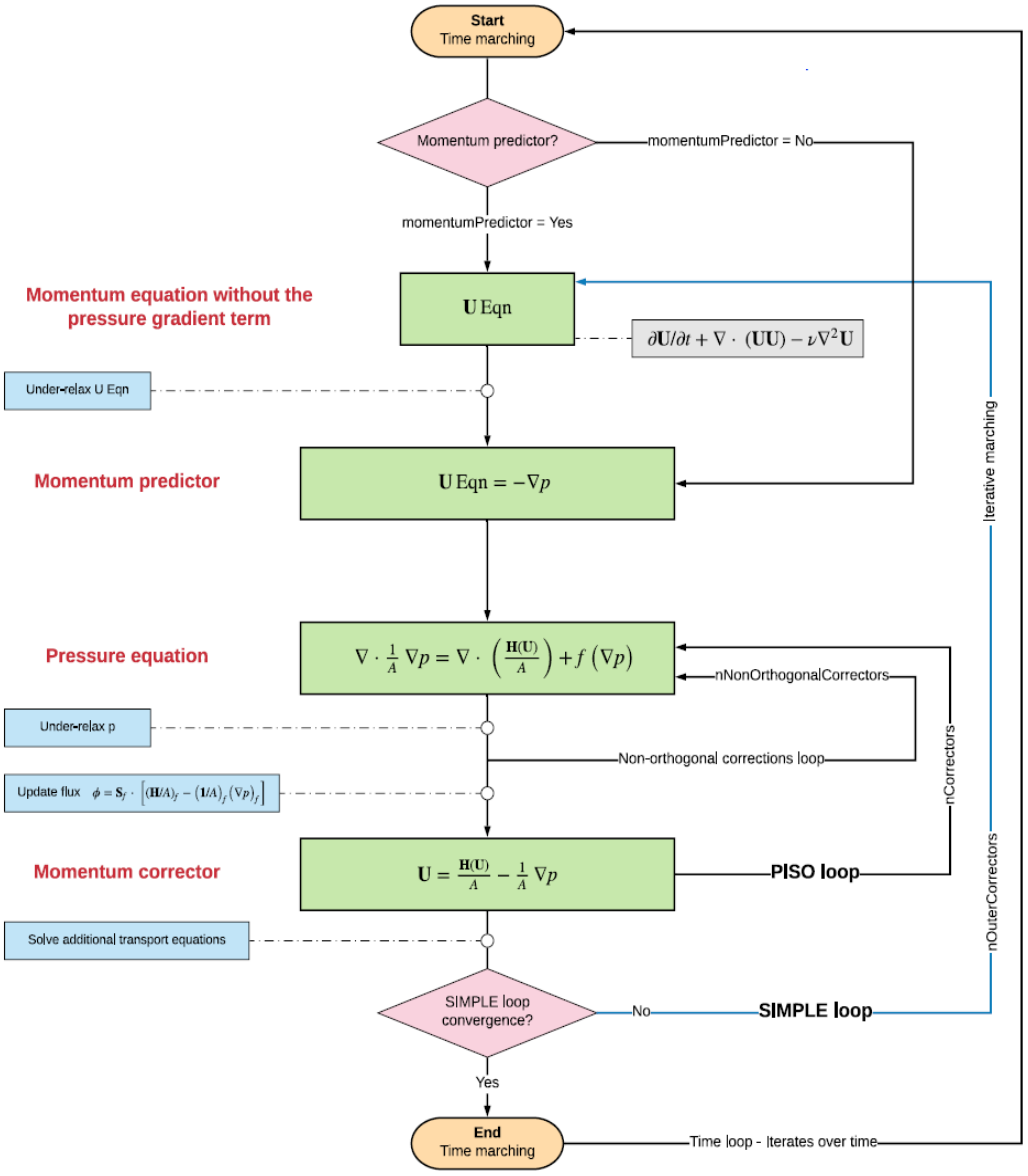

Figure 2.12: PIMPLE algorithm demonstration.

The convergence of the numerical solutions of simulations is observed through the Courant–Friedrichs–Lewy (CFL) number, which is defined as

$$CFL = \frac{U_{mag}\Delta t}{\Delta x} \leq U_{max} \tag{2.37}$$

2.2.5. Grid Creation

Meshes are used to discretize the computational domain for numerical flow simulations. Volumes or regions can be regulated at several points. Flow variables are represented by grid cells (see Section 2.2.1). The characteristic point, typically the cell's centre, is where the flow variables within a cell are kept constant (first-order technique). While organizing the grid points and combining them into cells, there is a distinction between structured and unstructured meshes [30].

2.2.5.1. Structured mesh

The arrangement of cells is the prime characteristic of structured meshes, either hexagonal or square. The cell positions can therefore be determined by I, J, and K coordinates, thereby describing the structured mesh in terms of neighborhood relationships. Structured mesh calculations are accelerated due to the continuous demand for neighborhood interactions. The arrangement of cells is the prime characteristic of structured meshes, either hexagonal or square. The cell positions can therefore be determined by I, J, and K coordinates, thereby describing the structured mesh in terms of neighborhood relationships. Structured mesh calculations are accelerated due to the continuous demand for neighborhood interactions.

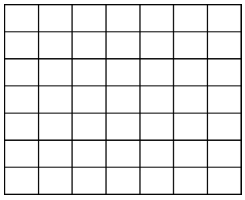

Figure 2.13: Cartesian grid, [30]

The most straightforward type of structured mesh is the Cartesian grid as shown in Figure 2.13. The distribution of points in space is entirely homogeneous since it is made up of square or cubic cells with constant spacing between the cell centers. In most cases, the lattice geometry must be adapted to an inhomogeneous flow field or body. On this basis, regions with substantial gradients in the flow variables, such as boundary or shear layers, can be resolved more precisely. Figure 2.14 shows the most important topologies of these body-adapted grids where mesh follows streamlines. For example, profile geometries like wings or rotor blades are discretized using c-grids or O-grids. If there are no bodies in the flow, spaces with a uniform flow frequently mesh with H-lattices. O-grids are mostly used for discretizing the bodies like cylinders. In the calculating area, various mesh topologies for complex and many bodies are split into so-called grid blocks. For example, the geometry of a cylinder can be embedded in a Cartesian computational grid.

This type of grid offers the advantage of parallelizing the calculations of different grid blocks and distributing them to various processors or computing

cores. During each iteration, the solution between the block structures must be exchanged, which requires the use of neighborhood relationships. Parallelization speeds up computation and makes it possible to use finer-resolution grids for calculations. To conclude, a structured grid is a network of well-organized blocks which help making calculations to simulate with maximal accuracy.

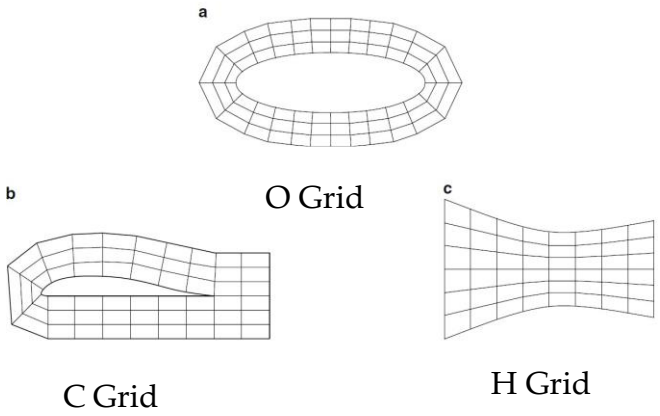

Figure 2.14: Grid topologies: O-, C- and H-grids, [30].

2.2.5.2. Unstructured mesh

Contrarily, using unstructured meshes has become more widespread in many CFD applications. Modern commercial codes use unstructured meshing, where cells can be assembled freely within the computational domain. Each face has its connectivity information, which is stored in some form of a table. Unstructured grids generally take the form of triangles or tetrahedrons in three dimensions. Nevertheless, any other elemental body, including quadrilateral or hexahedral cells, is also possible. Unstructured meshes can handle geometries with high-curvature boundaries well, particularly those with arbitrary shapes.

Despite the numerous benefits of unstructured meshing, several disadvantages exist with employing such a mesh for CFD simulations. Compared to structured meshes, points of unstructured meshes cannot be addressed using two indices (i, j), in two dimensions, or triple index (i, j, k), in three dimensions. An elemental cell may be attached to an arbitrary number of neighboring cells, making data processing and connection difficult. When it comes to resolving wall boundary layers, triangular (two-dimensional) and tetrahedral (three-dimensional) cells are usually less effective than quadrilateral (two-dimensional) or hexahedral (three-dimensional) cells. This grid type typically yields thin triangular or tetrahedral cells adjacent to boundary walls, complicating the approximation of diffusive fluxes. Flow-field variables require more complex solution algorithms to solve, which is another disadvantage with data treatment and connectivity of elemental cells. Hence, it may increase computation time and reduce computational efficiency [35].

2.2.5.3. Mesh modifier I: Cell layer addition/removal

In layer addition/removal, a set of mesh faces create an oriented surface with minimum and maximum layer thickness. The algorithm computes the approximate layer thickness based on the volume-to-area ratio (constant aspect ratio) between the cells in the master layer (nearest wall). Adding or removing layers is determined by the layer thickness from the previous step while preserving the global mesh quality. Upon reaching the maximum layer thickness, a cell layer is added to a predefined mesh surface; the layer is removed upon exceeding the minimum layer thickness. Based on the "set-and-forget" strategy, this topology modifier applies to static meshes without user intervention following mesh movement.
As shown schematically in Figure 2.15, adding, and removing cell layers (a set of mesh faces that create an oriented surface).

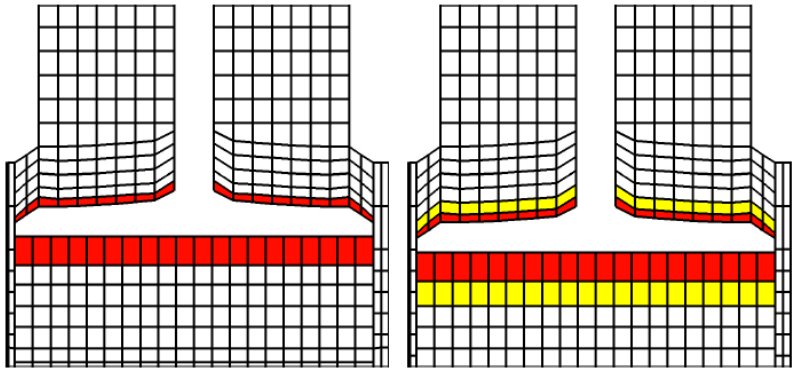

Figure 2.15: Cell layer addition (yellow) during motion, [36]

2.2.5.4. Mesh modifier II: Arbitrary Mesh Interface (AMI)

The arbitrary mesh interface (AMI) is the technique for coupling patches with the same outer bounds but different interior constructions.

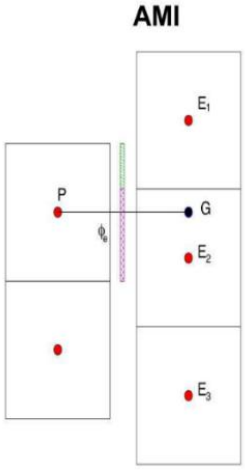

$$\phi_e = \phi_G \alpha + (1-\alpha)\phi_P\}$$

$$\alpha = \frac{x_e - x_p}{x_G - x_p}$$

$$\phi_G = \sum_i \alpha_i \phi_{Ei}$$

$$\alpha_i = \frac{A_i}{A} \qquad (2.38)$$

It enables the simulation of disconnected and adjacent meshes. Mesh domains can be stationary or rotating—the cyclicAMI boundary condition couples boundaries at patch boundaries between rotating and static geometry regions. Non-conformal interfaces connect mesh regions, maintaining mesh quality. Algorithms for connecting meshes work automatically. Simulation variables are determined by calculating face fluxes over the interface using second-order interpolation.

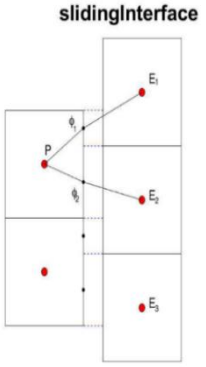

$$\phi_{e_1} = \phi_{E_1}\alpha_1 + (1-\alpha_1)\phi_P$$

$$\phi_{e_2} = \phi_{E_2}\alpha_2 + (1-\alpha_2)\phi_P$$

$$\alpha_i = \frac{x_{e_i} - x_p}{x_{E_i} - x_p} \tag{2.39}$$

Parallelization is fully supported, with AMIs distributed across several subdomains or restricted to one subdomain. AMI is integrated into boundary patch classes in OpenFOAM and can be used for unmatched/non-conformal cyclic patch pairs, sliding interfaces applied to rotating machinery, mapped patches, and coupling simulations between two mesh regions, e.g., surface film simulations and bulk flow simulations.

AMI projects the geometry of one patch onto the other. Alternatively, both patches can be projected onto an intermediate surface, such as triangulated surface geometry or a continuous character (determined by a function). In this study, sliding interface capability was employed. Figure 2.16 shows the sliding interface, where the two different but adjacent meshes are interacting.

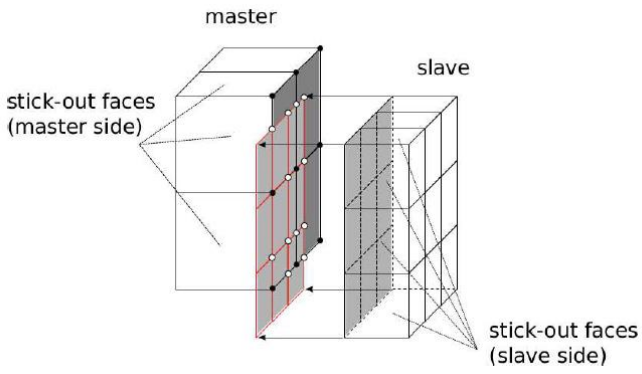

Figure 2.16: Operation of the Sliding Interface [37].

2.2.6. Quality criteria of structured grids

This section provides an overview of guidelines for generating structured grids. Compliance with the guidelines is of immense importance for the excellent quality of the simulation results.

2.2.6.1. Grid topology

Choosing the appropriate grid topology for a discretized calculation area or meshing geometry is crucial to the resolution of large gradients of flow variables. It establishes whether local high resolution is possible without extending beyond the restrictions on cell distortion, cell aspect ratio, or cell length growth rate. Additionally, selecting the appropriate grid topology reduces the time and effort needed to generate the grid. Different topologies are described in Section 2.2.4.

2.2.6.2. Extension of the computing area

The grid completely encloses the computational region. Flow amounts should be known at the far field's edge. The area must be chosen so that the boundary conditions at the boundaries of the computing area have a minimal impact on the simulated flow. For instance, the no-slip condition at body boundaries or a long distance from bodies in the flow achieves this. The boundary conditions can also reflect disturbances in the computing area. By making the computational area larger, this can be prevented. For profile flows, a far-field distance of 50 profile depths is advised. Since the flow gradients are smaller towards the far edge, the field's grid resolution can be decreased.

2.2.6.3. Cell skewness

The flow pattern or the following of body geometry can require a substantial deviation from the topology of a Cartesian grid (see Section 2.2.4).

Distortions of the grid occur, manifesting themselves in deviations of the internal angles of the cells from 90°. For example, the distortion can be specified with the so-called equiangular skewness. If this exceeds a limit, the grid will deliver worse results, or the convergence of the flow simulation will slow down.

Figure 2.17 shows the cell distortion in the transition from a Cartesian to an O lattice. The cells are almost square in the upper left corner, so they are hardly distorted, whereas the cell distortion in the upper right corner is relatively high. However, at 0.5, this is still below the limit of 0.85 specified in the literature. Compliance with this limit value is crucial in areas with large flow gradients.

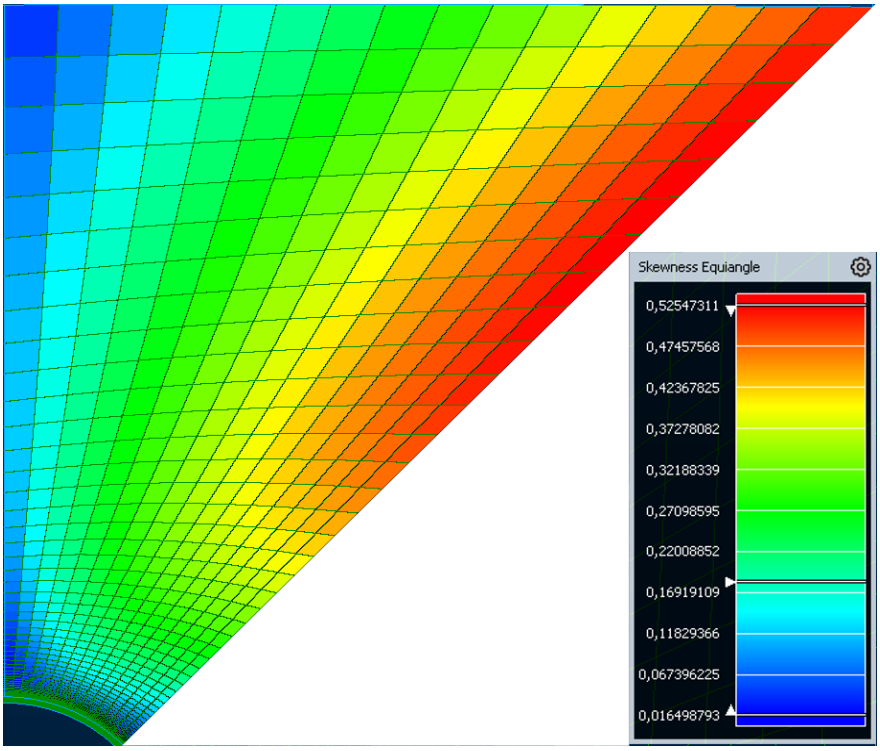

Figure 2.17: Cell distortion using the example of the transition of a Cartesian grid to an O-grid

2.2.6.4. Cell Aspect Ratio

An aspect ratio represents the ratio of a cell's longest to its shortest dimensions, $\frac{l_{max}}{l_{\mathrm{m}}}$

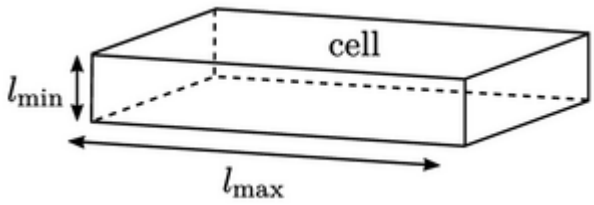

Figure 2.18: Single cell inside the mesh, [38]

In meshes, cells with a higher aspect ratio make it possible to exploit the fact that flow parameters' gradients, such as shear stress, deformation rate, and velocity, tend to be steeper in one direction than in another. They are most used to resolve the boundary layers at walls. The mesh resolution must be increased whenever the gradients normal to the wall are exceptionally high. To achieve lower y+, the central heights of cells adjacent to the boundary must be minimal. Introducing a high aspect ratio into one mesh area can cause problems in other areas, increasing the error associated with discretization. Thus, the aspect ratio increases by small indices from the blade and tower surface to the far field. GAMG performs much better in this case due to its agglomeration strategy that progressively reduces aspect ratios [38].
As shown in Figure 2.19, the aspect ratio at the airfoil's trailing edge is 10, increasing to 1000 towards the far field.

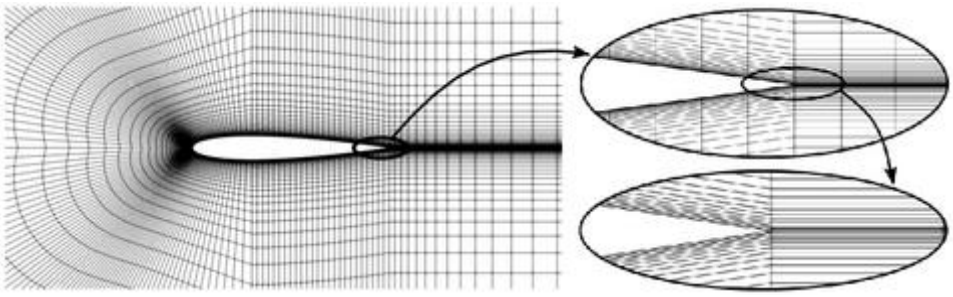

Figure 2.19: Single cell inside the mesh, [38]

2.2.6.5. Non-orthogonality

A non-orthogonality is defined as the angle formed by a vector connecting two adjacent cell centers across their common face and a normal to that face. It is recommended to keep non-orthogonality below 65 degrees to converge the solutions. The zero value indicates that the mesh is orthogonal and that two identical cells in the mesh are perfectly aligned. As non-orthogonality increases, the probability of numerical instability increases.

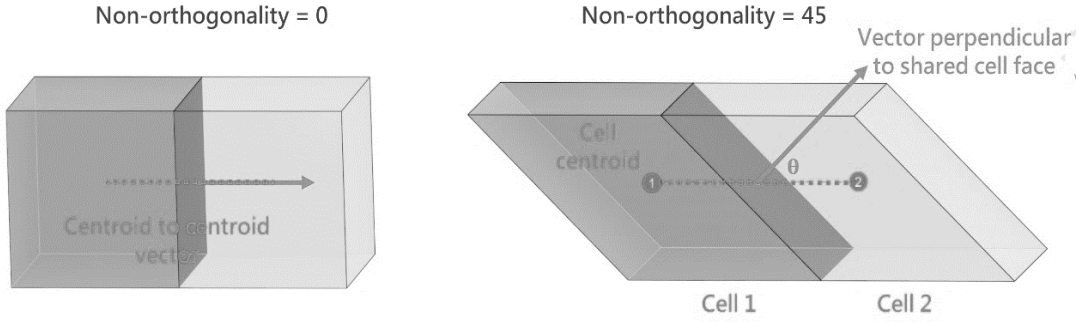

Figure 2.20: Single cell inside the mesh, [39]

2.2.6.6. Expansion rate

Another factor that needs to be considered when making the grid is the growing rate of the cell length. It must be below the limit value in all grid directions i, j, k. It usually is possible to define a specific cell growth in the software that generates the grid to produce a high-quality computational grid. Ideally, cell growth rate should not exceed 1.15-1.20 for smooth mesh transition [39].

$$\text{Growth rate} = \frac{\Delta y_2}{\Delta y_1}$$

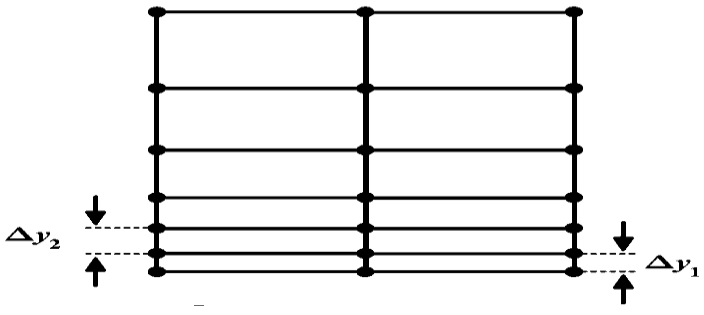

Figure 2.21: Smooth cell growth, [40]

Disproportionate growth rates cause diffusion in flow variables leading to a higher error rate.

2.2.6.7. Local refinement

To resolve high-flow gradients, the grid resolution must be increased locally by stretching the grid near around the desired point of the geometry, which is employed mostly around boundary and shear layers. While applying the stretched grid, sudden changes in the grid size must be avoided. Since the resolution of structured grids cannot be changed at a specific location, high-resolution regions in one spatial direction disperse along the grid lines. This frequently causes issues when considering the limit values for the cell aspect ratio, necessitating an increase in resolution in other spatial directions. Fig 2.17 illustrates the need for local refinement near the bottom wall.

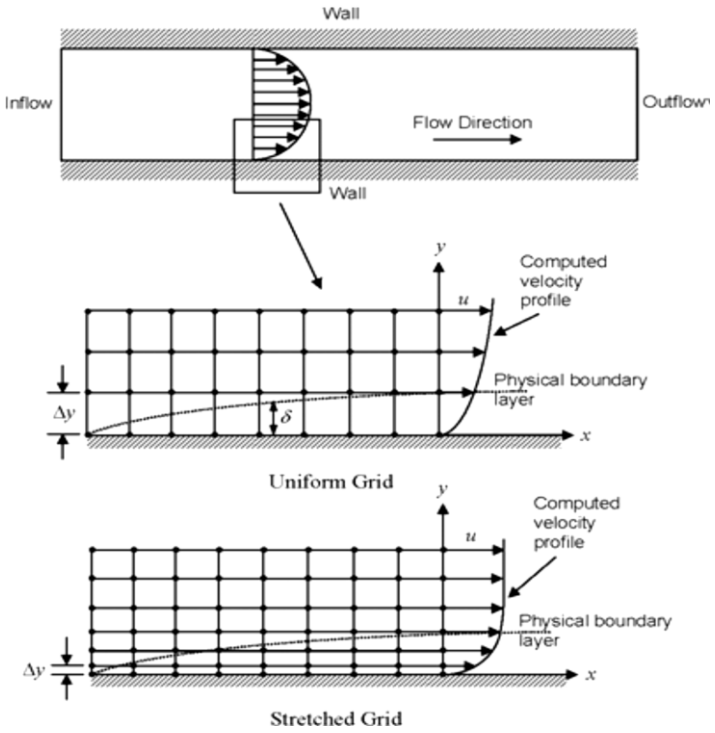

Figure 2.22: Unstretched and Stretched grids near the boundary, [40]

3 Software

This chapter provides an overview of the software used in this work to create the computational grid, carry out the simulation and evaluate the results.

3.1. Pointwise

Pointwise is a tool for creating both two-dimensional and three-dimensional structured and unstructured grids, which is supported by software from Pointwise, Inc. This work uses the version Pointwise V18.3R1 to smoothen profile geometry, especially the airfoil nose.

3.2. XFoil

XFOIL is open-source interactive software [41] to design and analyze subsonic isolated airfoils provided by MIT University. This tool is utilized to convert the profile's sharp to blunt trailing edge using 1.7% of trailing edge thickness to chord ratio.

3.3. OpenFOAM

Developed primarily by OpenCFD Ltd in 2004, OpenFOAM is also open-source Computational Continuum Mechanics (CCM) software in C++ [42]. It is widely used in various engineering and science fields, both in the commercial and academic sectors. OpenFOAM offers a wide range of features for solving various problems in fluid dynamics, including complex fluid flows with chemical reactions, turbulence, heat transfer, acoustics, solid mechanics, and electromagnetics. For this thesis, OpenFOAM v2112 is used to simulate the interaction of a wind turbine's rotor blade and the tower. The incompressible and unsteady solver pimpleFoam and its extension overPimpleDyMFoam are applied in this simulation setup. For structured multiblock meshing of the Far Field, profile, and tower, BlockMesh, an OpenFOAM's utility, is applied by providing point coordinates as well as boundary limits.

4 Spatial and Numerical Discretization

This chapter describes the discretization of the computational domain and the creation of the computational grid. Meshes were constructed using the guidelines provided in the master's thesis by Aljoscha Stein [27].

4.1. Computational Domain

This work primarily focuses on the simulation of a profile and tower section of a wind turbine in two dimensions. There are several advantages to this approach over a 3D setup.

Table 4.1: Data of the reference wind turbine and the cutting extraction

Size	Value	Description
$\mathbf{u_\infty}$	15 m/s	Nominal wind speed
$\mathbf{n_0}$	23.87 min^{-1}	Velocity of the 3D wind turbine at the operating point
$\mathbf{r_{profile}}$	41m	Radius of a rotor blade
$\mathbf{r_{cut}}$	30m	Velocity of the 3D wind turbine at the operating point
$\mathbf{t_{cut}}$	1m	Profile depth at the level of the cut
$\mathbf{(h/t)cut}$	6.88	Dimensionless distance of the t/4 point to the tower surface
$\mathbf{(D/t)cut}$	3	Dimensionless tower diameter
$\mathbf{\alpha_{cut}}$	10.53°	Angle of attack of the profile cut
$\mathbf{v_{profile,0}}$	75 m/s	Profile speed associated with n_0

Computing effort is reduced significantly, enabling detailed numerical and physical parameter analysis. Wind turbine blades pointing downward are cut horizontally at 30m from the axis of rotation in this 2D configuration. The cutting position can be seen in Figure 4.1. The resulting geometry is used for 2D simulation. Flow is in the x-direction, and the calculation is conducted in the by-plane. Rotor blades pass by the tower, moving in the Y-direction with the following velocity:

$$v_{profile,0} = 2\pi\frac{n_0}{60}r_{cut} = 75\ m/s. \tag{4.1}$$

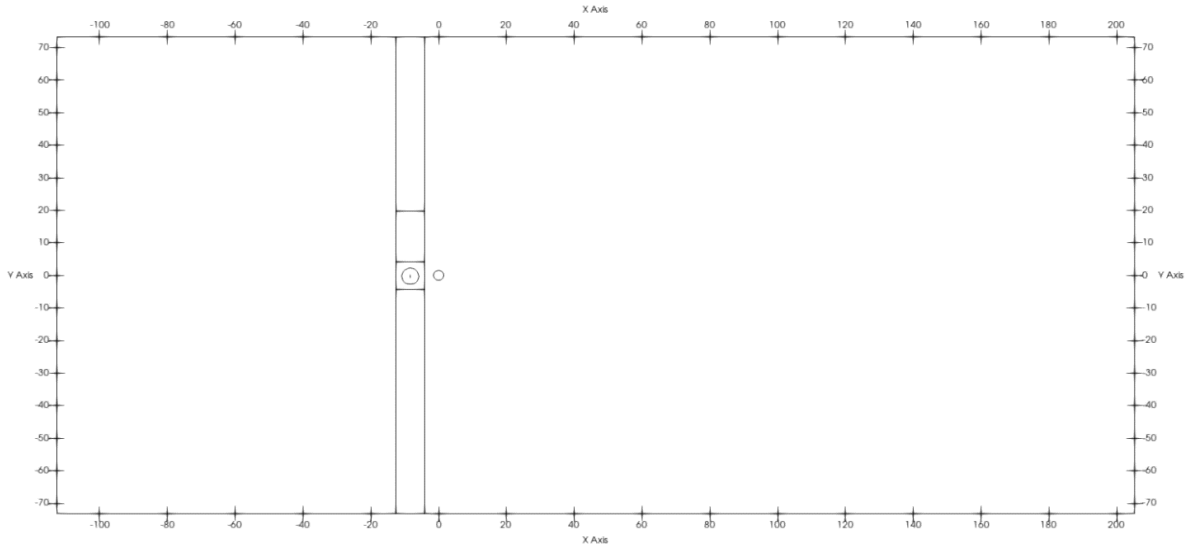

Figure 4.1: Layout of the meshing domain

As shown in Table 4.1, the essential data on the 3D wind turbine and its extraction from the 2D section are provided.

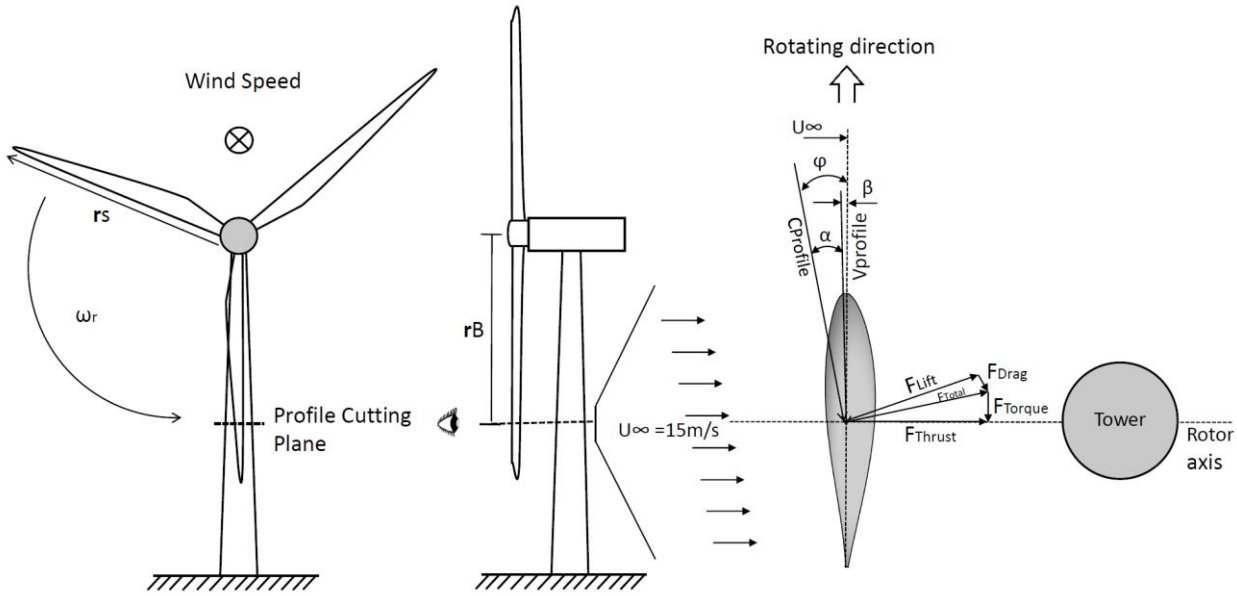

Figure 4.2: Schematic representation of the wind turbine and the extraction of the geometries for the 2D CFD setup

4.1 Airfoil geometrical modifications

4.1.1. Blunt Trailing Edge

The dataset for NACA 633418, taken from [43], was processed in Xfoil to convert the sharp leading edge to the blunt trailing edge. The geometric data file of NACA 633418,

placed in Xfoil's main folder, had been loaded into Xfoil using the command load naca633418.dat. After executing the 'gdes' command, the 'tgap' command was run, and the gap value was provided as 0.017. Following the specification of a gap size, a "blending distance/c" would also be requested, which was set to 1. Finally, the 'exec' command was entered, followed by the 'save naca633418blunt.dat' command.

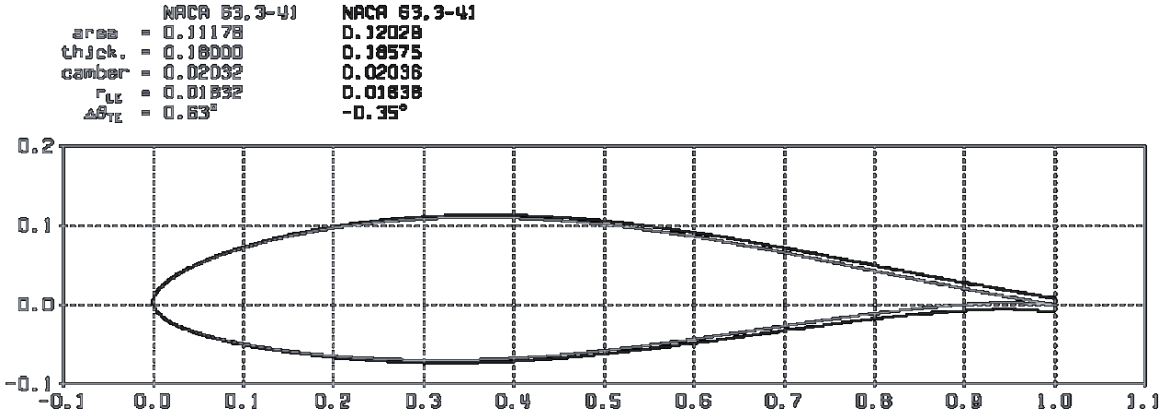

Figure 4.3: Modified NACA 633418 with Blunt Trailing Edge

In figure 4.4 and 4.5, pressure coefficients and pressure vectors are plotted for the profile (NACA 633418 with the blunt trailing edge) at two angles of attack $\alpha = 10^{o}$ and $\alpha = 1^{o}$ respectively, using Xfoil Software. The pressure distribution plots for a profile are presented when it is not influenced by profile-tower interaction ($\varphi = 0°$). The pressure distribution near the blade tip is reduced in magnitude because the profile's angle of attack is decreased due to the increase in blade pitch angle, as seen in Figures 4.4a and 4.5b. Consequently, the profile appears to have a weaker pressure region around it.

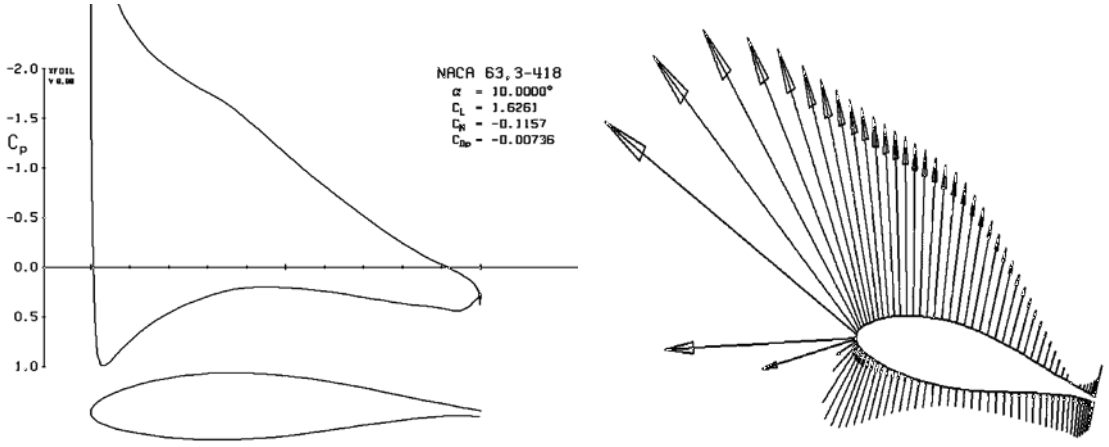

(a) Cp vs x/c (b) Airfoil with pressure vectors

Figure 4.4: Profile pressure distribution without account of profile-tower interactions when $\alpha=10^{o}$

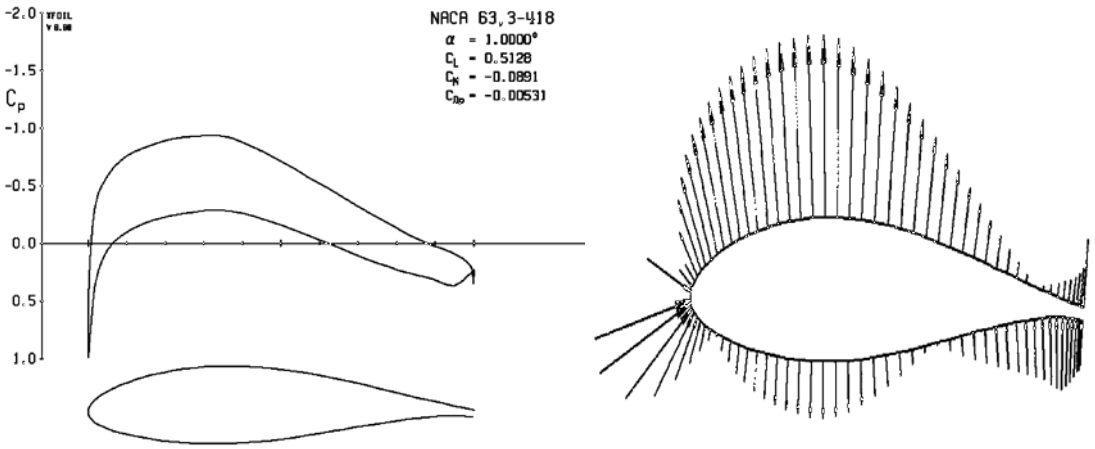

(a) Cp vs x/c (b) Airfoil with pressure vectors

Figure 4.5: Profile pressure distribution without account of profile-tower interactions when α=1°

4.1.2. Smoothening Airfoil's Geometry

The airfoil's geometry was rough and included bumps which could lead to undesirable separation of air at the surface of the airfoil. Therefore, the geometry of the airfoil was reshaped using pointwise software.

4.2 Grid Generation

Grid creation is usually the first step in setting up a CFD simulation. Here, the control volume is created, and some settings are fixed to describe how it is discretized. As in this case, the model focuses on the airfoil, tower, and the far-field. Objects can be defined in OpenFOAM in order to determine their impact on a grid. Following this process, the grid is ready for use. This section explains how this step was completed throughout this research. Physical domain is meshed as stationary and sliding grids; the details are explained below:

4.1.3. Stationary grid

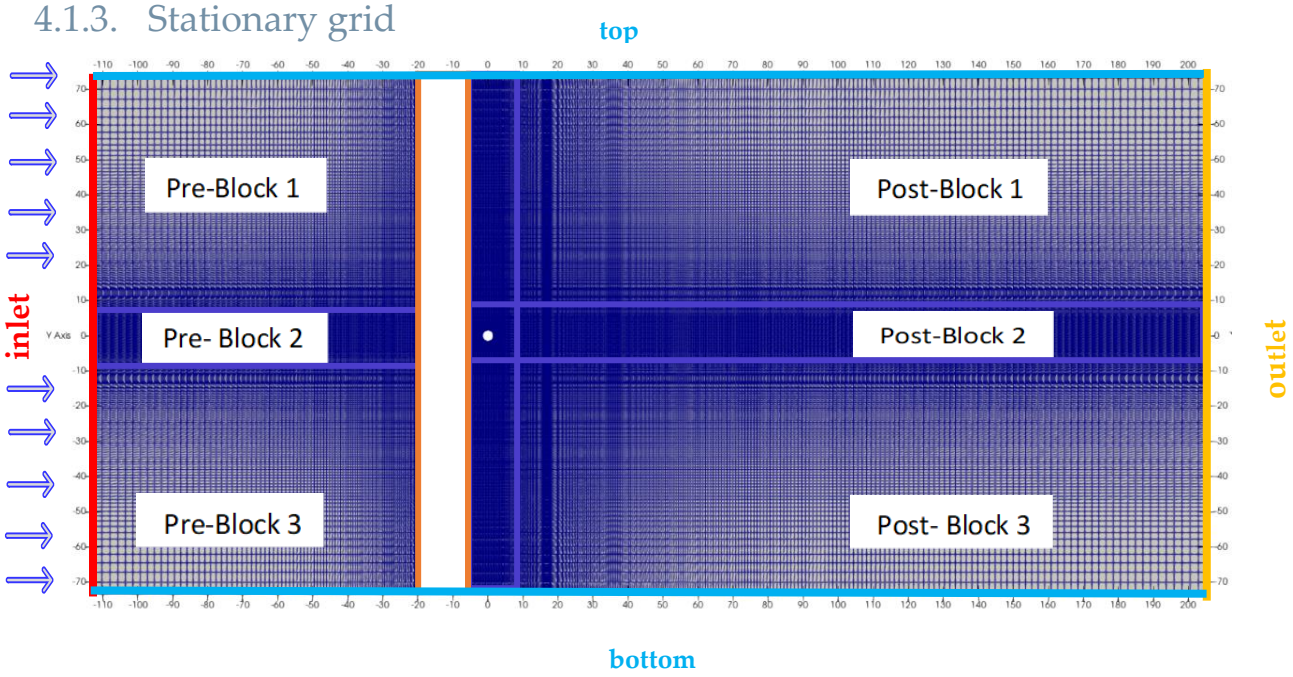

Figure 4.6: Stationary mesh blocks

In the stationary mesh, a dictionary file named blockMeshDict is processed, which can be accessed in the system directory. BlockMesh reads this dictionary, and the mesh is generated in the constant/polyMesh directory of the case in terms of faces, points, and boundary files. The stationary grid comprises the far-field and tower mesh blocks. This method decomposes the domain geometry into a set of hexahedral blocks in three dimensions [44]. It generates blocks with six faces that are arranged in a coordinate system. The grid faces are defined next. Boundary conditions are then considered based on the type of face. Each geometry block consists of 8 vertices, accessed by their labels, located at the corners of each hexahedron.

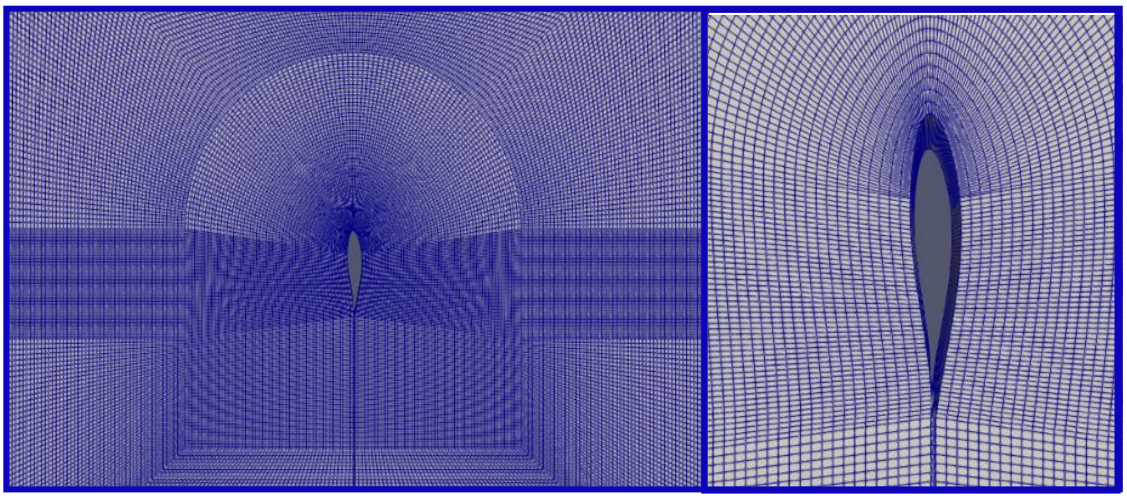

Figure 4.7: C-grid for the airfoil

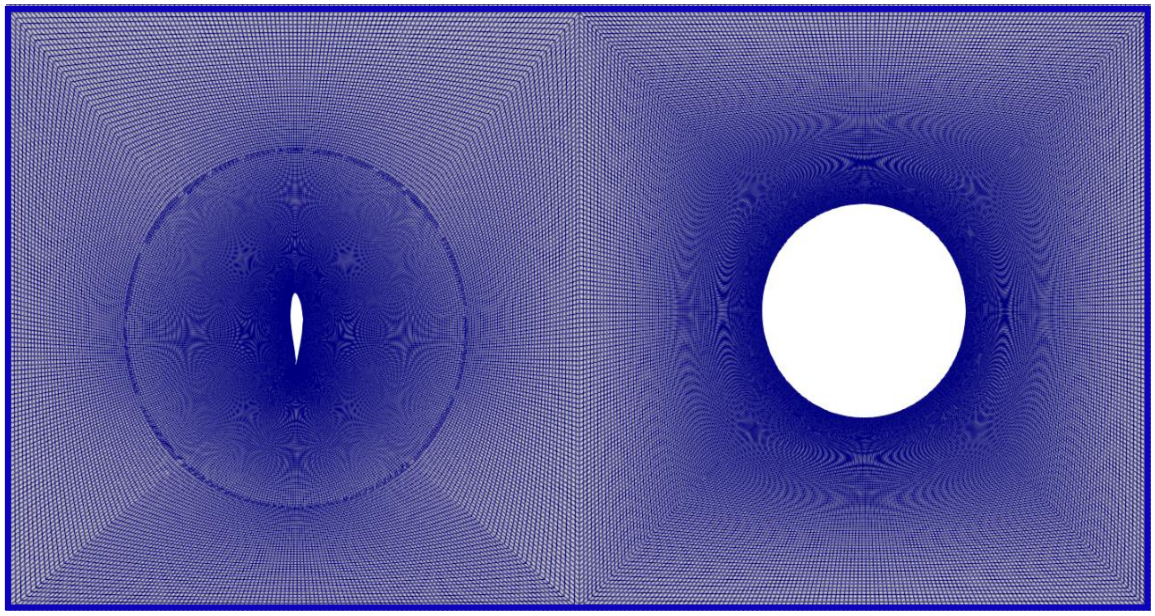

Figure 4.8: Representation of o-grid mesh for the tower and airfoil

Figures 4.8, 4.9 and 4.12 illustrate the o-grid meshes for the tower and profile for the considered setup. Mesh around the tower is divided into four blocks and meshed using the blockMesh utility in the OpenFOAM.

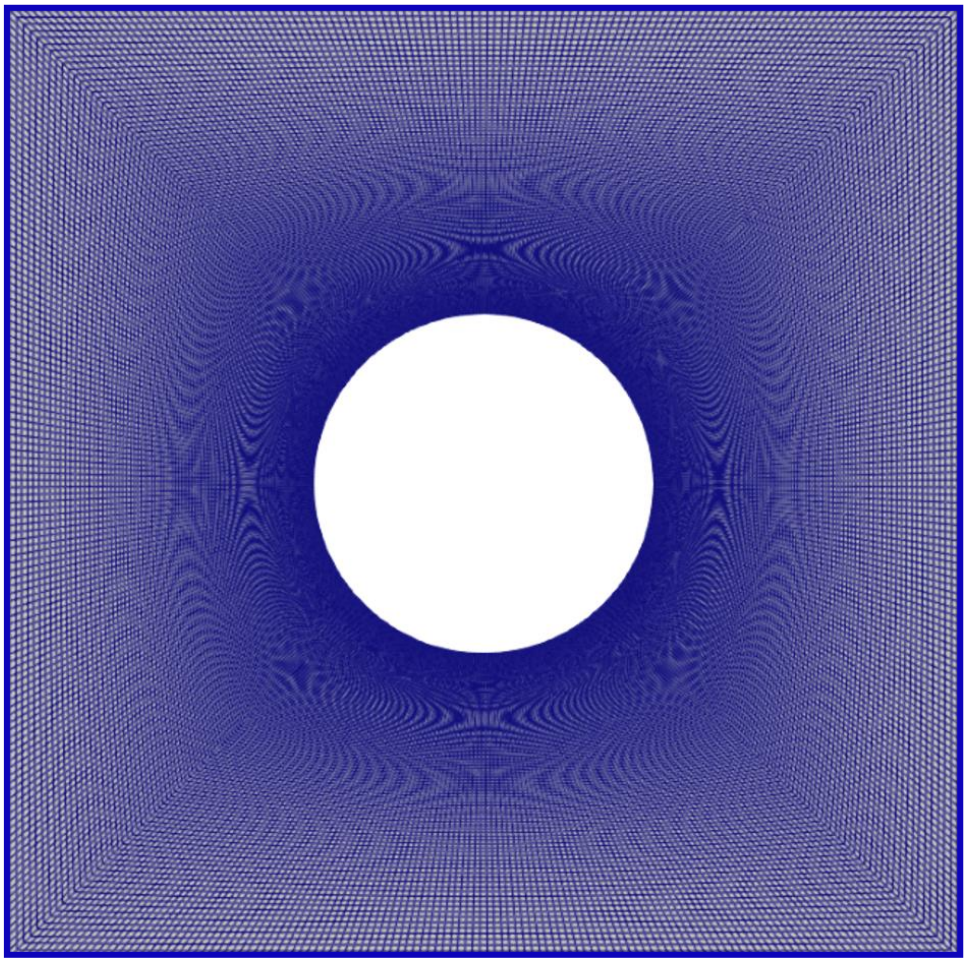

Figure 4.9: Tower Mesh

Using the optimal y^+=0.0001 near the tower and profile walls, which is calculated for the given conditions, 12 blocks are generated to represent the stationary flow domain shown in Figure 4.6. y^+decreases with distance away from the airfoil and tower walls, but it is kept optimal to get precise results in the least possible time. Different grid strategies are used for meshing including c-grid and o-grid (as shown in the figures 4.7 and 4.12), but o-grid is opted for the simulations.

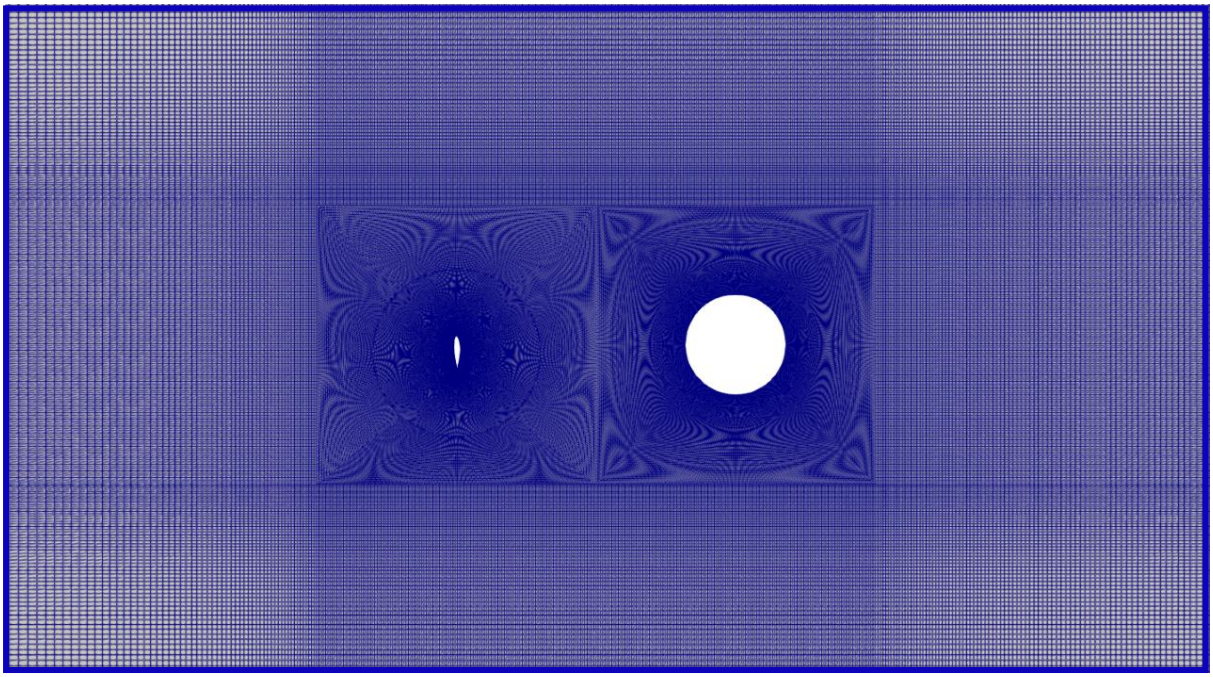

Figure 4.10: Mesh of the domain when y=0

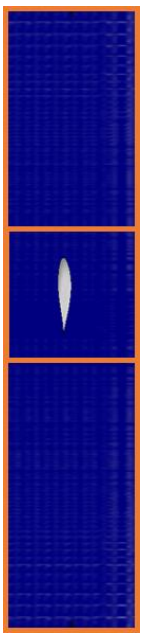

Figure 4.11: Moving grid

4.1.4. Moving Grid

The mesh around the airfoil is segmented into seven blocks: four of which surround the O-grid and three make an O-grid around the profile as shown in Figure 4.12.

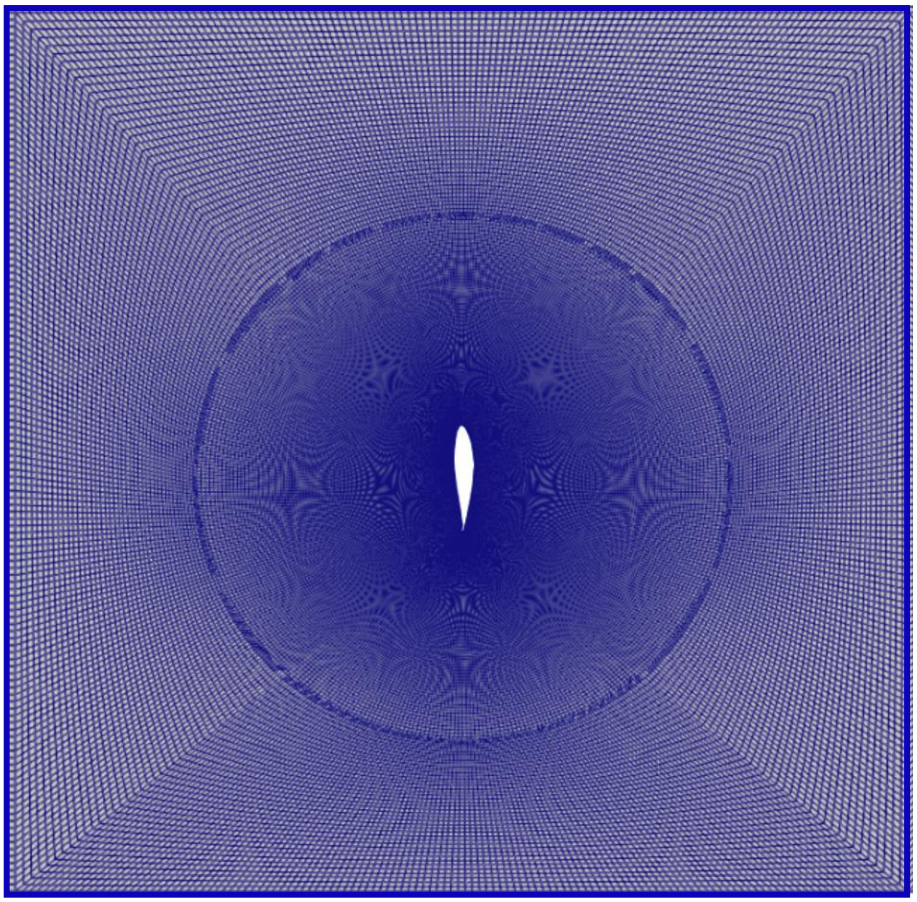

Figure 4.12: Profile Mesh

4.3 Mesh Quality Check

In order to solve the governing equations, a mesh has been created to discretize the domain. A partition into control volumes is necessary to discretize spaces, and the solution domain must be filled. The grid is then decomposed the domain geometry into a set of three-dimensional hexahedral blocks. Since the mesh is an approximate representation of the geometry, it is vital to check mesh quality and density to determine the simulation accuracy and stability. The first step is to generate the mesh information, which is checked through the CheckMesh tool available on OpenFOAM. CheckMesh is a utility that analyzes and evaluates mesh statistics and quality parameters. The information provided by CheckMesh contains mainly (1) Statistics about a number of points, faces, and cells, (2) the number of cells of each type and the number of cells to their face numbers, (3) topology checks and statistics, and (4) patch topology checks and statistics. The results are shown below:

```
"Create mesh for time = 3.14146951962

Time = 3.14146951962

Mesh stats
    points:         1198268
    internal points:  0
    faces:          2387883
    internal faces:   1190483
    cells:          596250
    faces per cell:   6.00145
    boundary patches: 15
    point zones:      3
    face zones:       14
    cell zones:       4

Overall number of cells of each type:
    hexahedra:    595414
    prisms:       0
    wedges:       0
    pyramids:     0
    tet wedges:   0
    tetrahedra:   0
    polyhedra:    836
    Breakdown of polyhedra by number of faces: faces   number of cells
                                          7   806
                                          8   30

Checking topology...
    Boundary definition OK.
    Cell to face addressing OK.
    Point usage OK.
    Upper triangular ordering OK.
    Face vertices OK.
```

```
 *Number of regions: 3
  The mesh has multiple regions which are not connected by any face.
 <<Writing region information to "3.14146951962/cellToRegion"
 <<Writing region 0 with 211500 cells to cellSet region0
 <<Writing region 1 with 63750 cells to cellSet region1
 <<Writing region 2 with 321000 cells to cellSet region2

Checking patch topology for multiply connected surfaces...
     Patch    Faces  Points    Surface      topology
airfoilSS_wall  180     362      ok    (non-closed singly connected)
airfoilPS_wall  180     362      ok    (non-closed singly connected)
airfoilTE_wall   90     182      ok    (non-closed singly connected)
mvTop_freestream_free 125 252     ok    (non-closed singly connected)
mvBottom_freestream_free 125  252  ok    (non-closed singly connected)
mvFront_empty   211500   212708   ok    (non-closed singly connected)
 mvBack_empty   211500   212708   ok    (non-closed singly connected)
freestream_free 2000    4004     ok    (non-closed singly connected)
tower_wall      500     1000     ok    (non-closed singly connected)
 front_empty  384750   386426     ok    (non-closed singly connected)
 back_empty   384750   386426     ok    (non-closed singly connected)
Interface_int_in_ami    425    852  ok   (non-closed singly connected)
Interface_int_foilIn_ami 425    852  ok   (non-closed singly connected)
Interface_int_out_ami    425    852  ok   (non-closed singly connected)
Interface_int_foilOut_ami425    852  ok   (non-closed singly connected)

Checking faceZone topology for multiply connected surfaces...
   FaceZone          Faces  Points   Surface     topology
patch_1patch_20MasterZone  0     0        ok       (empty)
patch_1patch_20SlaveZone   0     0        ok       (empty)
patch_1patch_20CutFaceZone 0     0        ok       (empty)
patch_3patch_41MasterZone  0     0        ok       (empty)
patch_3patch_41SlaveZone   0     0        ok       (empty)
patch_3patch_41CutFaceZone 0     0        ok       (empty)
patch_5patch_62MasterZone  92    284    ok (non-closed singly connected)
```

```
patch_5patch_62SlaveZone  0     0     ok        (empty)
patch_5patch_62CutFaceZone 816   1732   ok (non-closed singly connected)
                top  125   252   ok (non-closed singly connected)
          LARTopFaces  125   252   ok (non-closed singly connected)
       centralTopFaces  125   252   ok (non-closed singly connected)
    centralBottomFaces  125   252   ok (non-closed singly connected)
             bottom  125   252   ok (non-closed singly connected)

Checking basic cellZone addressing...
CellZone    Cells  Points          VolumeBoundingBox
cz_topLAR  7125  14616   195.876 (-12.57 49.8158 -0.5) (-4.19 73.19 0.5)
cz_top   11625  23688   130.944 (-12.57 34.19 -0.5) (-4.19 49.8158 0.5) cz_central  174000  349816 70.104
(-12.57 25.81 -0.5) (-4.19 34.19 0.5)
cz_bottom  18750  38052  829.62 (-12.57 -73.19 -0.5) (-4.19 25.81 0.5)

Checking geometry...
   Overall domain bounding box (-112.57 -73.19 -0.5) (205.19 73.19 0.5)
   Mesh has 2 geometric (non-empty/wedge) directions (1 1 0)
   Mesh has 2 solution (non-empty) directions (1 1 0)
   All edges aligned with or perpendicular to non-empty directions.
   Boundary openness (1.08981e-18 -1.8144e-18 9.26929e-15) OK.
   Max cell openness = 5.15671e-15 OK.
   Max aspect ratio = 188.614 OK.
   Minimum face area = 1.44181e-08. Maximum face area = 7.50368.  Face area magnitudes OK.

Min volume = 1.44181e-08. Max volume = 7.50368.  Total volume = 46506.5.
Cell volumes OK.

   Mesh non-orthogonality Max: 61.6286 average: 13.9103
   Non-orthogonality check OK.
   Face pyramids OK.
   Max skewness = 1.19131 OK.
   Coupled point location match (average 0) OK.

Mesh OK.
```

```
103
    End”
```

Once the information from the checkMesh tool is extracted using the command:

```
1 checkMesh > log.checkMesh &
```

This study uses four different mesh quality metrics to determine the mesh quality, and the mesh quality is compared to the recommended mesh quality obtainable as proposed by [1]. The main results of both meshes are listed in Table 1.

Table 4.2: Mesh Quality Metric comparison with the recommendations

Mesh Quality Metric	Value from the checkMesh tool	Maximum/ recommended
Number of cells	596,250	---
Maximum, Aspect Ratio	188.614	The ideal aspect ratio is 1
Mean, Aspect Ratio	1	The ideal aspect ratio is 1
Maximum, Non-orthogonality	61.6286	0 (ideal) and 90 (worst)
Mean, Non-orthogonality	13.9103	0 (ideal) and 90 (worst)
Maximum, Skewness	1.19131	0 (ideal) to 1 (worst).
Mean, Skewness	0	0 (ideal) to 1 (worst).

From table 4.2, it is observed that the average aspect ratio is 1.4, close to 0 (the ideal limit); the average non-orthogonality is roughly 13.9 degrees, close to 0 (the ideal limit); and the average skewness is 0, which is also consistent with the ideal range of values. Generally, the values of the main mesh quality parameters are kept within the ranges specified in the defaults. Hence, overall mesh quality is acceptable to proceed with the simulation study.

Further, two types of grids are generated: the O-type and C-type. A detailed study has been conducted to determine the appropriate grid type. O-type grid (see figures 6 and 7) is selected to proceed to the simulation, and the detailed information of the grid is presented in table 4.3.

Table 4.3: Grid study

Parameter	Value
Number of cells	596,250
Number of points	1,198, 268
y^+	< 1

4.4 Temporal Study

It is necessary to select a time step based on the mesh motion and the duration of the simulation. This choice must take into account the complexity of the geometry and the physical parameters of the setup. Profiles pass the tower between -30m and +30m in the Y-direction, affected by the changing flow surrounding it. Settings must therefore be chosen to guarantee that the turbulence model achieves stability, and the tower-profile interaction is simulated.

Table 4.4: Time step evaluation as a function of velocity variation

Case	1st investigation: Velocity variation $V_{profile}$				Simulation time	
	v_{profle}	ω	Time Step	RPM	Start	End
1	60	2	1.570796	19.09859	2.3561	3.9269
2	65	2.166667	1.449966	20.69014	2.1749	3.6249
3	70	2.33333	1.346397	22.28169	2.0195	3.3659
4	**75**	**2.5**	**1.256637**	**23.87324**	**1.8849**	**3.1415**

The time step is set according to the profile's movement (translational velocity). Next, the impact of the time step and number of intermediates within a simulation step on

simulation results has been examined. Doing so can determine the optimal parameters for studying physical factors. It was examined in a case setup with the angle of attack of the profile set at 10.53°, tower spacing of the profile h equal to 6.88 m (see table 4.3), and a tower diameter of 3 m (see table 4.3 and 4.4), where the angle of attack of the profile was set at 10° and the design speed n_{rotor} = 23.87 min^{-1}. The airfoil movement occurs in 60 steps, which correspond to the 180-time steps that were divided into each step, which implies that the azimuthal movement for this given movement is 180 degrees. Table 4.4 presents the time step study performed considering different velocity profiles and at various time steps. Hence, a time step of 1.256637s has been chosen as a base case for the simulation study.

Further to investigate the tower diameter and height variation a base time step of 1.256637s is used and the values of the variables are illustrated in Table 4.5.

Table 4.5: Time step evaluation as a function of height and tower diameter variation

2nd investigation Tower-profile spacing h/t				3rd investigation Tower diameter D/t	
4.5				2	
5.5				2.5	
6.88				3	
7.5				3.5	
Calculated parameters for Simulations				Simulation time	
v_{profle}	ω	Time Step	RPM	Start	End
75	2.5	1.256637	23.87324	1.8849	3.1415

4.5 Numerical Setup

The numerical case setup for the tower-profile interaction is presented, which is kept the same for all the investigative studies, except for changing the blockMeshDict, topoSetDict, and controlDict, which are modifed as per case requirements. All the simulations are run on high performance computational system, named as pradtl, at IAG, University of Stuttgart was utilized for running the simulations. Prandtl had 20

nodes with 2 Xeon Gold 6140 processors where 96 GB of DDR4-2666 RAM is available for each node. The OpenFOAM settings are presented to explain the numerical setup used, then the details of each setup are explained in more detail.

4.5.1 Case structure

The structure of the files in OpenFOAM cases includes an optimal set of files that are available for the simulation to be carried out, and the structure of the files can be seen in Figure 4.13. The base case setup comprise system, constant, 1.8849, Meshfactory and log folders. In the system directory, In the system directory, simulation-controlling parametric files are provided, including ControlDict, blockMeshDict, and various discretization schemes. Constant folder contains flow properties (turbulence and transport) and dynamicMeshDict files. 1.8849, a directory, contains the meshModifiers and starting conditions for all flow variables at t=1.8849s.

In the postProcessing directory, all the output files are stored once the solution has converged and the simulation is finished. In addition, the simulation was distributed to 36 subdomains using the Scotch method to speed up the processing, and this information had been passed to the system via decomposeParDict.

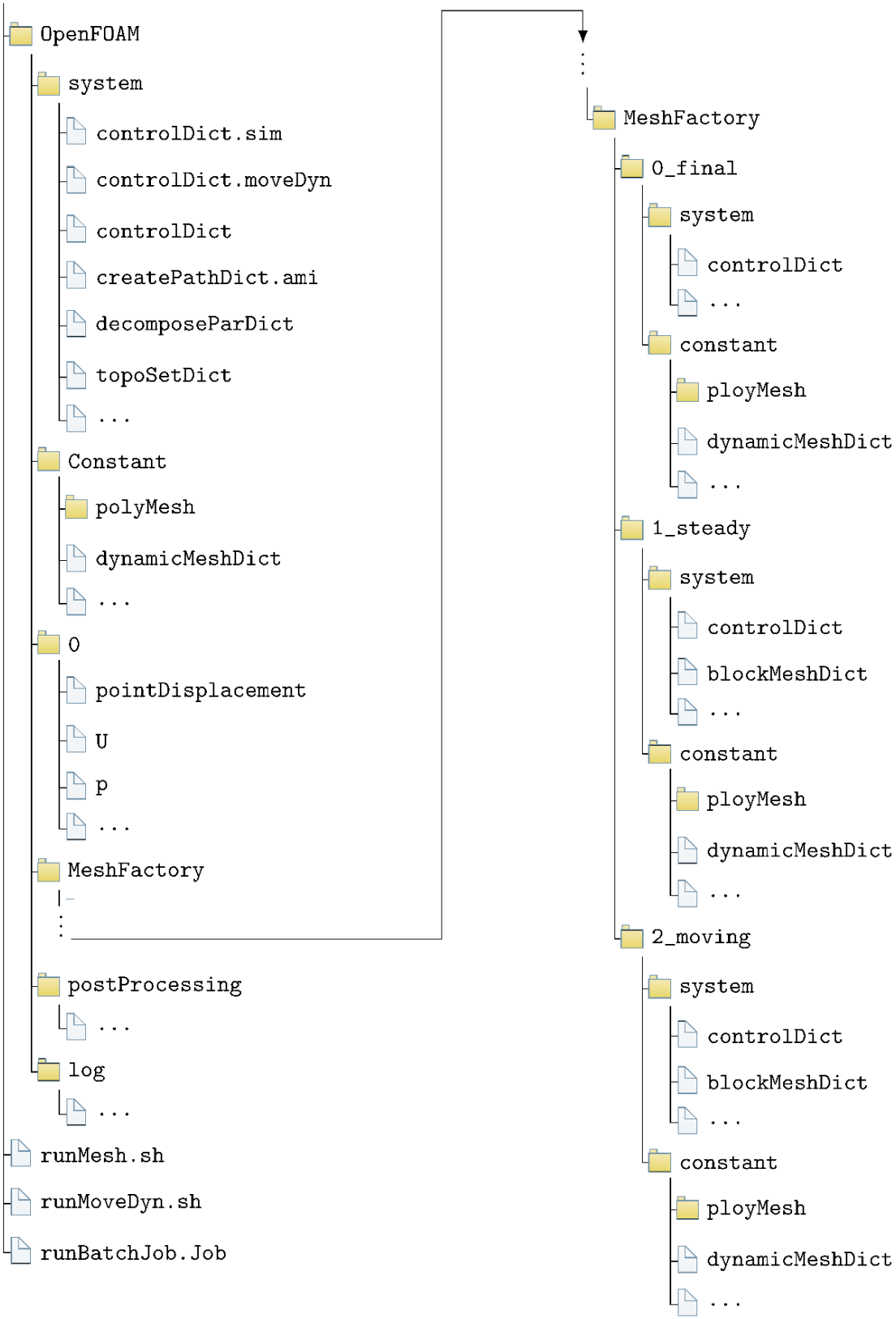

Figure 4.13: Overview of the OpenFOAM case setup directory.

4.5.2 Solver and the turbulence model

PimpleFoam (as explained in section 2.2.4), a flow solver within OpenFOAM, is used for this unsteady simulation whereas the kOmegaSST model (as discussed in section 2.2.3) has been employed to resolve the flow turbulence.

4.5.3 Numerical schemes

Table 4.6: Divergence Schemes

	Type of scheme	Variable used
	$div\ (\varphi, U)$	Gauss linear Upwind grad(U)
Turbulenc	$div\ (\varphi, k)$	Gauss upwind
	$div\ (\varphi, \varepsilon)$	Gauss upwind
	$div\ (\varphi, \omega)$	Gauss upwind
	$div\ (\varphi, nutilda)$	Gauss upwind
	$div\ (\varphi, R)$	Gauss upwind
	$div\ (R)$	Gauss linear
	$div\ ((nuEff * dev2(T(grad(u)))))$	Gauss linear

Table 4.6 and 4.7 shows that the numerical schemes for discretization are treated in the *fvSchemes* directory. During the scheme specification, all the interpolation is set to be linear type. Time schemes are backward Second order, implicit. Gradient and divergence schemes are mainly Gauss linear. Usually, adding a few limiters that ensure greater stability is sufficient. In this study, the divergence techniques have been directly replaced by Gauss upwind to eliminate this issue. It has been used for the k and epsilon flux parameters. Laplacian scheme is Unbounded, second order, and conservative. It indicates that the scheme has been adjusted to account for the mesh non-orthogonality, which frequently arises in actual meshes. The divergence schemes, as given in Table4.6, are vital for the simulations. In this study, Gauss linearUpwind, Gauss upwind and Gauss linear schemes are utilized for the divergence.

Table 4.7: Discretization Schemes

Variable	Type of scheme
Interpolation schemes	Linear
Surface normal gradient	Corrected (ψ=1)
Gradient schemes	Gauss linear
Laplacian schemes	Gauss linear corrected
Time schemes	Backward (second order implicit)

4.5.4 Mesh motion

For the mesh motion, layerAdditionRemoval method, a mesh modifier, is opted in for this research. A topoSetDict is provided in the system folder which includes the details on the limits and coordinates of the mesh. Airfoil moves between +30m and -30m in y-direction to simulate BTI. Below is code containing commands for executing the layering mechanism as illustrated in figure 4.14.

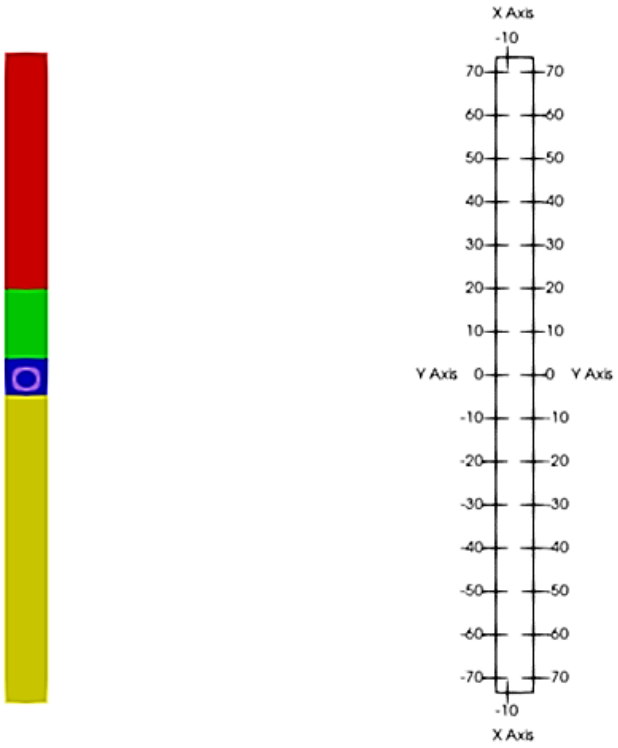

Figure 4.13: Distribution of patches on the moving mesh for layerAdditionRemoval

TopoSetDict can be reported as in Algorithm 1.

Algorithm 1 topoSetDict

```
"//#################################################
//Create cellZone Blocks
//#################################################

  //Prefix cs_cellSet cz_cellZone
  //Prefox fs faceSet fz_faceZone
  // 1. Create cellZones wich includes all moving cells
  // Create cellSet cs_movingCellsAll
  {
    name    cs_movingCells;
    type    cellSet;
    action  new;
    source  boxToCell;
    box     (-24 0 -10)(-12 130 10);
  }

  {
    name    cz_movingCells;
    type    cellZoneSet;
    action  new;
    source  setToCellZone;
    set     cs_movingCells;
  }

  // 4. Here we create a special zone to enable layer addition removal
  // create cell zone at top of domain for LAR region
  {
    name    cs_LARCells;
    type    cellSet;
    action  new;
    source  boxToCell;
```

```
32      box     (-24 130 -10)(-12 150 10);
33    }
34
35    {
36      name    cz_LARCells;
37      type    cellZoneSet;
38      action  new;
39      source  setToCellZone;
40      set     cs_LARCells;
41    }
42
43
44  //################################################
45  //Create faceZone top bottom lar
46  //################################################
47
48
49    // 2. Create fz_top
50    {
51      name    fs_top;
52      type    faceSet;
53      action  new;
54      source  patchToFace;
55      patch   top_freestream_free;
56    }
57
58    {
59      name    fz_top;
60      type    faceZoneSet;
61      action  new;
62      source  setAndNormalToFaceZone;
63      faceSet fs_top;
64      normal  (0 -1 0);
65    }
66
```

```
67
68   // 2. Create fz_bottom
69   {
70       name    fs_bottom;
71       type    faceSet;
72       action  new;
73       source  patchToFace;
74       patch   bottom_freestream_free;
75   }
76
77   {
78       name    fz_bottom;
79       type    faceZoneSet;
80       action  new;
81       source  setAndNormalToFaceZone;
82       faceSet fs_bottom;
83       normal  (0 1 0);
84   }
85   // 2. Create fz_lar ; face in between LARCells and movingCells
86
87  {
88       name    fs_lar;
89       type    faceSet;
90       action  new;
91       source  cellToFace;
92       set     cs_LARCells;
93       option  all;
94   }
95
96   {
97       name    fs_lar;
98       type    faceSet;
99       action  subset;
100      source  cellToFace;
101      set     cs_movingCells;
```

```
    option  all;
  }
  {
    name    fz_lar;
    type    faceZoneSet;
    action  new;
    source  setsToFaceZone;
    faceSet fs_lar;
    cellSet cs_movingCells;
  }"
```

4.6.5 Initial Boundary Conditions

In table 4.8, initial boundary conditions are utilized for this numerical investigation.

Table 4.8: Initial Boundary Conditions

Boundary Conditions	
Variable	Values
Ambient Temperature	288 K (15 degree Centigrade)
Ambient Presssure	10^5 Pa
Wind Velocity (u_∞)	15 m/s
Air Viscosity	1.81×10^{-5} kg/(m·s)
Air Density	1.225 kg/m^3
h/t	6.88
d/t	3
$V_{profile}$	75 m/s

5 Results and Discussion

This chapter presents the influence of physical parameters on the pressure fluctuations due to tower-profile interaction (TPI). These play a decisive role in noise emission and material fatigue due to load fluctuations on the rotor blades. The results for the three variables are presented in four configurations for each variable (case), including the dimensionless tower-profile spacing (h/t), the dimensionless tower diameter (D/t), and the profile's translation speed ($V_{Profile}$). For example, when the speed of the wind turbine varies, which implies a proportional change in the speed of the profile section, the resulting variation in the angle of attack α is compensated. Table 5.1 shows the parameters and operating conditions considered for the base case.

Table 5.1: Parameters of the base case (2.3MW Wind Turbine)

Size	Value	Description
h/t	6.88	Dimensionless distance of the t/4 point to the tower surface
D/t	3	Dimensionless tower diameter
$\boldsymbol{\alpha}$	10.53^o	Angle of attack of the profile cut relative to the direction of movement at r = 36.83 m
$\boldsymbol{\beta}$	1^o	Profile's pitch angle
$\mathbf{n_0}$	18 min^{-1}	Speed of the 3D wind turbine in the operating point to n_o
$\mathbf{v_{Profile,0}}$	75 m/s	Profile translational speed
$\mathbf{u_\infty}$	15 m/s	Wind speed

5.1. Profile-tower interaction region

5.1.1. Velocity Field

In figures 5.1 and 5.2, the velocity fields during the profile-tower interaction are plotted for six different instants of time (φ = 80°, 85°,90°,95°,100°,105°) on the plane at the maximum interaction location. As shown in Figure 5.1a, the bottom side of a tower is

where the blade approaches from, while the top side is where the blade passes the tower and moves away.

During the absence of TPI, a velocity deficit area can be observed in the vicinity of the tower immediately upwind of the blade due to the tower's presence, as illustrated in Figure 5.1 and Figure 5.2. Due to the velocity deficit, the blade's aerodynamic forces change transiently when passing through the velocity deficit region in front of the tower, a known TPI mechanism.

A profile approaching the tower at an azimuth angle of 85° can be seen in Figures 5.1b and 5.2c, where the accelerated flow can be seen on the downwind side of the profile, and decelerated flow can be seen on the upwind side of the profile. Circulation combined with leading-edge flow produces an accelerated flow near the profile's leading edge on the downwind side, which interacts with the tower. For h/t = 4.5, it results in a significantly accelerated flow on the bottom side of the tower. In contrast, the effect diminishes significantly for the same interaction when h/t increases to 7.5.

When the blade comes into alignment with the tower at φ =90°, wind flow is reduced around the profile for h/t = 4.5, as demonstrated by the lower intensity of flow asymmetry upwind and downwind. Due to the strong accelerated flow on the downwind side of the blade, the gap between the passing blade and the tower experiences an increase in flow velocity. In contrast, at h/t = 7.5, the blade and tower experience a reduced velocity field. Because the tower's position is sufficiently far from the region of high-velocity deficit near the profile, the profile extracts more energy from the oncoming wind and reduces its velocity downwind.

Immediately after passing the tower at φ =95°, the induced flow around the trailing edge of the profile interacts with the surface on the top side of the tower for h/t = 4.5. Nevertheless, this interaction is much weaker than the leading-edge interaction at φ = 85°, as the downwind acceleration of the flow toward the trailing edge is lowered. As h/t increases to 7.5, the magnitude of the tower-profile velocity field is reduced, which is similar to the interaction at φ =90°. As the translational velocity of the profile increases, it is expected that circulation around the profile will be strengthened. This is true when approaching, aligning with, and passing the tower.

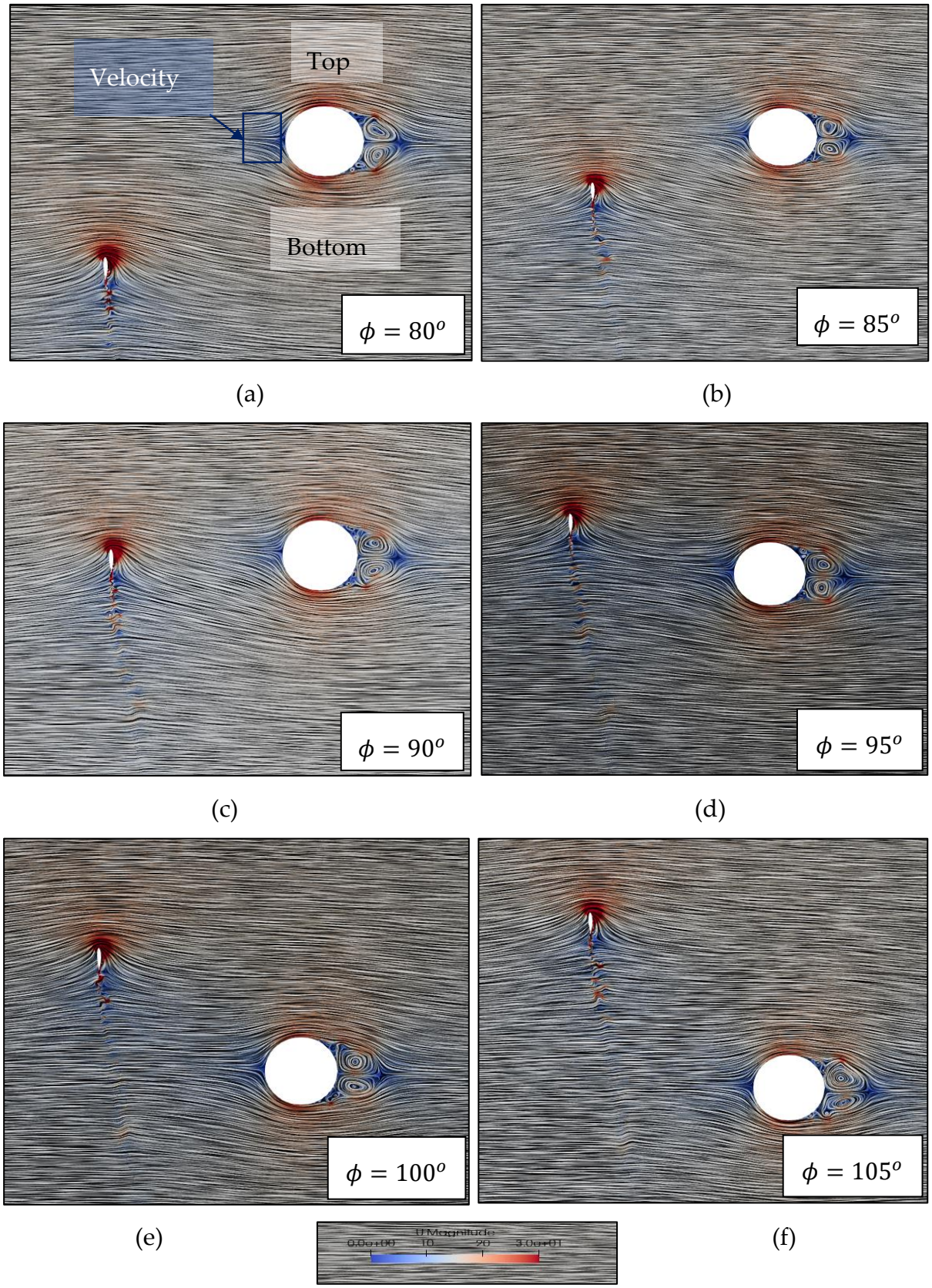

Figure 5. 1: Velocity magnitudes (y and z directions) of a 2D simulation at various azimuth angles.

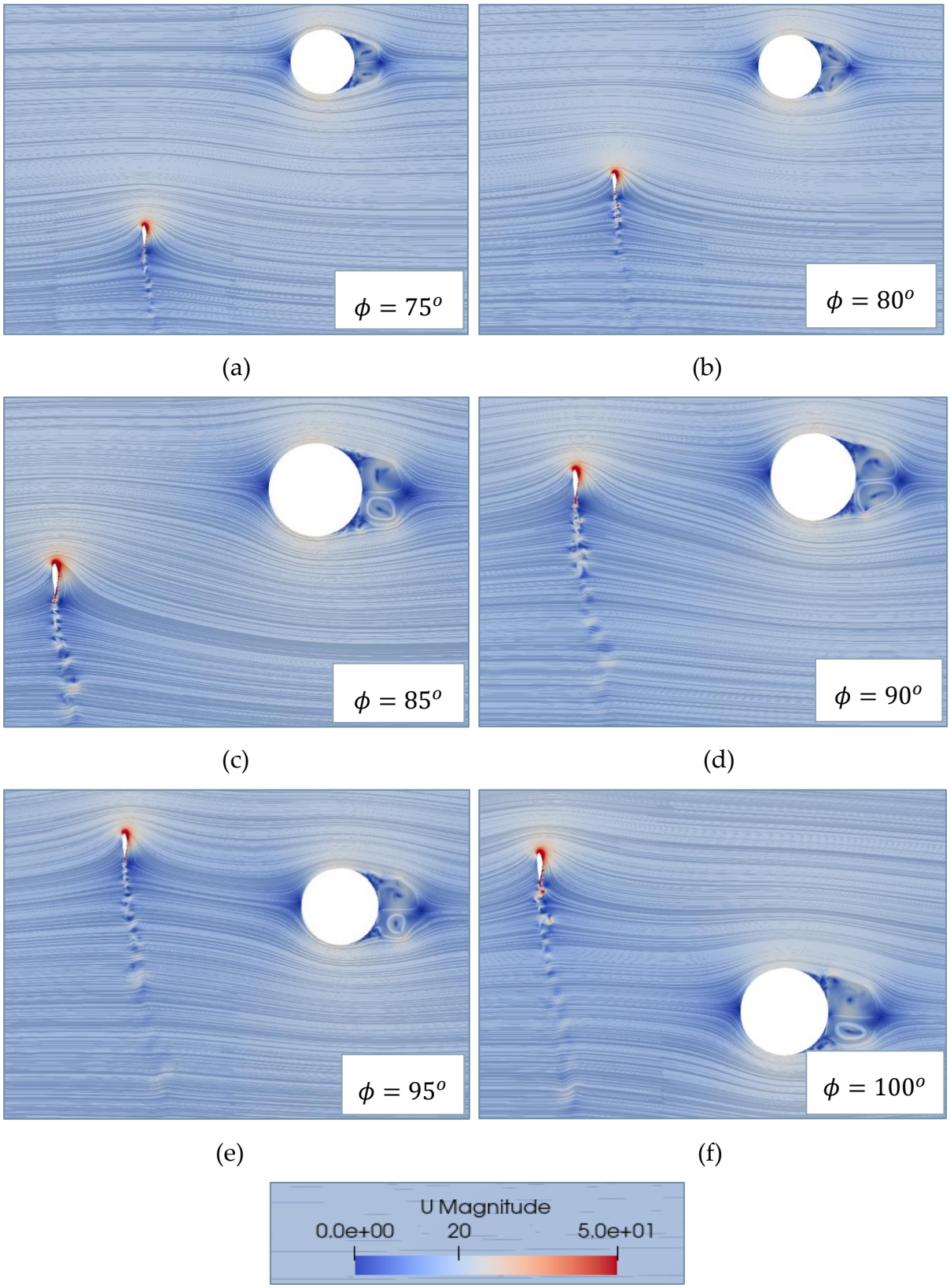

Figure 5.2: Velocity magnitudes and flow streamlines of a 2D simulation at various azimuth angles.

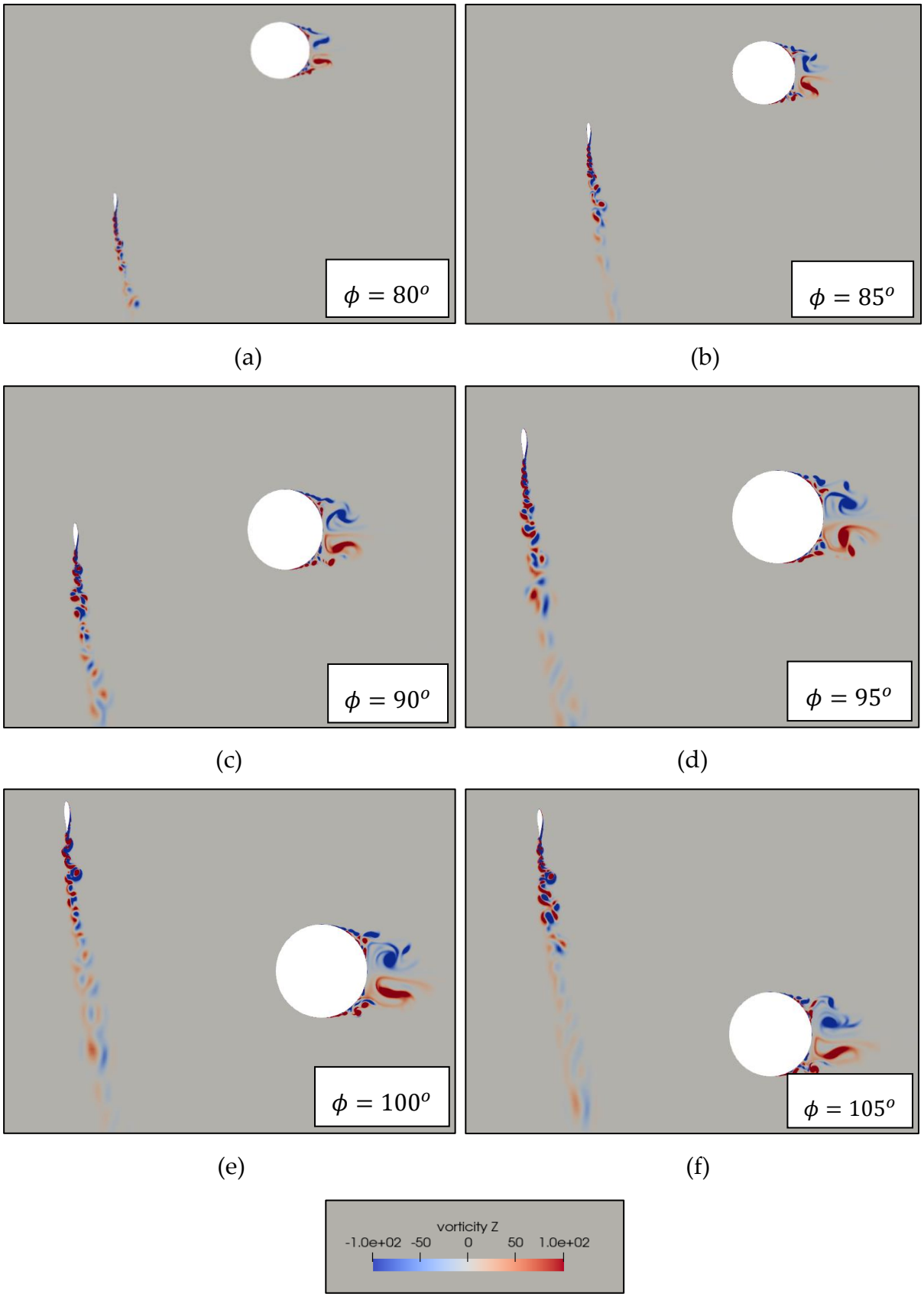

Figure 5.3: Vorticity in the z direction at various azimuth angles for 2D simulation of the base case.

5.1.2. Pressure field

Pressure fluctuations occur on the tower and the suction side of the profile due to the profile passage across the tower and the reduced inflow velocity fields, resulting in infrasonic emissions from wind turbines, as described in [11]. The aim of this study is, therefore, to quantify and qualitatively assess pressure fluctuations. Pressure curves over time are analyzed at various points on the tower and profile surfaces. Further, the results separately report the noise components emanating from the profile (pressure side, suction side, and profile as a whole) and the tower. Both the tower and suction side of the profile have in-phase acoustic components, which reinforce one another, when the profile is in alignment with the tower.

As shown in the figure 5.1, the pressure field for the profile passage is shown for six different azimuthal profile positions, including $\varphi = 70^o$, 75^o,80^o, 85^o, 90^o,95^o, and 100^o. A typical pressure distribution around an airfoil is characterized by high-pressure regions at both its leading and trailing edges. In addition, the low-pressure area is most prominent near the blade's leading edge, which, in this case, lies at approximately 30% of the chord, the thickest part of the blade. This leads to an asymmetrical force locus when the blade and tower are aligned, resulting in a decrease in force. For the nominal angle of attack of 10° (with profile's pitch angle of 1°) shown in Figure 5.4, at profile spacing h/t = 6.88, various pressure zones are generated around the profile, distinguishing between the pressure and suction sides at any profile angle.

As the profile approaches the tower at $\varphi = 75^o$,which particularly can be seen in Figure 5.4 (a), the high-pressure region at the leading edge of the profile interacts with the tower. When the profile aligns with the tower during the passage at $\varphi = 90^o$, a profile's low-pressure region (suction side) interacts with the tower for all the configurations, as illustrated in Figure 5.4 (d). The reduced pressure regions are due to the profile passing through the velocity deficit region caused by the tower's presence. Similar interaction can be seen when a profile passes by a tower and is positioned at position $\varphi = 95^o$. For lower h/t tower-profile spacings, however, the high-pressure region due to the trailing edge also interacts with the tower. Comparatively, as the tower-profile spacing increases, only the low-pressure region impacts the tower, as the high-pressure regions surrounding the blade are located far from it. When the profile is moving away from the tower, as seen in Figure 5.4(f), only the high-pressure region at the trailing edge of the profile affects the tower. Due to a higher induced velocity towards the blade tip, the profile-tower pressure interaction is more prominent there.

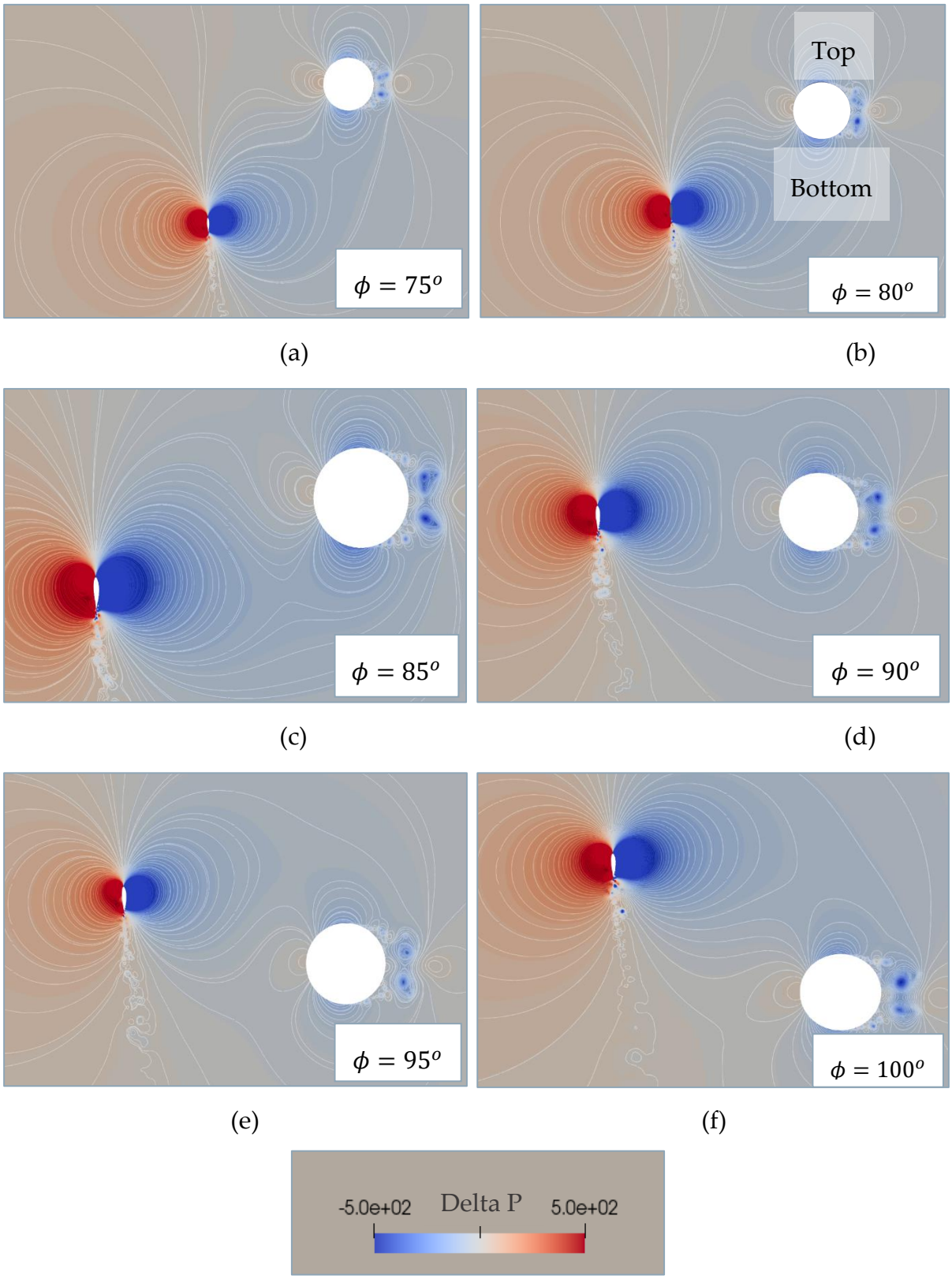

Figure 5.4: Pressure contours at various azimuth angles for 2D simulation of the base case.

5.2. Influence of tower spacing

5.2.1. Force

The lift and drag coefficients are plotted versus time for the profile and tower, as shown in Figure 5.5. The profile's drag and lift coefficients decrease slightly when the profile passes the tower. For the various H/t values, the lift and drag coefficients for the blade profile follow the same trend. However, as H/t values increase, the lift and drag coefficient curves increase for the tower. The tower's drag increases when the profile passes through the tower while its lift reduces.

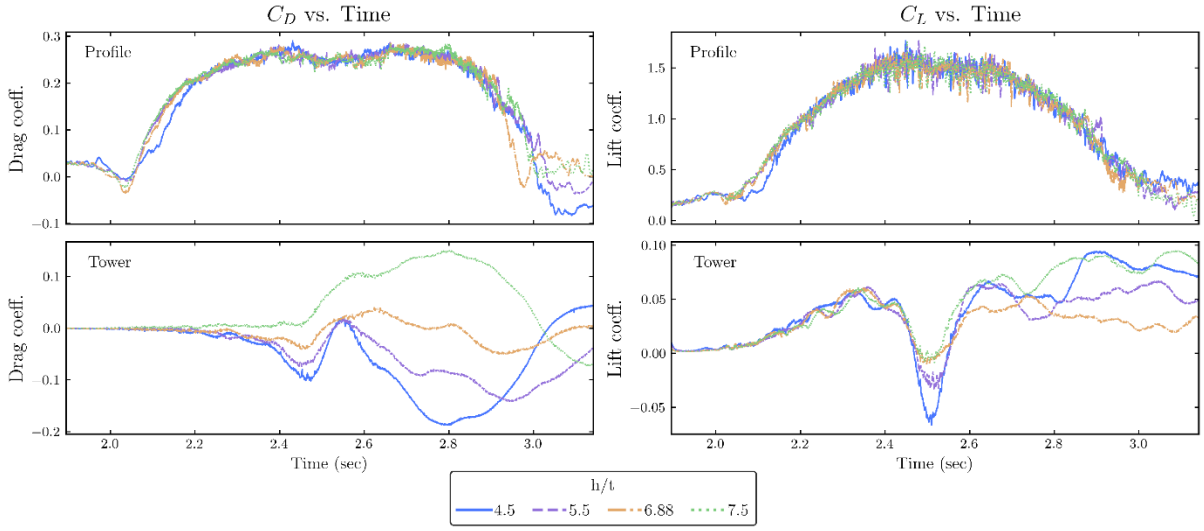

Figure 5.5: Force coefficients for four different configurations of tower-profile spacing during the 2D simulations

5.2.2. Pressure field

5.2.2.1. Tower surface

Pressure variations (Δp) on the tower's surface when the profile is in the tower's vicinity for the four different configurations of tower-profile spacing h/t for profile movement along the y-axis are plotted and compared in Figure 5.6. Tower-profile spacing is indicated in a dimensionless manner, the distance from the tower's surface to the t/4 point on the chord line. Four cases (as shown in Table 5.2) are simulated for dimensionless tower-profile spacing, h/t, considering that the dimensionless tower diameter, profile velocity, and the profile's pitch angle are taken as 3m, 75 m/s, and 1°, respectively (see Table 5.1).

According to Curle's formulation, the acoustic pressure emanating from a surface is determined by the rate at which the force acting on it changes. Based on the computed acoustic pressure curves, it is evident that the profile component dominates the tower components in all directions and this, therefore, determines the overall shape of the acoustic pressure waveform. Both the tower and suction side of the profile have in-

phase acoustic components, which reinforce one another, when the profile is in alignment with the tower. In all configurations, the acoustic pressure waves are similar except when the profile crosses the tower, where a sharp decrease in the pressure can be observed and the pressure variation is reduced for wider tower-profile spacing.

Table 5.2: First Variable: Dimensionless tower spacing

	Case 1	Case 2	Case 3 (Base)	Case 4
h/t	4.5	5.5	6.88	7.5

During the approach of the blade to the tower, a pressure drop occurs on the tower's bottom side, resulting from the low-pressure region on the suction side of the profile, depicted in Figure 5.4(b). When comparing pressure curves for different tower-profile spacings, the pressure decrease is maximal at the shortest tower-profile spacing h/t of 4.5, which occurs at the same location. Moreover, for h/t = 4.5, a weak area of pressure increase can be observed on the tower, which can be attributed to the high-pressure region around the leading edge of the blade interfering with the tower, as appears when φ = 85° in Figure 5.4(c). When the profile aligns with the tower at φ = 90°, the tower experiences the highest pressure drop for the shortest tower-profile distances, as shown in Figure 5.4(d). At h/t = 7.5, the TPI effect is also similar to what is seen at 85°, showing a slight pressure reduction.

At φ = 95°, when the profile moves away from the tower, a low-pressure region on the suction side of the profile for all the h/t cases primarily affects the top side of the tower. At φ = 90° (y=0), there is a sharp pressure increase due to high pressure around the blade's trailing edge interacting with the tower, as shown in Figure 5.6.

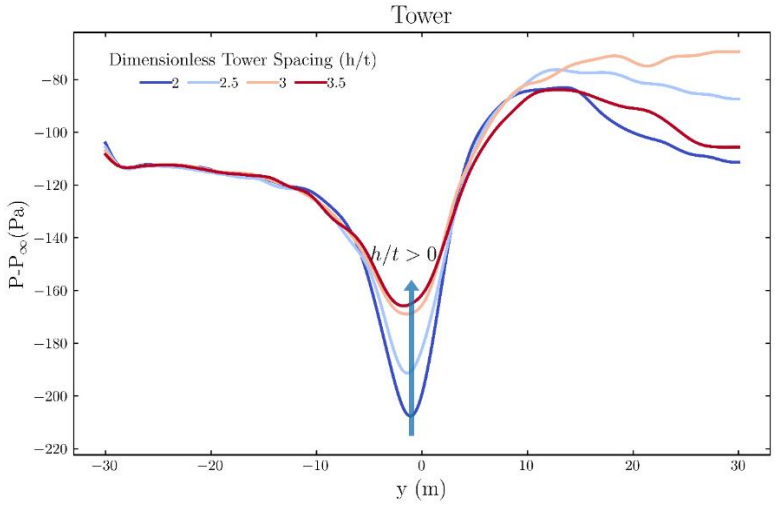

Figure 5.6: Pressure variations at the tower surface for four different configurations of tower-profile spacing.

5.2.2.2. Airfoil surface

Figure 5.7 shows the Δp amplitude plotted for the suction and pressure sides of the profile during the profile passage (y-direction). The pressure curves for all configurations (h/t) are almost identical with slight pressure fluctuations when the profile passes the tower.

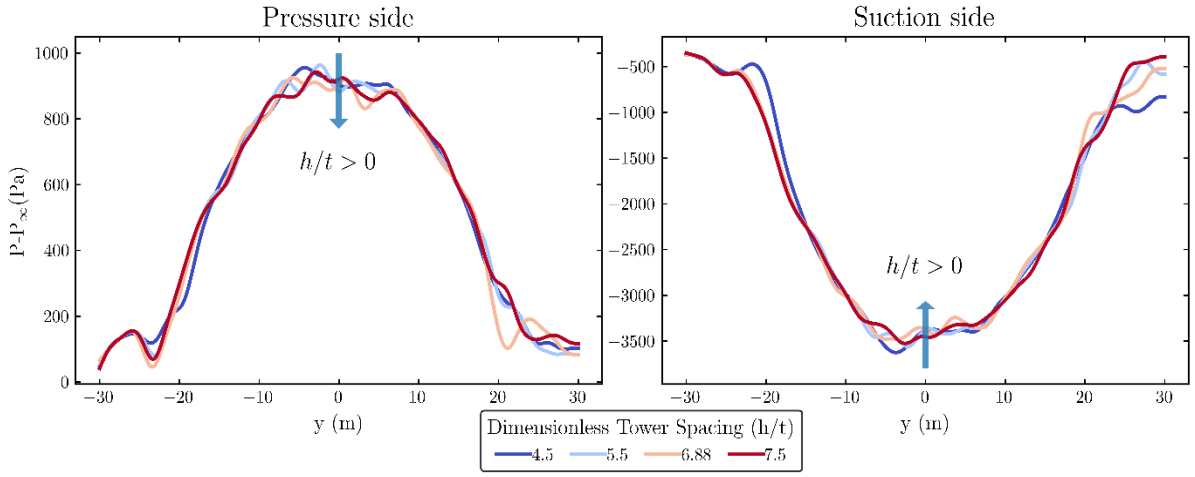

Figure 5.7: Pressure variation on the profile's surface for four distinct tower-profile (h/t) spacing configurations.

On the suction side, pressure drops as the profile approaches and aligns with the tower at 90°; pressure increases as the profile moves away from the tower. Contrarily, on the pressure side, pressure variation increases when the profile approaches and aligns with the tower at y=0 then drops as it moves away. TPI affects the surface pressure on the blade around φ = 90°, with the pattern being consistent in all cases. ΔP peaks at approximately φ = 90° when the blade and tower are aligned. During TPI, the suction side experiences a positive change in pressure, indicating a weaker low-pressure area. In contrast, the pressure side shows a negative change, indicating a weaker high-pressure area. As shown in Figure 5.8, the profile as a whole exhibits reduced lift during TPI in all cases.

Figure 5.8 illustrates the pressure distribution on the surface of the profile as it passes around the tower at a pitch angle of 1°. For four different configurations of tower-profile spacing, pressure distribution plots are presented to demonstrate the changes around the profile at different azimuthal positions (60°, 90°, 120°, and 150°). Pressure on the blade is defined by Equation 5.1 as C_p.

$$C_p = \frac{P - P_\infty}{\frac{1}{2}\rho_\infty {u_\infty}^2} \tag{5.1}$$

Where P_∞, ρ_∞ and u_∞ are the freestream fluid's static pressure, density, and velocity. TPI reduces airflow and lift around the blade for a short duration for all configurations, peaking at φ = 90°. On the suction side of the blade, the effect is more prominent, particularly near the leading edge, and weaker toward the trailing edge. TPI effects on blades are significantly reduced when the tower-profile distance is increased from 4.5

to 7.5, as seen in Figure 5.8. The pressure distribution curve of the suction side of the profile is interestingly characterized by spikes from the trailing edge to the leading edge, which is attributed to the blade stalling on the inner part of the blade due to the high angle of attack, α = 10.5°. Furthermore, when the profile aligns with the tower at φ = 90°, the pressure curve on the suction side is less spikey for 0.2>x/c >0.1.

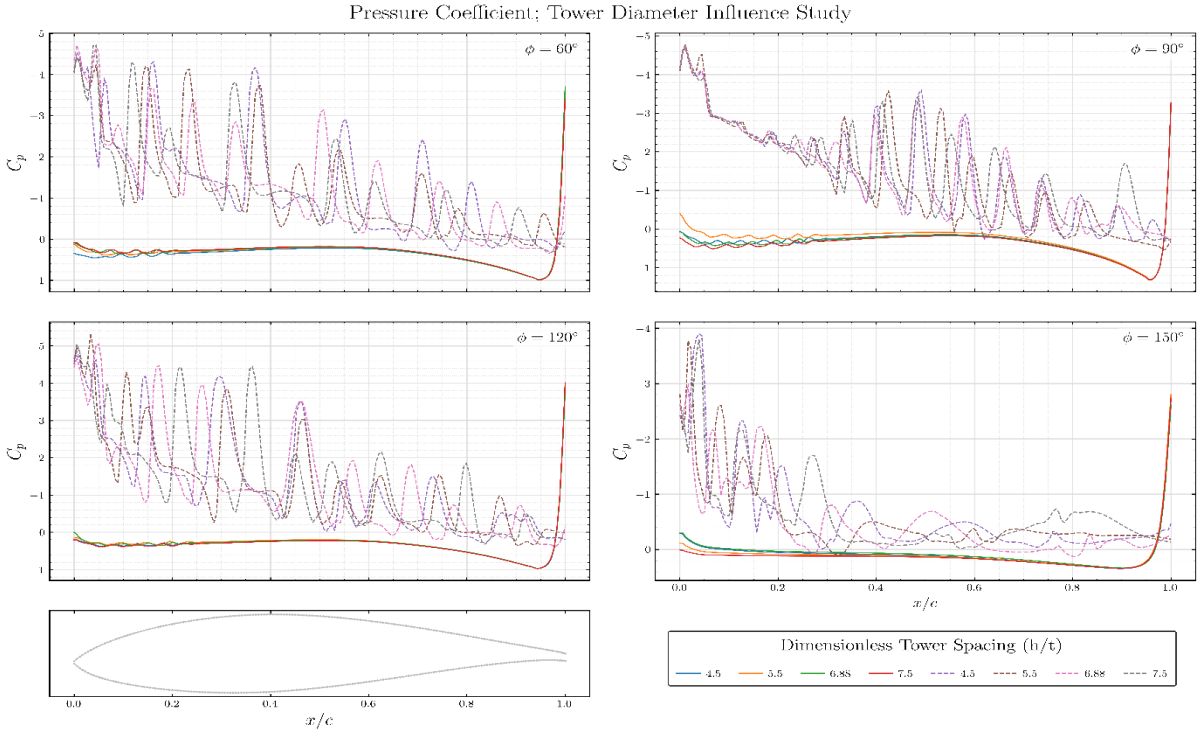

Figure 5.8: Pressure distribution around the profile at various azimuth angles for four different configurations of tower-profile spacing.

5.2.2.3. Trends

As shown in Figure 5.9, the pressure slope is influenced by tower-profile spacing: pressure variation increases as tower-profile spacing decreases. Pressure variations on the tower surface are highly sensitive to the parameter h/t, which decreases with increasing tower-profile spacing. Mathematically, the variable h/t is inversely proportional to Δp. For higher h/t values, the effect on the pressure fluctuation becomes negligible since the influence of the flow fields on the tower and profile is minimal.

As h/t increases, the profile size across the rotor radius shrinks after the minimum of the corresponding pressure curves until it no longer accounts for the most significant value in the interval under consideration. Increasing profile-tower spacing, the high-pressure region is moved further from the tower, allowing only the low-pressure region on the suction side to interact with it. For h/t = 4.5, there is a big gap in the Δp values for the profile and tower, which decreases with increasing tower-profile spacing. The pressure fluctuations on the profile surfaces have about the same order

of magnitude for the different tower-profile distances. When pressure variations are considered, the tower is more severely impacted than the profile.

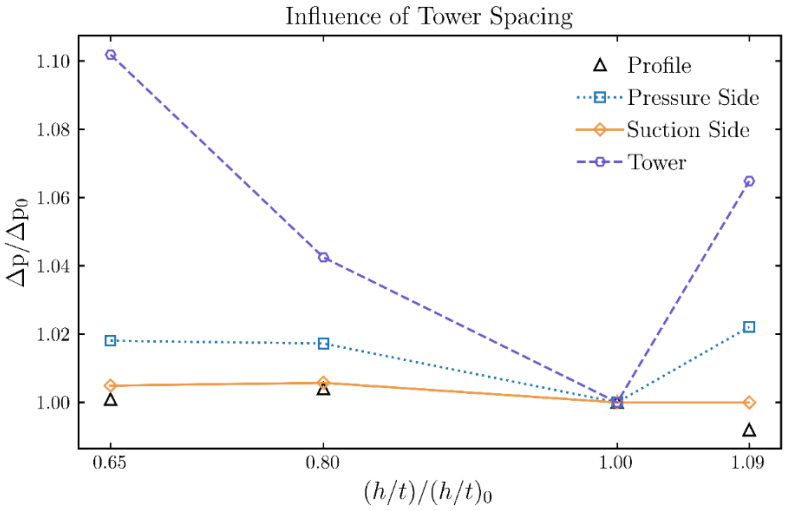

Figure 5.9: Influence of dimensionless tower-profile spacing on tower-profile interactions

5.2.3. Acoustics

Figure 5.10a shows the periodic pressure curves for four different dimensionless tower-profile distances to investigate the effect of the tower-profile distance on the shape of the pressure fluctuations. When a profile passes the tower, three pulses occur over one rotation (one for the tower, second for the suction side, and third for the pressure side of the profile), indicating the acoustic pressure due to the TPI. The pressure curve for the tower is characterized by two pulses, first a strong negative pulse, then a weak positive pulse. When the thrust is reduced to its minimum (when the profile moves away), the negative peak appears, while the positive peak appears once the thrust has been restored to its steady state (when the profile moves away). The peaks in the profile and tower pressure waveforms are in-phase, amplifying the amplitude. Based on measurements of operational wind turbines, the highly impulsive noise generated by TPI is consistent with that reported in [45].

Additionally, the wave shape matches that of Doolan et al. [15], which only considered profile noise. The results indicate that a velocity deficit is the primary cause of the profile's TPI effect. The tower contributes significantly to the TPI noise, as illustrated in Figure 5.10a, which implies that the noise is not solely generated by the profile as is commonly assumed. Profile pressure peaks around 20 times that of tower pressure at its highest and around 16 times that at its lowest. Increasing the tower-profile distance reduces the magnitude of tower pressure, profile pressure, and the overall pressure between the tower and profile, as shown in Figure 5.10a. Because of this, the interaction weakens as the tower-profile distance is widened, as discussed in Section 5.3.1.

Figure 5.10b presents discrete Fourier transforms for four differing tower-profile distances to evaluate the influence of tower-profile distance on acoustic pressure fluctuations. The amplitude of the higher harmonic frequencies is normalized to the fundamental frequency (A1) for comparison. As tower-profile spacing increases, the noise spectra become more noticeable as the overall magnitude and the relative significance of harmonics are decreased. It is due to the reduced overall pressure variation for larger tower-profile spacing values.

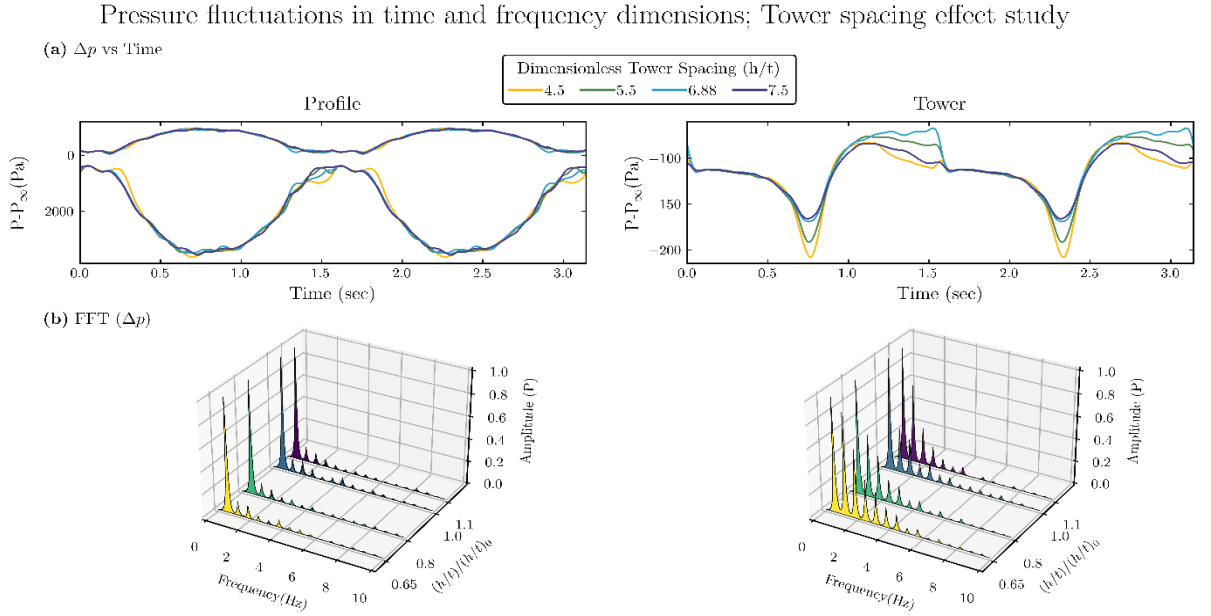

Figure 5.10: Discrete Fourier transform of the periodic pressure curve as a function of the dimensionless tower-profile spacing h/t

5.3. Influence of tower diameter

5.3.1. Force

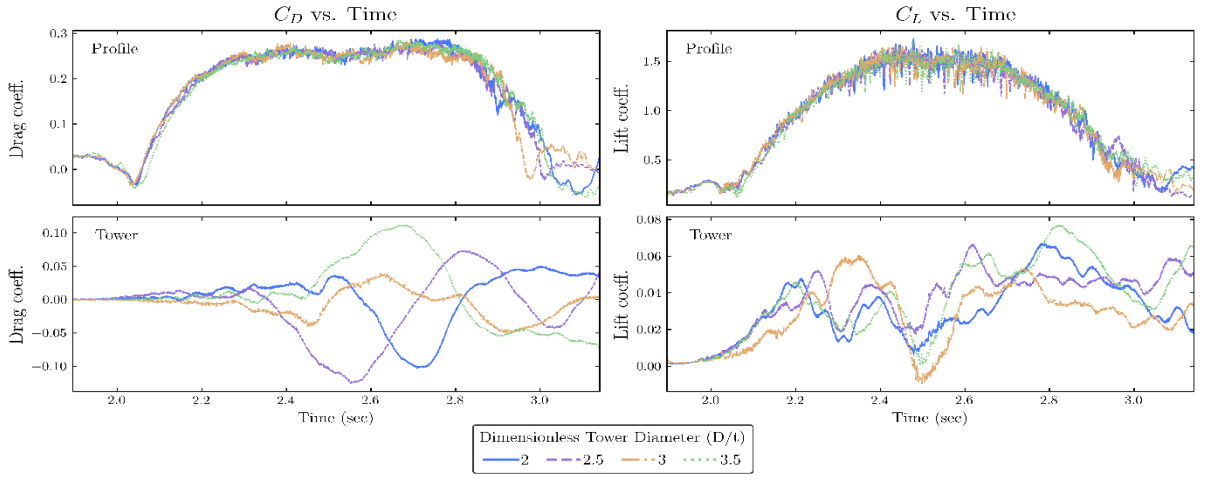

Figure 5.11: Profile and tower lift and drag coefficients for four different tower diameters during the 2D simulations

Figure 5.5 illustrates the lift and drag coefficients of the profile and tower over time. Upon passing the tower, the profile's drag and lift coefficients decrease slightly. Regardless of the tower diameter, the lift and drag coefficients for the blade profile follow the same trend. In contrast, as the tower diameter increases, the tower's lift and drag coefficient curves also increase. As the profile passes through the tower, drag increases while the tower's lift is reduced.

5.3.2. Pressure Field

5.3.2.1. Tower surface

In Figure 5.12, pressure variations on the tower's surface are plotted for four different tower diameters D/t along the y-axis when the profile is in the vicinity of the tower. The tower diameter is indicated in a dimensionless manner, the distance from the tower's surface to the t/4 point on the chord line. Simulations are carried out for four dimensionless tower diameters, D/t (as shown in Table 5.3), taking the dimensionless tower-profile distance, speed of the profile, and a pitch angle of the profile as 6.88, 75 m/s, and 1°, respectively (see Table 5.1).

Table 5.3: Second Variable: Dimensionless tower diameter

	Case 1	**Case 2**	**Case 3 (Base)**	**Case 4**
D/t	2	2.5	3	3.5

As can be observed from the computed acoustic pressure curves, the profile component dominates the tower component in all directions, determining the overall shape of the acoustic pressure waveform. As the profile is aligned with the tower, both the tower and the profile's suction side exhibit in-phase acoustic pressure components that reinforce one another. Acoustic pressure waves in all configurations are similar except when the profile crosses the tower, where there is a sharp decrease in pressure, and pressure variation decreases as the tower diameter increases.

When the profile is approaching the tower, a pressure drop occurs on the bottom side, resulting from the decreased pressure region on the suction side of the profile. Compared to other tower diameters, the pressure decrease is minimal at the lowest tower diameter, D/t =2, which takes place at y=0 when the profile aligns with the tower. Additionally, for smaller D/t values, the tower surface pressure decreases less, which can be attributed to the change in the tower-profile distance h/t. When the dimensionless tower diameter is taken as 3, and the profile aligns with the tower at y=0, the tower experiences the highest pressure drop of around 170 pa, as shown in

Figure 5.50. When D/t = 2 and 3.5, a slight reduction in pressure is present unless the blade is aligned with the tower, followed by an increase in pressure. At φ = 95°, a high-pressure region surrounds the trailing edge of the profile for all D/t cases, which causes an increase in pressure on the tower's top side. The pressure curve for D/t=2.5 is inclined to higher y values, indicating that the pressure increase is significant and more prolonged in this case.

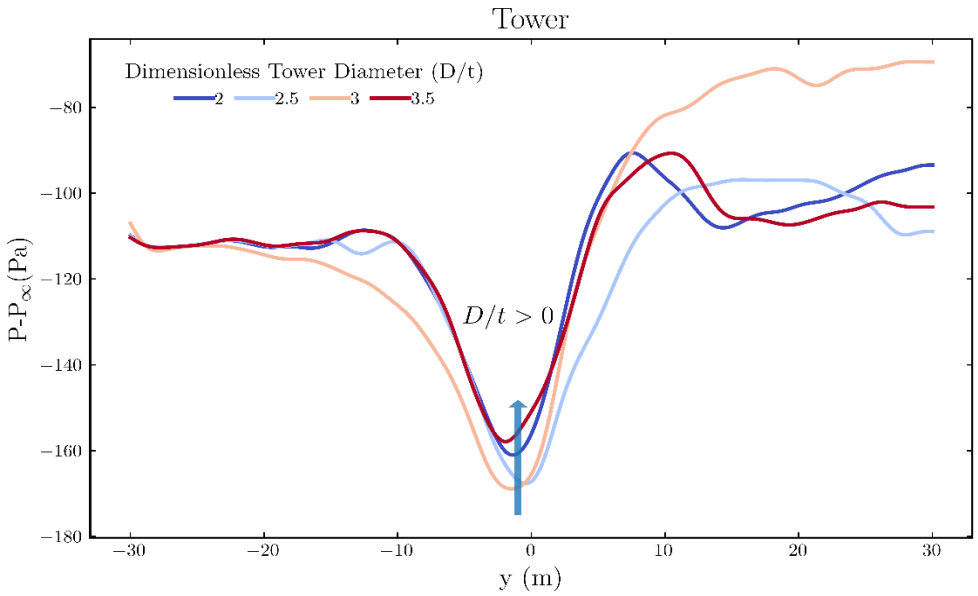

Figure 5.12: Pressure variations at the tower surface for four different configurations of dimensionless tower diameter

5.3.2.2. Profile surface

For four dimensionless tower diameters, Figure 5.13 illustrates the pressure variation on the suction and pressure sides of the profile when it passes the tower (y-direction). In all configurations of D/t, the pressure curves exhibit similar characteristics with slight pressure fluctuations when the profile is aligned with the tower.

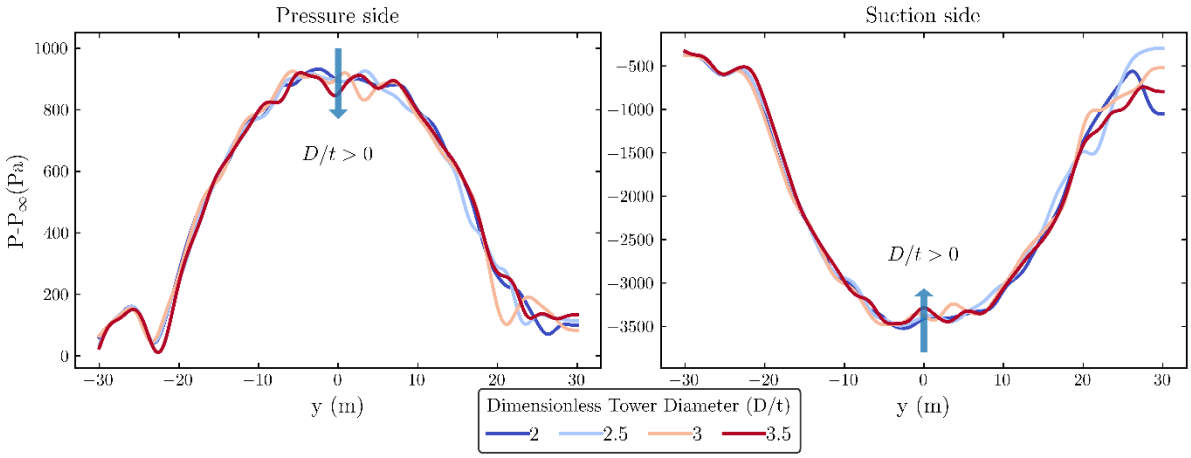

Figure 5.13: Profile pressure variation for four distinct dimensionless tower diameter configurations

As the profile approaches the tower, the suction pressure drops, and the upwind side pressure increases; as the profile moves away from the tower, the suction pressure decreases, and the upwind side pressure increases unless the profile has reached its normal thrust. When the blade and tower are in line, TPI impacts the profile surface pressure, which peaks around y=0, exhibiting the same pattern for all configurations of tower diameters. During TPI, the suction side experiences a positive change in pressure, indicating a weaker low-pressure area. In contrast, the pressure side shows a negative change, indicating a weaker high-pressure area. As shown in Figure 5.13, the profile as a whole exhibits reduced lift during TPI in all cases.

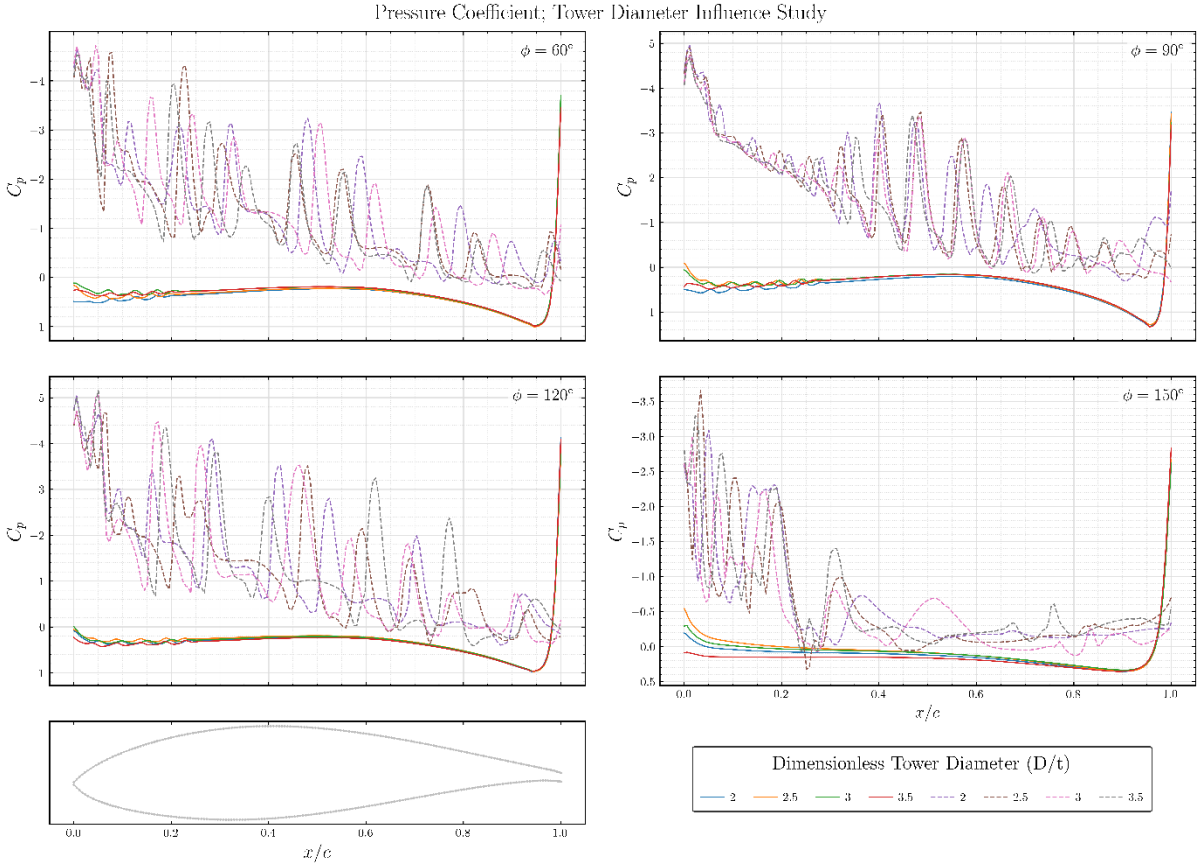

Figure 5.14: Pressure coefficients at various azimuth angles for four different configurations of dimensionless tower diameter

A pressure distribution of the profile is presented in Figure 5.14 as it passes around the tower at a pitch angle of one degree. The profile's pressure distribution plots are analyzed and compared for four different tower diameters to demonstrate how the pressure varies at different azimuthal angles (60°, 90°, 120°, and 150°). For all the cases, airflow and blade lift are reduced during the tower-profile interaction for a short duration, which peaks at y=0. Specifically, the effect is more pronounced near the blade's leading edge and less prominent toward the blade's trailing edge on the suction side of the profile. TPI effects on blades are slightly reduced when the tower diameter is increased from 2 to 3.5, as seen in Figure 5.14. Interestingly, spikes can be seen on the pressure distribution curve along the trailing edge of the profile due to stalling

occurring at the bottom of the blade due to its high angle of attack, $\alpha = 10°$. The profile alignment with the tower at 90° produces a less spikey pressure curve on the suction side for 0.2>x/c >0.1, which is attributed to TPI. A similar pattern can be seen on the suction side of the pressure curve when 1>x/c >0.4 is applied at an angle of 150°.

5.3.2.3. Trend

Figure 5.16 shows trends in pressure fluctuations as a function of a dimensionless tower diameter, where the respective base values normalize the tower diameter and each pressure value. As the tower diameter increases, the distance between the tower and the profile h/t decreases. The pressure fluctuations on the profile exhibit a nonlinear rise with a low gradient as the tower diameter increases. Similarly, tower surface pressure variations are highly sensitive to D/t, which fluctuates slightly more as the tower diameter increases. Contrary to the tower, however, the changes are significantly lower on the profile's surface, so no clear patterns of pressure fluctuations due to variation in tower diameter can be detected on the profile surface.

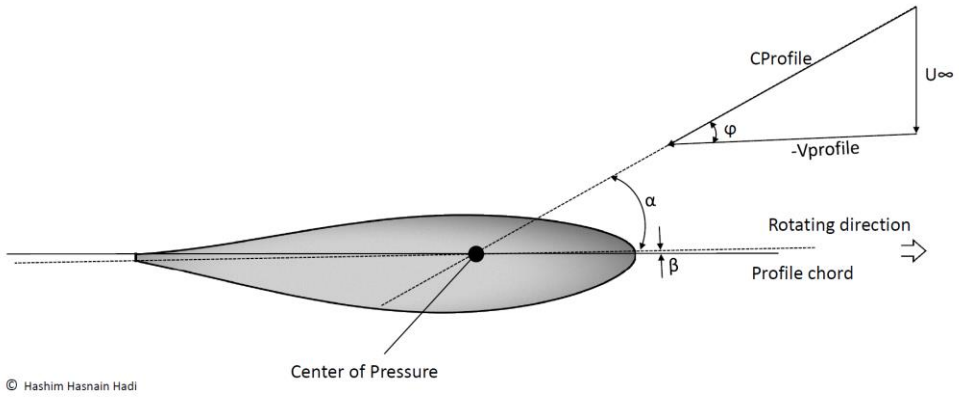

Figure 5.15: Pitch angle and angle of attack of the profile as a function of the translation speed $V_{profile}$

The strong dependence on Δp and D/t for the tower and the low dependency on D/t for the profile can be explained by a congestion effect in front of the tower. This causes the increase in the pressure variation Δp on the profile. Assumedly, the negative pressure area on the profile suction side has no relevant dependence on the tower diameter if the tower-profile spacing h/t is kept constant, however h/t varies in this study due to the variation in the tower diameter. For different tower diameters, the pressure fluctuations on the profile surfaces are about the same order of magnitude. As can be observed, pressure variations affect the tower more than the profile. Increasing the D/t value by 17% results in approximately 4% variation in tower surface pressure and around a 2% variation in profile surface pressure, as illustrated in Figure 5.16.

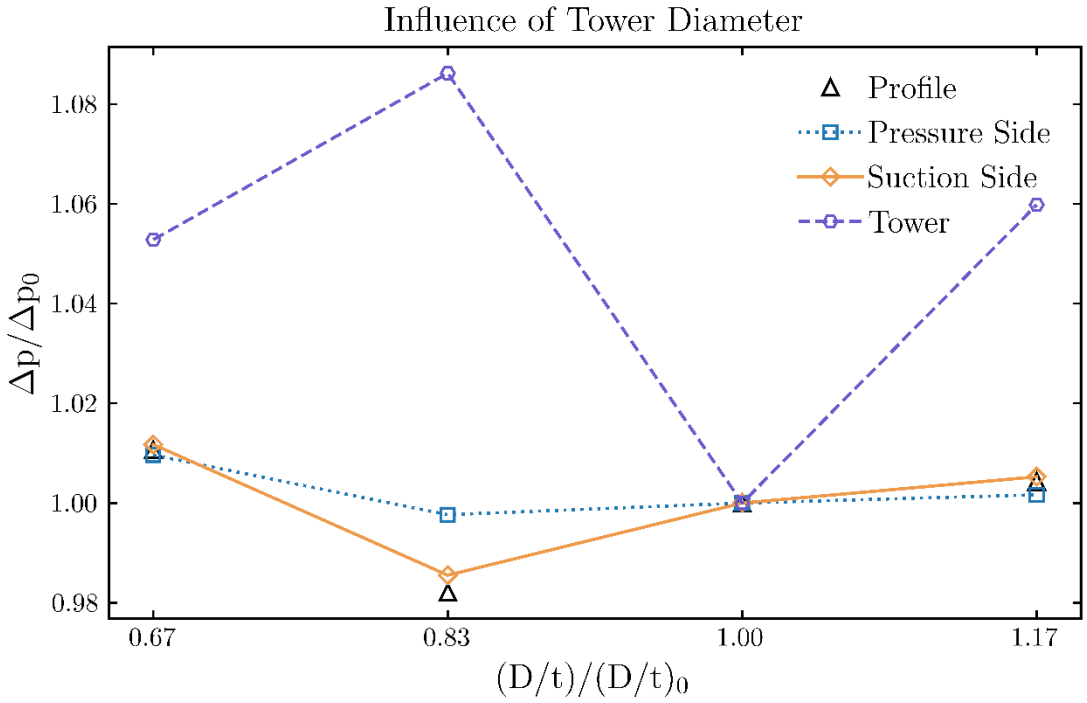

Figure 5.16: Influence of dimensionless tower diameter on tower-profile interactions.

5.3.3. Acoustics

Figure 5.17a illustrates the periodic pressure curves for four different dimensionless tower diameters for two profile passages to analyze how tower diameter affects pressure fluctuations. For each profile passage, three waveforms are generated over time: first for the tower, second for the suction side, and third for the pressure side of the profile. It is evident from the tower's pressure curve that there are two strong but opposite peaks. The negative peak appears when the thrust is reduced to its minimum (i.e., the profile is approaching), while the positive peak appears when the thrust is restored to its steady state (i.e., the profile is moving away). The peaks are in phase in both the profile and tower pressure waveforms, thereby amplifying the amplitude. TPI is responsible for the highly impulsive noise generated by wind turbines, which is described in section 5.3.2.

The pressure curves, in this case, exhibit similar variations to those observed with varying tower-profile spacings h/t, which can be attributed to the variation in tower-profile distances due to varying tower diameters. This study confirms that the profile and the tower contribute significantly to the noise associated with TPI. When the tower diameter is increased from 2 to 3.5 meters, the peak pressure varies by around 25%. Profile pressure peaks around 20 times that of tower pressure at its highest and lowest. Mathematically, increasing the tower diameter decreases the tower profile spacing but increases the tower's surface area for the pressure interaction between the tower and profile, thus, resulting in increased pressure fluctuations. Consequently, the

magnitude of surface pressures on towers and profiles appears to vary inconsistently contrary to the tower-profile distance variation as discussed in the previous section.

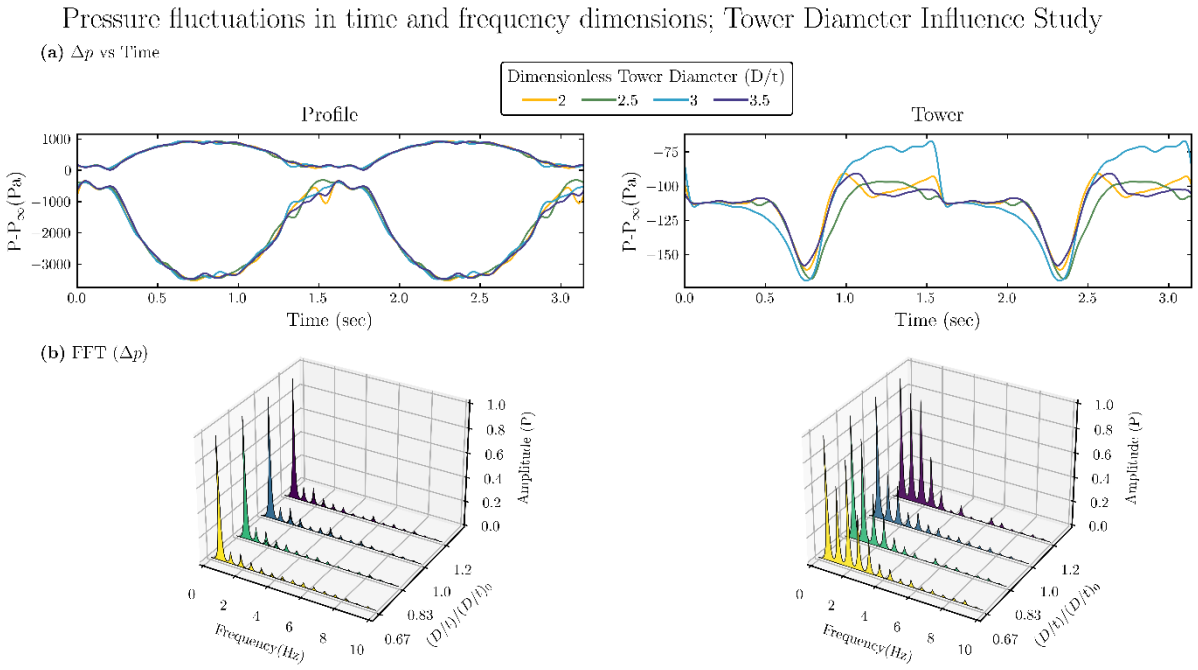

Figure 5.17: (a) Pressure variation, and (b) Fast Fourier Transform for various dimensionless tower diameters are presented.

In Figure 5.17b, discrete Fourier transforms are presented for four different tower-profile distances in order to evaluate the effect of tower-profile distance on the fluctuations in acoustic pressure. With variation in tower diameter, the discrete Fourier transform only shows minor changes for the profile, but notable changes for the tower. When the diameter of the tower increases, the noise spectrum becomes more noticeable as the magnitude and significance of harmonics increase, potentially reaching audible levels. It is due to the increased overall pressure variation for thicker tower diameters caused by the larger surface area of the tower, contributing to congestion. With D/t=3.5, f3 = 1.8 Hz is the strongest 3rd harmonic for the tower. For D/t=2, the highest number of prominent harmonics appears, with f5 = 3.0 Hz as its fifth harmonic. The harmonics with the highest amplitudes are most concerning when a frequency is increased.

5.4. Influence of translational velocity of the profile

5.4.1. Force

The lift and drag coefficients of the profile and tower are shown in Figure 5.5 over time. Upon passing the tower, the profile's drag and lift coefficients decrease slightly. Increasing the profile velocity, the lift and drag coefficient curves for the profile move up in the Y-axis, increasing lift and drag. In contrast, as the profile velocity increases, the tower's lift and drag coefficient

curves also increase. As the profile passes through the tower, drag increases while the tower's lift is reduced, similar to the D/t and H/t cases.

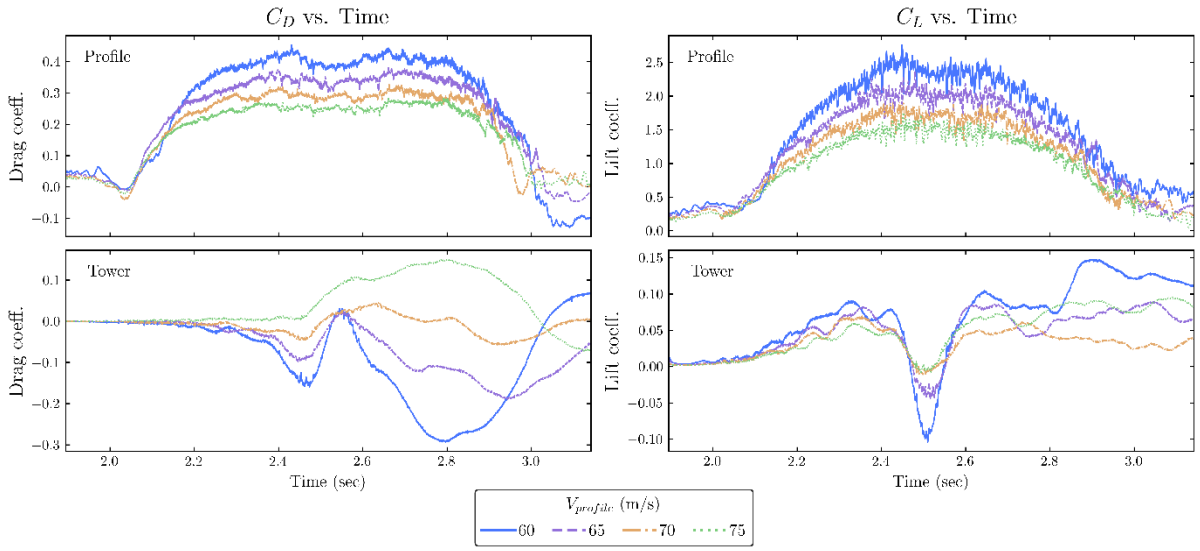

Figure 5.18: Profile and tower lift and drag coefficients for four different profile velocities during the 2D simulations

5.4.2. Pressure field

5.4.2.1. Tower Surface

When the profile is in proximity to the tower, pressure variations are plotted along the y-axis for four translational velocities, as illustrated in Figure 5.19. Using four different profile velocity values, $V_{profile}$ (as indicated in Table 5.4), simulations are performed, taking the dimensionless distance between towers and profiles, the dimensionless tower diameter, the profile speed, and a pitch angle of the profile as 6.88, 3, and 1° respectively (see Table 5.1).

Table 5.4: Third Variable: Profile's Translational Velocity

	Case 1	Case 2	Case 3 (Base)	Case 4
$V_{Profile}$ (m/s)	60	65	70	75

As can be seen in Figures 5.19 and 5.20, tower pressure is dominated by the profile component in all directions, ultimately shaping the total acoustic pressure waveform. As the profile and tower are aligned, both have in-phase acoustic pressure components that contribute to constructive interference, thus amplifying the overall pressure. With all profile velocities, acoustic pressure waves are similar except for the lowest profile

velocity, which is taken as $V_{profile} = 60m/s$, where the pressure curve during approach and move away exhibits notable fluctuations. On approaching the tower, the suction side pressure decreases, resulting in a pressure drop on the bottom side. Contrarily, there is a sharp increase in the tower pressure curve after y=0, which can be attributed to the interaction of high pressure around the trailing edge with the top side of the tower when the profile is moving away.

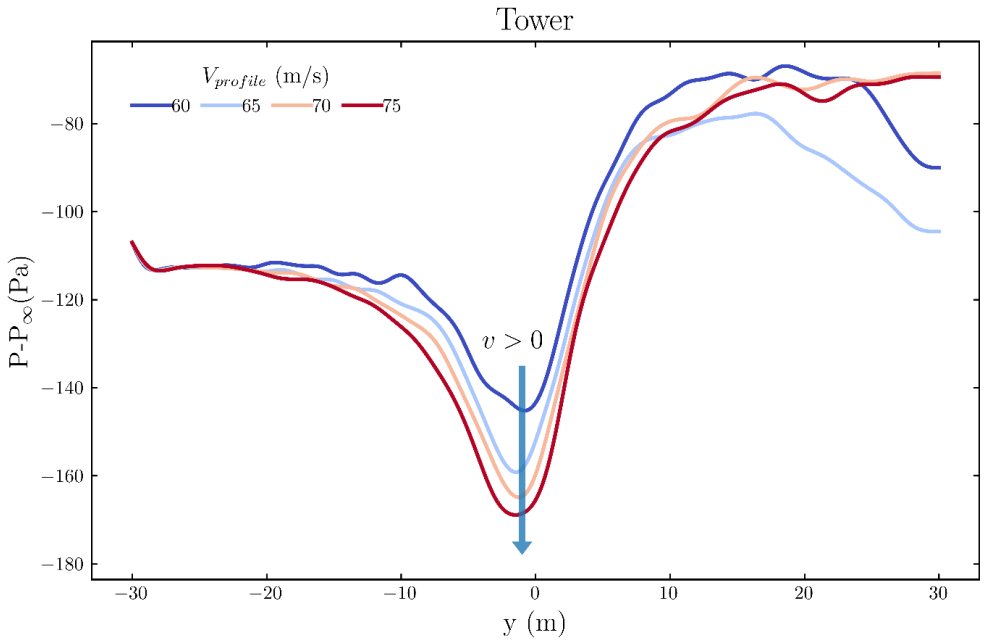

Figure 5.19: Pressure variations at the tower surface for four different profile velocities

Additionally, at slower profile velocities, the surface pressure on the tower drops less, which can be attributed to the reduction in the momentum of the air within the gap between the tower and the profile. With fast-moving profiles, the pressure drops much earlier than the point of alignment. However, the pressure rises slowly when the profile moves away, resulting in the highest pressure drop affecting more surface area of the profile and tower. When the profile velocity is taken as 65m/s, and the profile aligns with the tower at y=0, the tower experiences a pressure drop of around 158pa, as shown in Figure 5.19. When $V_{profile}$ is taken as 65m/s and 70m/s, the tower pressure curves follow the same trend, but the curves are shifted up in the x-axis, decreasing the profile velocities. When the profile aligns with the tower at y=0, when the profile has the slowest velocity, the pressure variation on the tower decreases the least compared to other profile velocities. At $\varphi = 95°$, as the profile moves away, the top side of the tower experiences an increase in pressure as a high-pressure region surrounds the trailing edge of the profile.

5.4.2.2. Profile surface

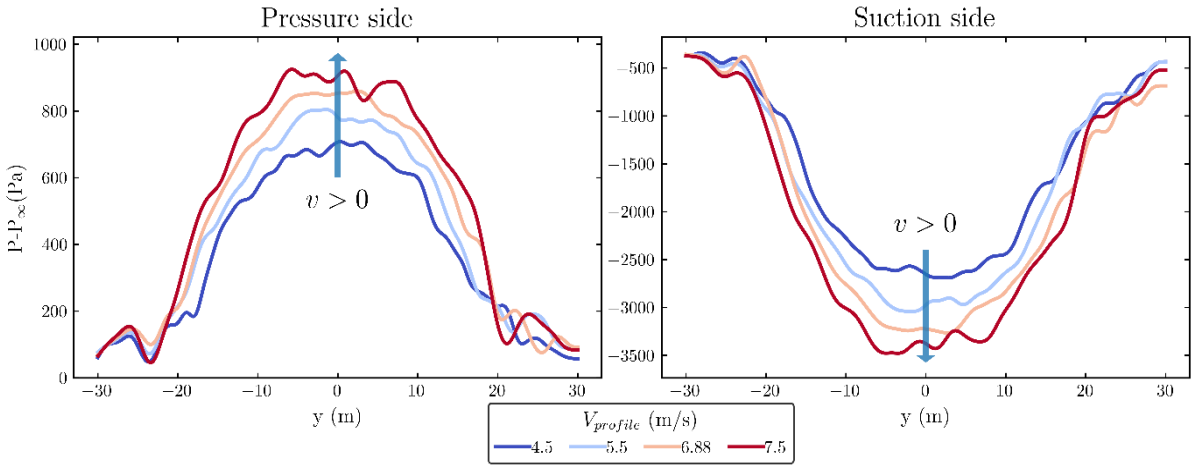

Figure 5.20: Profile pressure variation for four distinct profile velocities

In Figure 5.20, the pressure variation on the suction and pressure sides of the profile is presented and compared for four different profile velocities as the profile passes the tower (y-direction). By varying the translation speed of the profile, a change in the direction of inflow is generated in the profile when the pitch angle β and the wind velocity u_∞ are kept constant, resulting in a change in the angle of attack α (which is shown in table 5.5), as shown in Figure 5.15. In all cases of profile velocity, the pressure curves exhibit similar characteristics with slight pressure fluctuations when the profile is aligned with the tower.

Table 5.5: Variation in angle of attack α with varying profile's translational velocity

	profile velocity (m/s)	n_{rotor} (min^{-1})	**A**
1	60	19.09	13.47°
2	65	20.69	12.34°
3	70	22.28	11.37°
4	75	23.87	10.53°

While moving toward the tower, the profile experiences low suction pressure and high upwind side pressure; when moving away, the suction pressure increases whereas the upwind side pressure decreases, unless the profile reaches its normal thrust. TPI

impacts the profile surface pressure when the profile and tower are aligned such that the pressure curves for both the suction and pressure sides exhibit multiple bumps.

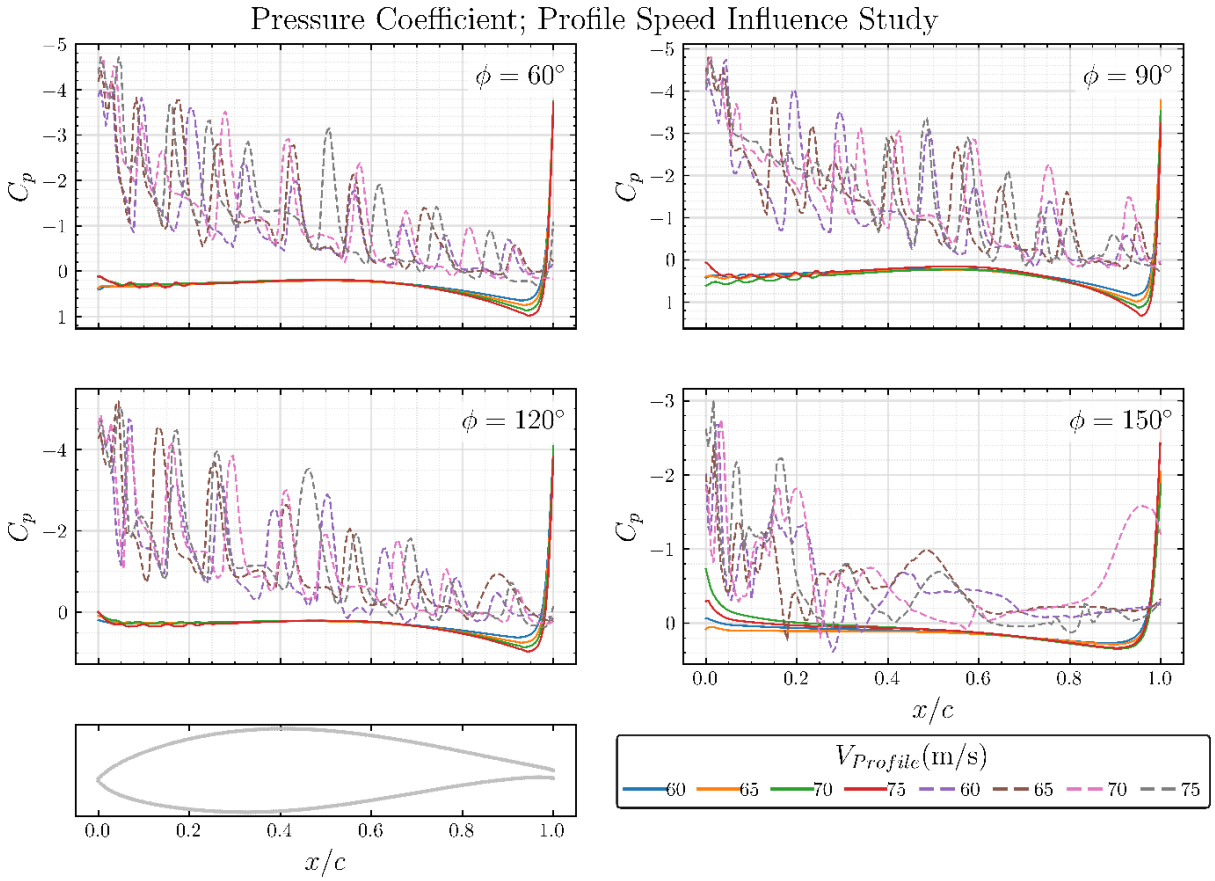

Figure 5.21: Pressure coefficients at various azimuth angles for four different profile velocities

On the pressure side, the maximum variation in pressure experienced by the profile is around 900pa, whereas on the suction side, the maximum variation in pressure is approximately four times that of the pressure side. The pressure variations on the suction side of the profile and tower are major contributors to the infrasonic noise generated during TPI, which must be addressed to minimize wind turbine noise. Slower profile velocities cause less pressure variations on the profile surface, where the acoustic pressure curves move upward in the x-direction, and vice versa. As shown in Figure 5.21, in all cases, the profile exhibits reduced lift during TPI.

Figure 5.21 shows the pressure distribution of the profile as it passes around the tower at a pitch angle of one degree. For four different profile velocities, the pressure distribution plots are analyzed and compared to demonstrate the pressure changes at different azimuthal angles (60°, 90°, 120°, and 150°). During tower-profile interaction, blade lift is reduced in all cases, with a peak at y=0 for a short period. This effect is more prominent on the suction side than the pressure side of the profile. TPI effects on blades slightly increase when the profile velocity is elevated from 60m/s to 75m/s. Stalling occurs at the bottom of the blades when the angle of attack is high, as shown

by spikes along the trailing edge. For 0.2>x/c >0.1, the suction side pressure curve is equally spikey, as opposed to the cases with varying h/t and D/t, when the profile is parallel with the tower.

5.4.2.3. Trend

Pressure variations are illustrated in figure 5.22 as a function of profile velocity, with the respective base values normalizing all velocity and pressure values. With increasing profile velocity, the fast-moving airfoil imparts more momentum to the air around it, displacing the air between the profile and the tower, which leads to increased pressure fluctuations between the profile and the tower. The pressure curve for the tower surface exhibits a nonlinear rise with a low gradient as profile velocity increases. In contrast, profile waves are highly sensitive to the $V_{profile}$, which fluctuates steeply and linearly as profile velocity increases. Variation in the surface pressure on the tower and profile is directly proportional to the translational velocity of the profile. Contrary to the profile, however, the changes are significantly lower on the tower's surface.

$$C_{profile} = \sqrt{u_{\infty}^2 - v_{profile}^2} \tag{5.1}$$

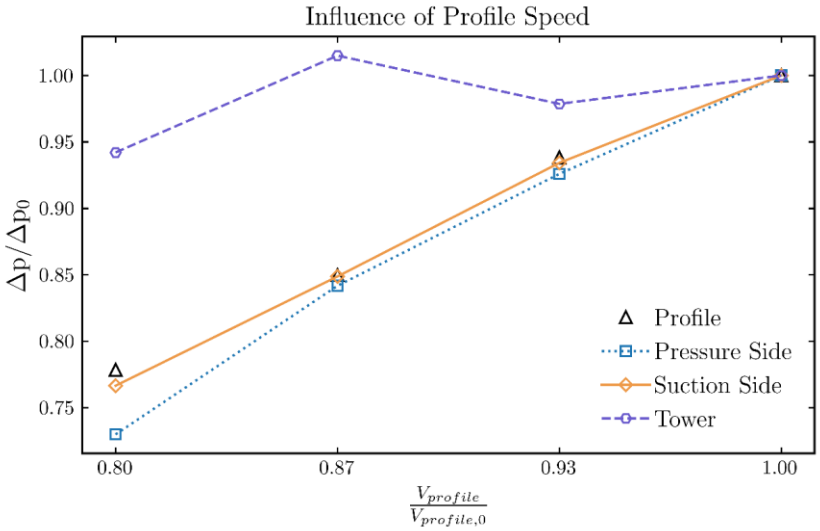

Figure 5.22: Influence of dimensionless profile velocity on tower-profile interactions.

Profile surfaces exhibit similar pressure fluctuations at different profile speeds. Observably, pressure variations are more pronounced on the tower than on the profile. Changing profile velocity by 10% induces approximately 2.5% variation in tower surface pressure and approximately 11.5% fluctuation in profile surface pressure, as shown in Figure 5.22.

5.4.3. Acoustics

The periodic pressure curves for four different profile velocities for two profile passages are illustrated in figure 5.23a to evaluate the effect of profile velocities on pressure fluctuations. The tower's pressure curve shows that each blade passage has two strong but opposing peaks. When the thrust is reduced to its minimum (i.e., the profile approaches), a negative peak appears, whereas a positive peak appears when the thrust is restored to its steady state (i.e., the profile moves away). Profile and tower pressure waveforms exhibit synchronous peaks, which increase the amplitude.

Unlike h/t and D/t case studies, velocity variations exhibit more pressure variation on the profile, apparent in the profile pressure plot as pressure curves ascend. TPI noise is significantly influenced by the profile and the tower, as demonstrated in this study. During TPI, the peak pressure varies by approximately 50% when the profile velocity increases from 60 m/s to 75 m/s. At its highest point, the profile pressure is approximately 20 times the tower pressure. Increasing profile velocity increases air displacement between the profile and tower, causing pressure fluctuations on the profile and tower, which contributes to the noise associated with TPI. Consequently, the magnitude of surface pressure on towers and profiles appears to vary directly with profile velocity, contrary to the profile velocity variation discussed in the previous section.

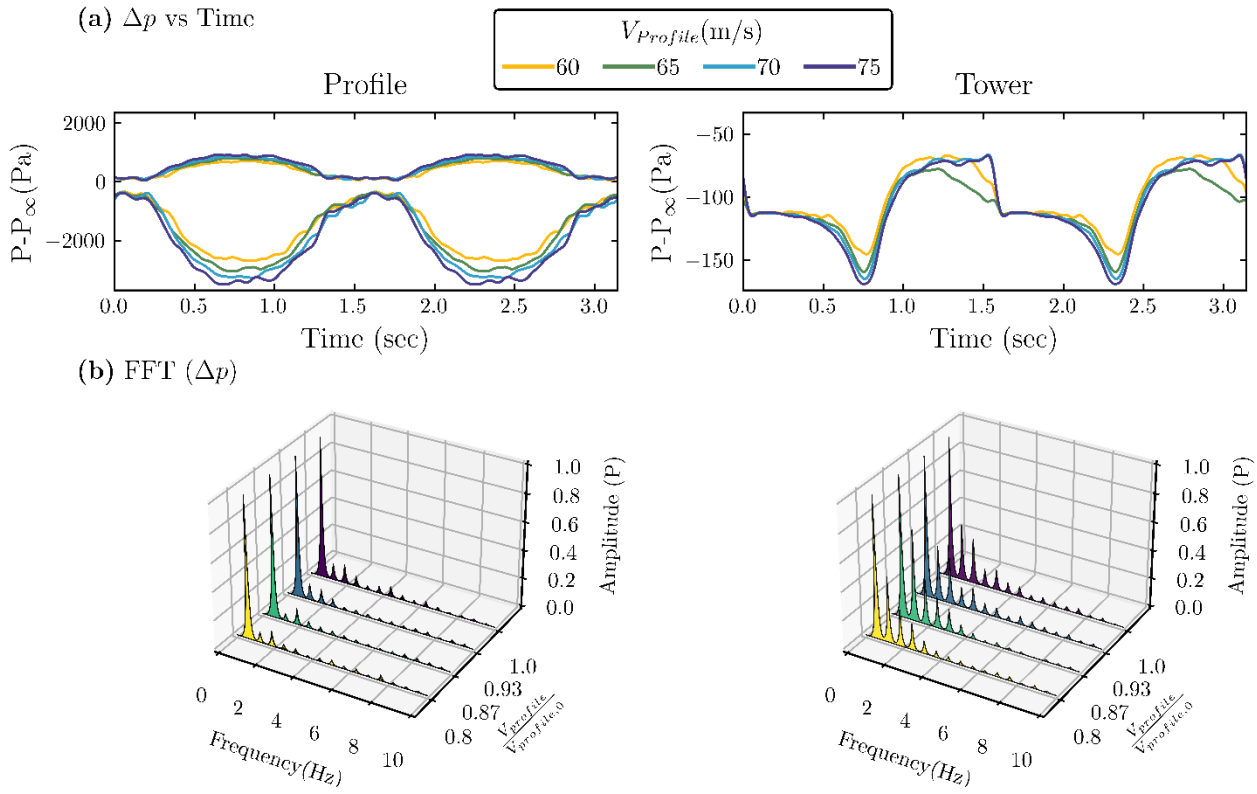

Figure 5.23: (a) Pressure variation, and (b) Fast Fourier Transform for four different profile velocities are presented.

For four different profile velocities, Discrete Fourier Transforms are presented in Figure 5.23b to investigate the effect of profile velocity on the fluctuations in acoustic pressure. With variation in profile velocity, the discrete Fourier transform only shows minor changes for the profile but significant changes for the tower. In the Discrete Fourier Transform for the tower, harmonic amplitudes rise, whereas frequencies decrease when profile velocity decreases, and vice versa, as profile velocity increases. Similarly, the FFT of the profile indicates that amplitude and frequency are increased as profile velocity increases, and vice versa. The strongest 2nd harmonic for the tower is f_2 = 0.5 Hz when $V_{profile}$=65 m/s. $V_{profile}$= 75 m/s has the highest number of prominent harmonics, with f_5 = 2.5 Hz being the fifth harmonic.

5.5. Assessment of the impact of physical parameters on the pressure fluctuation

This study examines and compares various influencing variables regarding pressure fluctuations on 2D tower and profile surfaces to determine which parameters are most appropriate for controlling these fluctuations. In comparing influences on amplitude, $\Delta p_{amplitude}$ or $\Delta p_{fluctuation}$ the ratio of the change in Δp to the change in the influencing variable g should be considered. In this way, it is assessed how ΔP changes due to the change in g. The ratio is

$$\frac{\Delta(\Delta p)}{\Delta g} \tag{5.4}$$

Here g stands for any influencing variables: tower-profile distance h, tower diameter D, angle of attack α and profile velocity $v_{profile}$. The quotient is converted into a dimensionless variable to be compared with various influencing variables. The initial setup value determines the dividend and divisor. Here is ΔP_0 for the dividend and g_0 for the divisor. That's how to get

$$S = \frac{\frac{\Delta(\Delta p)}{\Delta p_0}}{\frac{\Delta g}{g_0}} \tag{5.5}$$

As a function of the change in an influencing variable normalized with the initial state, the expression indicates the change in pressure fluctuation normalized with pressure fluctuation in the initial setup. Here, the dimensionless quotient is referred to as sensitivity. It is a dimensionless gradient in the graph of Δp over the varied influence quantity. However, the difference quotient is always set up with the status in the initial setup ($\Delta(\Delta p) = \Delta p - \Delta p_0$)). The slope of the graph of "p" of the profile changes with h, for instance, and so does the sensitivity to changes in influence.

5.5.1. Sensitivity of pressure fluctuations on the profile surface

Figure 5.24 illustrates the sensitivity of the pressure fluctuation Δp for the profile based on the change in the influencing variable relative to its value for the base setup ($\Delta g/g_0$). The initial values of the influential variables being investigated are presented in Table 5.3. Considering the influence of tower-profile spacing on pressure variation (Section 5.2), Δ*p* for the profile decreases with increasing tower spacing *h/t*, *the* sensitivity line is comparatively flat, and only low sensitivities of $S_{max,h,profile}$=0.009 and $S_{min,h,profile}$=−0.015 appears since the calculated changes in the tower-profile spacing are minor compared to the initial value of h_o = *6.88*. In contrast to other influencing variables evaluated, the calculated sensitivity values of the cases are significant along the y-axis. It can be observed that the changes in pressure fluctuation caused by this process are approximately of the same magnitude as those caused by other factors. However, the quotient *S* of the related changes is comparatively small. The mean sensitivity of the pressure fluctuation to a change in the tower-profile distance is $\overline{S}_{h,profile}$= 0.001.

Table 5.6: Values of the influencing variables g^0 in the initial setup

Influencing variable	g_0	Initial value
Tower profile distance	**h**	6.88 m
Tower diameter	**D**	3 m
Profile speed	$\mathbf{v_{profile}}$	75 m/s

Based on the variation of tower diameter, *S* is predominantly positive, and one case provides a slight decrease of $\Delta p - \Delta p_0$, which is why there is a slightly negative value for the sensitivity at $\Delta g/g_0$=0.8. With increasing, $\Delta g/g_0$, the sensitivity falls sharply between $\Delta g/g_0$ = 0.64 and $\Delta g/g_0$ = 0.08 and then rises again. Choosing a reference point is essential to determining the model's sensitivity because all changes to this point are compared with the initial condition. The maximum magnitude of the sensitivity because of a change in the tower diameter occurs for $\Delta g/g_0$ =0.64. It gives $S_{max,D,profile}$ =0.02, i.e., a value of approximately double the magnitude for the variation of the tower spacing. The mean sensitivity is $\overline{S}_{D,profile}$ =0.005, slightly lower than the maximum absolute value. Varying tower diameter appears more sensitive to pressure fluctuations than varying tower-profile distance but less sensitive than varying profile velocity.

Table 5.7: Summary of the sensitivity of the pressure fluctuation on the profile surface for all influencing variables

Influencing factor g	Maximum/minimum value, $S_{max,profile}$ or $S_{min,profile}$	Mean $\bar{S}_{profile}$	Note
Tower profile distance h	0.009	0.001	Change of sign at D =75m/s
Tower diameter D	0.02	0.005	
Profile speed $v_{profile}$	0	- 0.37	

Considering the influence of the translational velocity of the profile on pressure variation (Section 5.4), Δp for the profile increases with increasing profile velocity. The Δp implies that $\Delta(\Delta p)/\Delta v_{profile}$ is always negative for the analyzed region. As the magnitude of the variation increases with increasing sensitivity, the influence of profile velocity only becomes stronger.

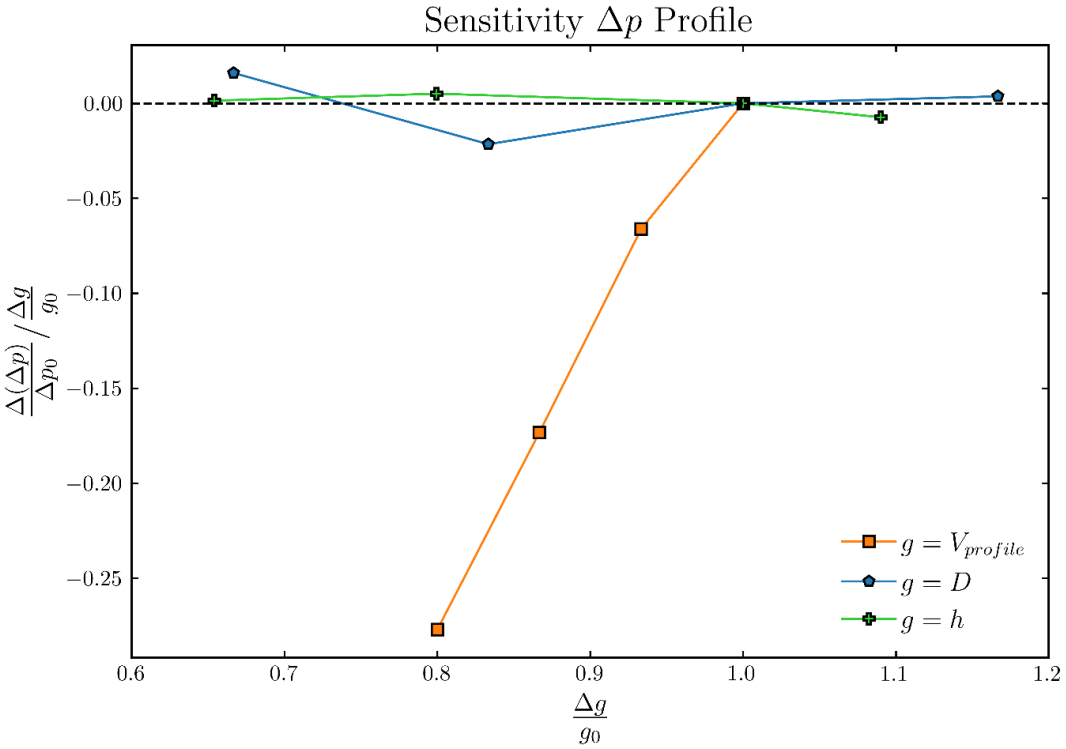

Figure 5.24: Sensitivity of the pressure variation (Δp) Amplitude on the profile surface to changes in the influencing variables g: tower-profile distance h, tower diameter D, and profile velocity $V_{Profile}$.

A negative change Δg leads to a positive change in the pressure fluctuation Δ(Δp) for the variation in profile velocity, thereby maintaining the negative values for sensitivity. Since Δg vanishes at g = g_0, the sensitivity cannot be defined at that point. The maximum sensitivity for the variation in profile velocity occurs at $\Delta g/g_0$=1, which is $S_{max,v_{profile},profile}$= 0. The mean sensitivity of the pressure fluctuation to a change in the tower-profile distance is $\overline{S}_{v_{profile},profile}$= -0.37. The values provided are based on calculated variations and do not represent general statements regarding the sensitivity of parameters.

5.5.2. Sensitivity of pressure fluctuations on the tower surface

Based on relative changes in the influencing variables, figure 5.25 illustrates the sensitivity of the tower's pressure fluctuations. Unlike the profile, the sensitivity to the tower does not change in sign. It is noteworthy that the sensitivity of the pressure change on the tower surface to variations in the tower-profile distance h is very similar to the sensitivity observed for tower diameters. For the case discussed, the maximum sensitivity is $S_{max,h,Tower}$ = 0.17, and the mean value is $\overline{S}_{h,Tower}$ =0.07. In section 5.2, it was concluded that the influence of pressure fluctuations decreases with increasing the tower-profile distance, which is verified in Figure 5.25.

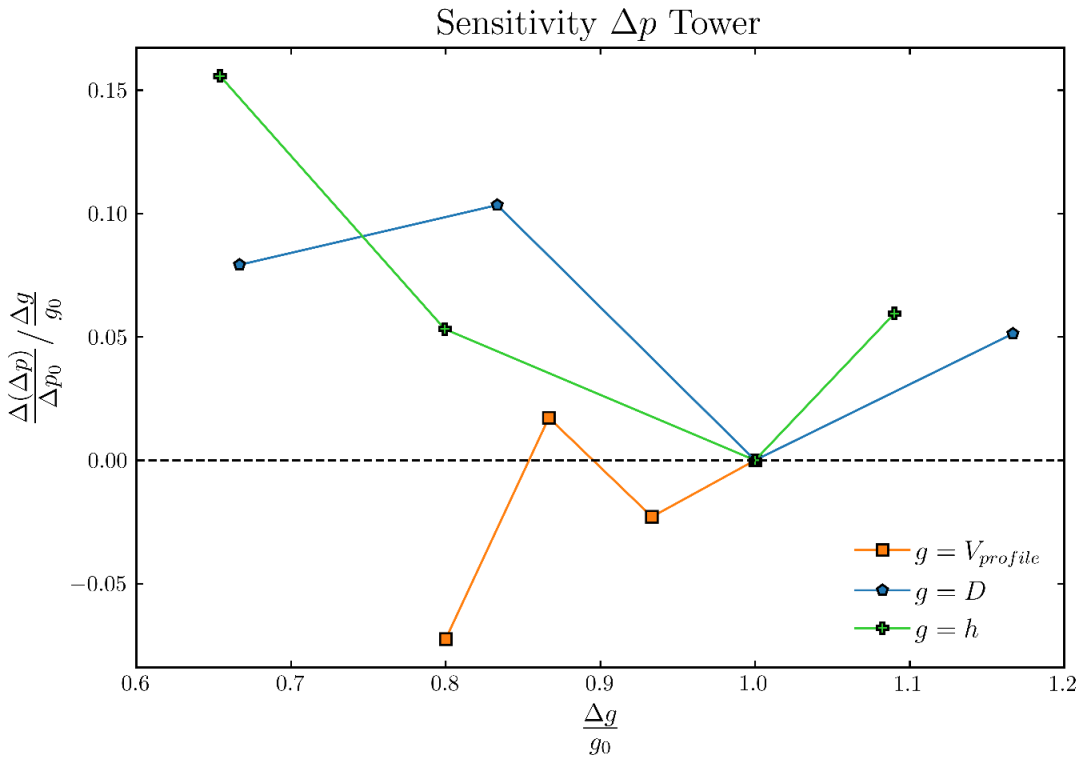

Figure 5.25: Sensitivity of the pressure variation (Δp) on the tower surface to changes in the influencing variables g: tower-profile distance h/t, tower diameter D/t, and profile velocity $V_{Profile}$.

Considering the influence of tower diameter on pressure fluctuations on the tower surface, section 5.3 concluded that there is no clear relationship between pressure fluctuations on the tower surface and tower diameter. As with tower profile spacing h, the sensitivity of the tower diameter retains all points within the positive region for the tower. The pressure fluctuation Δp fluctuates strongly with tower diameter. Consequently, the sensitivity varies strongly with changing tower diameter, sometimes reaching very high values. This result would appear to contradict the statement that the variables cannot be determined to be interdependent. Following section 5.3, the sensitivity varies with the pressure profile on the tower surface and does not reflect the actual dependence. The mean value should be considered when evaluating the sensitivity to changes in tower diameter. At g/g_0=0.8, Smax is $S_{max,D,Tower}$ =0.12, while the mean sensitivity is $\overline{S}_{D,Tower}$ = 0.0625.

Although $v_{profile}$ has a similar effect on pressure variation on the profile surface as the sensitivity of pressure variation on the tower surface, one positive value is observed. Following this pattern, the sensitivity value increased after a significant decrease. The sensitivity curve shows sharp but irregular variations. The $S_{max,v_{profile},Tower}$=0.02 at $g/g0$=0.88 is the only positive value for this variable. The $\overline{S}_{v_{profile},Tower}$ is -0.0225, which is also negative, like most of the values of the variable.

Table 5.8: Summary of the sensitivity of the pressure fluctuation on the tower surface for all influencing variables.

Influencing factor g	**Maximum/minimum value, $S_{max,Tower}$ or $S_{min,Tower}$**	**Mean $\overline{S}_{Tower}$**	**Note**
Tower profile distance h	0.17	0.07	Strongly fluctuating *S*
Tower diameter D	0.12	0.0625	
Profile speed $v_{profile}$	0.02	-0.0225	

6 Conclusion & Outlook

This thesis investigates the effects of several variables on the aerodynamic interaction between the blades of a rotor and the tower of a wind turbine. When the rotor blade and tower surface interact, pressure fluctuations on the rotor blade and tower surface play a decisive role in noise emissions. In addition, they contribute to the fatigue of materials in wind turbines. An evaluation of two-dimensional simulations using OpenFOAM is carried out in this study. To derive the 2D configuration, a real wind turbine with a nominal output of 2.3 megawatts is used as a reference. A 2D flow simulation is based on intersection geometries. The mesh is enabled for sliding through layerAdditionRemoval and cyclic boundary conditions. The geometry of the airfoil is modified to make the conditions more realistic to get precise results from the simulations. The pressure profile in the flow field is also examined transversely to the profile's direction of movement at the tower's height. A comparison between the respective calculation cases and a setup demonstrates improved convergence.

The physical domain is segmented into stationary and moving meshes. Various meshes are created using different meshing strategies, including C-grid and O-grid, but O-grid has opted for the final setup. The pressure curves across the profile position for different surface points on the profile and tower are analyzed to extract pressure fluctuations. While the profile is passing the tower, there is a drop in pressure at the front of the tower and a decrease in the lift coefficient of the profile, which can be attributed to the negative pressure area on the suction side of the profile. Variable sensitivity is introduced to compare the effects on the analyzed variable of pressure fluctuation. The variable sensitivity is the dimensionless ratio between the change in a target variable and an influencing variable. A negative correlation exists between the change in dimensionless tower distance h/t and the change in pressure fluctuation for both tower and profile. The influence decreases with increasing tower distance in response to the decreasing influence of the tower and profile flow fields on each other. For both tower and profile, the dependency is approximately the same. This can be interpreted as a similar value for sensitivity S. With an increase in the dimensionless tower diameter D/t, a non-linear increase in Δp can be seen for the profile. Pressure fluctuation sensitivity for a change in D/t is about the same as for a change in h/t for the profile. On the tower surface, Δp shows slight decrease. It is assumed that the mean value of the sensitivity is about half as significant as that of the profile. With increasing angle of attack, Δp for the tower increases.

Due to the dropping pressure on the suction side of the profile, the pressure fluctuates on the tower surface. On the profile, Δp initially increases and decreases again. Combined with the tower's influence, the drop in pressure on the profile suction side can explain the increase. The pressure distribution on the profile surface is examined

to investigate the cause of the subsequent decline in Δp simultaneously with the fall; a suction peak occurs on the profile suction side that is considered a possible cause. There is a positive correlation between the change in profile speed and the change in Δp on the profile and tower surfaces. The decrease in pressure on the profile suction side causes pressure fluctuations in the tower-profile interaction. The mean sensitivity for the tower is almost twice as high as for the profile.

The average sensitivity is about the same for the profile measuring point as for the tower-profile distance. In the case of the tower, the sensitivity to airfoil speed is approximately twice as high as that of the tower-airfoil distance. As a function of the change in the influencing variables, the discrete Fourier transform of the pressure over time is applied to examine the difference in pressure fluctuation. Increasing h/t results in a reduced pressure variation along the profile and tower. As a result, the time-to-amplitude ratio of the pressure excursion increases. Even though the tower diameter changes, there is no noticeable change in pressure deflection when the tower-profile distance h/t is maintained constant and vice versa if the h/t varies. Increasing profile speed shortens the duration of the interaction and increasing negative pressure on the suction side of the profile increases pressure variation amplitude. In the case studies conducted, an increase in the tower-profile distance and a reduction in profile speed were effective. To reduce Δp on the profile surface, the recommendations are supplemented by reducing the tower diameter.

The numerical investigation conducted using a 2D setup of the tower and profile can serve as a base for further research. The solid surface of the turbine blades reflects the effects of wind which can be minimized with flexible blades. A numerical study can be conducted by coupling OpenFOAM-Mbdyn to investigate the effectiveness of using flexible blades. Another possibility of reducing the noise effect due to the tower is by applying a layer of porous (damping) material to the tower surface as investigated by [46-47]. During tower-profile interaction, only the front side of the tower contributes to aerodynamic interaction noise. To study pressure variations locally and more precisely on the tower surface, another 2D setup could be created in which the tower diameter is divided into front and back. Additionally, an automatic blockMeshDict file writing code can be written for 6-digit NACA airfoils. It is also possible to study the directivity of the TPI noise which can help identify the type of noise and reduce it accordingly by using Ffowcs Williams Hawkings analogy as implemented in [46] and Curle's analogy as analyzed in [18]. Furthermore, an analysis can be conducted for the change in influencing variables with variable wind turbine power and varying profile. It is also possible to conduct a techno-economic study for a wind turbine with flexible blades.

7 References

[1] Renewable Capacity Statistics 2015 (IRENA, 2015) https://irena.org/-/media/Files/IRENA/Agency/Publication/2015/IRENA_RE_Capacity_Statistics_2015.pdf, (Accessed: 1.08.2022)

[2] Renewable Capacity Statistics 2022 (IRENA, 2022) https://irena.org/media/-/Files/IRENA/Agency/Publication/2022/Apr/IRENA_RE_Capacity_Statistics_2022.pdf, (Accessed: 1.08.2022)

[3] "Entwurf eines Gesetzes zur Erhöhung und Beschleunigung des Ausbaus von Windenergieanlagen an Land（Wind-an-Land-Gesetz)", BMWK (August 2, 2022) "Gemeinsame Pressmitteilung: Bundeskabinett beschleunigt naturverträglichen Windkraft-Ausbau deutlich", BMWK (August 2, 2022) "Erklärvideo zum Wind-an-Land-Gesetz".

[4] Prometeus, «Fire». Olympus BrevSayed, M., Bucher, P., Guma, G., Lutz, T., Wüchner, R. (2021). Aeroelastic Simulations Based on High-Fidelity CFD and CSD Models. In: Stoevesandt, B., Schepers, G., Fuglsang, P., Yuping, S. (eds) Handbook of Wind Energy Aerodynamics. Springer, Cham.etto 1, 300.000 BC.

[5] H. Møller and C. S. Pedersen, "Low-frequency noise from large wind turbines," J. Acoust. Soc. Am., vol. 129, no. 6, pp. 3727–3744, Jun. 2011.

[6] G. Guidati, J. Ostertag, and S. Wagner, "Prediction and reduction of wind turbine noise an overview of research activities in europe," 2000 ASME Wind Energy Symp., pp. 219–229, 2000.

[7] G. V. d. Berg, "The beat is getting stronger: the effect of atmospheric stability on low frequency modulated sound of wind turbines", J. Low Freq. Noise Vib., vol. 24, pp. 1–23.

[8] C. Doolan, D.J. Moreau, L.A. Brooks, Wind turbine noise mechanisms and some concepts for its control, Acoust Aust., vol. 40, pp. 7-13, 2022.

[9] N. Curle, “The influence of solid boundaries upon aerodynamic sound,” Proc. R. Soc. London. Ser. A. Math. Phys. Sci., vol. 231, no. 1187, pp. 505–514, Sep. 1955.

[10] Y. Yauwenas, B. Zajamšek, J. Reizes, V. Timchenko, and C. J. Doolan, “Numerical simulation of blade-passage noise,” J. Acoust. Soc. Am., vol. 142, no. 3, p. 1575, Sep. 2017.

[11] H. H. Hubbard and K. P. Shepherd, “Aeroacoustics of large wind turbines,” J. Acoust. Soc. Am., vol. 89, no. 6, p. 2495, Jul. 1999.

[12] G. C. Greene, Greene, and G. C., “Measured and calculated characteristics of wind turbine noise,” wtd, pp. 355–362, 198.

[13] N. D. Kelley, H. E. Mckenna, E. W. Jacobs, R. R. Hemphill, and N. J. Birkenheuer, “The MOD-2 Wind Turbine: Aeroacoustical Noise Sources, Emissions, and Potential Impact,” 1988.

[14] L. A. Viterna, "The NASA-LERC wind turbine noise prediction", code, NASA CP, 2185, 1981. https://ntrs.nasa.gov/search.jsp?R=19820015854 (last Accessed: 9 October 2018).

[15] C. Doolan, “Wind turbine noise mechanisms and some concepts for its control,” vol. 17, 2011.

[16] H. A. Madsen, “Low Frequency Noise from Wind Turbines Mechanisms of Generation and its Modelling,” vol. 29, no. 4, pp. 239–251, Dec. 2010.

[17] C.C. Nelson, A.B. Cain, G. Raman, T. Chan, M. Saunders, J. Noble, R. Engeln, R. Dougherty, K.S. Brentner, P.J. Morris, Numerical studies of wind turbine acoustics, 50th AIAA Aerospace Sciences Meeting Including the New Horizons Forum and Aerospace Exposition, Nashville, Tennessee, 2012.

[18] Y. Yauwenas, B. Zajamšek, J. Reizes, V. Timchenko, C.Doolan,”Directivity of blade-tower interaction noise”, JASA Express Letter, vol. 6, Jun. 2011.

[19] M.-C. Hsu, Y. Bazilevs, “Fluid-structure interaction modeling of wind turbines: simulating the full machine”, Comput. Mech., vol. 50 (6), pp. 821–833, 2012.

[20] J.-O. Mo, A. Choudhry, M. Arjomandi, Y.-H. Lee, “Large eddy simulation of the wind turbine wake characteristics in the numerical wind tunnel model”, J. Wind Eng. Ind. Aerod., vol. 112, pp.11–24, 2013.

[21] F. Zahle, N. N. Sørensen, and J. Johansen, “Wind turbine rotor-tower interaction using an incompressible overset grid method,” Wind Energy, vol. 12, no. 6, pp. 594–619, Sep. 2009.

[22] Q. Wang, H. Zhou, and D. Wan, “Numerical simulation of wind turbine blade-tower interaction,” J. Mar. Sci. Appl. 2012 113, vol. 11, no. 3, pp. 321–327, Sep. 2012.

[23] The Feynman Lectures on Physics. Eingesehen am url: https://www.feynmanlectures.caltech.edu/II_41.html, (accessed: 7.10.2022).

[24] G. K. Batchelor: An Introduction to Fluid Dynamics. Cambridge University Press, 1970.

[25] H.Schlichtingund, K.Gersten, Boundary Layer Theory. BerlinHeidelberg: SpringerVerlag, 2017.

[26] H.Oertel Jr.:Prandtl - Führer durch die Strömungslehre. Wiesbaden: SpringerVieweg, 2017.

[27] Numerische Untersuchungen der Interaktion von Rotorblatt und Turm einer Windenergieanlage mit dem Strömungslöser FLOWer, Masterarbeit, von Aljoscha Stein, December 2020.

[28] I. Janajreh, I. Talab und J. Macpherson,” Numerical Simulation of Tower Rotor Interaction for Downwind Wind Turbine,” Modelling and Simulation in Engineering, 2010.

[29] A. Gomez und J. R. Seume, “Aerodynamic Coupling of Rotor and Tower in HAWTs”, EWEC. Marseille, 2009.

[30] R. Schwarze, “CFD-Modellierung Grundlagen und Anwendungen bei Strömungsprozessen“, Berlin Heidelberg: Springer, 2013.

[31] F. R. Menter, “Two-Equation Eddy-Viscosity Turbulence Models for Engineering Applications”, AIA A JOURNAL, vol. 32. no.8, 1994.

[32] F. Municchi, P. P. Nagrani, and I. C. Christov,”A two-fluid model for numerical simulation of shear-dominated suspension flows”, International Journal of Multiphase Flow, vol. 120, pp. 103079, 2019.

[33] OpenFOAMWiki. OpenFOAM guide/The SIMPLE algorithm in OpenFOAM - Open-FOAMWiki, URL:

https://openfoamwiki.net/index.php/OpenFOAM_guide/The_SIMPLE_algorithm_in_OpenFOAM, (accessed 8.10.2022).

[34] OpenFOAMWiki. OpenFOAM guide/The PIMPLE algorithm in OpenFOAM - Open-FOAMWiki, URL: https://openfoamwiki.net/index.php/OpenFOAM_guide/The_PIMPLE_algorithm_in_OpenFOAM, (accessed 8.10.2022).

[35] Jiyuan Tu, Guan-Heng Yeoh, Chaoqun Liu, Chapter 4 - CFD Mesh Generation: A Practical Guideline, Editor(s): Jiyuan Tu, Guan-Heng Yeoh, Chaoqun Liu, Computational Fluid Dynamics (Third Edition), Butterworth-Heinemann, 2018.

[36] Hrvoje Jasak, Book Chapter, 47th AIAA Aerospace Sciences Meeting including The New Horizons Forum and Aerospace Exposition.

[37] Piscaglia, F., Montorfano, A., and Onorati, A., "Development of Fully-Automatic Parallel Algorithms for Mesh Handling in the OpenFOAM®-2.2.x Technology," SAE Technical Paper 2013-24-0027, 2013.

[38] Greenshields, Christopher and Weller, Henry, "Notes on Computational Fluid Dynamics: General Principles", CFD Direct Ltd, 2022.

[39] http://www.wolfdynamics.com/wiki/meshing_preliminaries_and_quality_assessment.pdf (accessed 1.11.2022)

[40] https://opencourses.emu.edu.tr/pluginfile.php/13882/mod_resource/content/1/chapter%207.pdf (accessed 1.11.2022)

[41] https://web.mit.edu/drela/Public/web/xfoil/ (accessed 1.11.2022)

[42] H. G. Weller, G. Tabor, H. Jasak, and C. Fureby, “A tensorial approach to computational continuum mechanics using object-oriented techniques”, Computers in Physics, vol. 12, pp. 620, 1998.

[43] https://m-selig.ae.illinois.edu/ads/coord/naca633418.dat (accessed 1.2.2022)

[44] https://www.openfoam.com/documentation/user-guide/4-mesh-generation-and-conversion/4.3-mesh-generation-with-the-blockmesh-utility/(accessed30.05.2022)

[45] C. Pilger and L. Ceranna, "The influence of periodic wind turbine noise on infrasound array measurements", Journal of Sound and Vibration, vol. 388, pp.188–200, 2017.

[46] S. Sharma, T. F. Geyer, and E. J. G. Arcondoulis, "Effect of Coating Thickness on Aerodynamic Noise Reduction by Porous-Coated Cylinders," 28th AIAA/CEAS Aeroacoustics Conf. 2022, 2022.

[47] E. J. G. Arcondoulis, Y. Liu, Z. Li, Y. Yang, and Y. Wang, "Structured Porous Material Design for Passive Flow and Noise Control of Cylinders in Uniform Flow," Mater. (Basel, Switzerland), vol. 12, no. 18, Sep. 2019.

A Appendix A

A.1. BlockMesh: Stationary Part

```
/*--------------------------------*- C++ -*----------------------------------*\
| =========                 |                                                 |
| \\      /  F ield         | OpenFOAM: The Open Source CFD Toolbox           |
|  \\    /   O peration     | Version:  v2112                                 |
|   \\  /    A nd           | Website:  www.openfoam.com                      |
|    \\/     M anipulation  |                                                 |
\*---------------------------------------------------------------------------*/
FoamFile
{
    version     2.0;
    format      ascii;
    class       dictionary;
    object      blockMeshDict;
}
// * * * * * * * * * * * * * * * * * * * * * * * * * * * * * * * * * * * * //

scale   1;

vertices
(
 //Pre-Block 1 (bottom)
        (-112.57 -73.19  0.5) //0
        ( -12.57 -73.19  0.5) //1
        ( -12.57 -73.19 -0.5) //2
```

(-112.57 -73.19 -0.5) //3
(-112.57 -4.19 0.5) //4
(-12.57 -4.19 0.5) //5
(-12.57 -4.19 -0.5) //6
(-112.57 -4.19 -0.5) //7

//Pre-Block 2 (center)
(-112.57 4.19 0.5) //8
(-12.57 4.19 0.5) //9
(-12.57 4.19 -0.5) //10
(-112.57 4.19 -0.5) //11

//Pre-Block 3 (top)
(-112.57 73.19 0.5) //12
(-12.57 73.19 0.5) //13
(-12.57 73.19 -0.5) //14
(-112.57 73.19 -0.5) //15

//Below Tower (Block 4)
(-4.19 -73.19 0.5) //16
(4.19 -73.19 0.5) //17
(4.19 -73.19 -0.5) //18
(-4.19 -73.19 -0.5) //19
(-4.19 -4.19 0.5) //20
(4.19 -4.19 0.5) //21
(4.19 -4.19 -0.5) //22
(-4.19 -4.19 -0.5) //23

// Tower
(-1.060660172 -1.060660172 0.5) //24
(1.060660172 -1.060660172 0.5) //25

```
        (   1.060660172 -1.060660172 -0.5)  //26
        (  -1.060660172 -1.060660172 -0.5)  //27

      (  -1.060660172  1.060660172  0.5)  //28
        (   1.060660172  1.060660172  0.5)  //29
        (   1.060660172  1.060660172 -0.5)  //30
        (  -1.060660172  1.060660172 -0.5)  //31

      (  -4.19        4.19        0.5)  //32
        (   4.19        4.19        0.5)  //33
        (   4.19        4.19       -0.5)  //34
        (  -4.19        4.19       -0.5)  //35

// Above Tower Block
        (  -4.19  73.19  0.5)  //36
        (   4.19  73.19  0.5)  //37
        (   4.19  73.19 -0.5)  //38
        (  -4.19  73.19 -0.5)  //39

// Post Block 1 (Below)
        ( 205.19 -73.19  0.5)  //40
        ( 205.19 -73.19 -0.5)  //41
        ( 205.19  -4.19  0.5)  //42
        ( 205.19  -4.19 -0.5)  //43

// Post Block 2 (Center)
        ( 205.19   4.19  0.5)  //44
        ( 205.19   4.19 -0.5)  //45

// Post Block 3 (Above)
        ( 205.19  73.19  0.5)  //46
```

```
        ( 205.19  73.19 -0.5)  //47

);

blocks
(
 //Pre-Blocks
   hex ( 3  2  6  7  0  1  5  4) ( 150  150  1  ) //Below 0
   simpleGrading
   ( 0.03291176817                 //x Direction
   (                   //y Direction
    (0.4 0.10 0.29199)
    (0.6 0.90 0.06) //50% Geo, 50% Cell, 0.1 Expansion Ratio   //(0.5 0.5 10)
    )
        1 )     //z Direction
   hex ( 7  6 10 11  4  5  9  8)( 150  125  1  ) //Center 1
   simpleGrading //center 1 central point give errors
   ( 0.03291176817                 //x Direction
   (                   //y Direction
    (1 1 1) //50% Geo, 50% Cell, 0.1 Expansion Ratio
    //(0.5 0.5 10)
    )
        1 )     //z Direction
   hex (11 10 14 15  8  9 13 12) (  150  150  1  ) //Above 2
   simpleGrading
   ( 0.03291176817                 //x Direction
   (                   //y Direction
    (0.6 0.90 16.67) //50% Geo, 50% Cell, 0.1 Expansion Ratio //(0.5 0.5 10)
    (0.4 0.10 3.424792525)
    )
        1 )     //z Direction
```

```
// Below Tower
  hex (19 18 22 23 16 17 21 20) ( 125  150  1  ) //Below 3
  simpleGrading
  ( 1                //x Direction
  (                   //y Direction
   (0.4 0.10 0.29199)
   (0.6 0.90 0.06) //50% Geo, 50% Cell, 0.1 Expansion Ratio //(0.5 0.5 10)

   )
       1 )    //z Direction
// Tower blocks
  hex ( 31 30 34 35 28 29 33 32) ( 125  312   1 ) simpleGrading ( 1  540  1)  // top  4
  hex ( 26 27 23 22 25 24 20 21) ( 125  312   1 ) simpleGrading ( 1  540  1)  // bottom 5
  hex ( 27 31 35 23 24 28 32 20) ( 125  312   1 ) simpleGrading ( 1  540  1)  // left  6
  hex ( 30 26 22 34 29 25 21 33) ( 125  312   1 ) simpleGrading ( 1  540  1)  // right 7

// Above Tower
  hex ( 35 34 38 39 32 33 37 36) ( 125  150  1  ) //Above 8
  simpleGrading
  ( 1                //x Direction
  (                  //y Direction
   (0.6 0.90 16.67)   //70% Geo, 80% Cell, 16.67 Expansion Ratio //(0.5 0.5 10)
   (0.4 0.10 3.424792525)
  )
       1 )          //z Direction

// post-block 1 (below)
  hex ( 18 41 43 22 17 40 42 21) ( 300  150  1  ) //Below 9
  simpleGrading
  ( 30.75866694           //x Direction
```

```
    (                   //y Direction
     (0.4 0.10 0.29199 )
     (0.6 0.90 0.06) //50% Geo, 50% Cell, 0.1 Expansion Ratio //(0.5 0.5 10)
      )
        1 )             //z Direction

 // post-block 2 (Center) //10
    hex ( 22 43 45 34 21 42 44 33) ( 300 125  1 )
    simpleGrading
    ( 30.75866694               //x Direction
    (
            //y Direction
      (1 1 1) //50% Geo, 50% Cell, 0.1 Expansion Ratio
      //(0.5 0.5 10)
      )
        1 )             //z Direction

 // post-block 3 (top)
    hex ( 34 45 47 38 33 44 46 37) ( 300  150  1 ) //Above 11
    simpleGrading
    ( 30.75866694               //x Direction
    (                   //y Direction
      (0.6 0.90 16.67) //70% Geo, 80% Cell, 16.67 Expansion Ratio //(0.5 0.5 10)
      (0.4 0.10 3.424792525)
      )
        1 )     //z Direction
);

edges
(
    arc 24 25 (   0 -1.5  0.5)
```

```
    arc 26 27 (   0 -1.5 -0.5)
    arc 28 24 (-1.5    0  0.5)
    arc 31 27 (-1.5    0 -0.5)
    arc 28 29 (   0  1.5  0.5)
    arc 31 30 (   0  1.5 -0.5)
    arc 29 25 ( 1.5    0  0.5)
    arc 30 26 ( 1.5    0 -0.5)
);

boundary
(
    freestream_free
    {
        type patch;
        faces
        (
            ( 0  4  7  3)
            ( 4  8 11  7)
            ( 8 12 15 11)
            (12 13 14 15)
            ( 0  1  2  3)
            (36 37 38 39)
            (37 46 47 38)
            (45 47 46 44)
            (43 45 44 42)
            (41 43 42 40)
            (17 40 41 18)
            (16 17 18 19)
        );
    }
```

```
int_out_ami
{
    type patch;
    faces
    (
        (16  20  23 19)
        (20  32  35 23)
        (32  36  39 35)
    );
}

int_in_ami
{
    type patch;
    faces
    (
        ( 2  6  5 1)
        ( 6 10  9 5)
        (10 14 13 9)
    );
}

tower_wall
{
    type wall;
    faces
    (
        ( 24 25 26 27)
        ( 25 29 30 26)
        ( 28 29 30 31)
        ( 24 28 31 27)
```

```
    );
}

front_empty
{
    type empty;
    faces
    (
        ( 0  1  5  4) //pre-block
        ( 4  5  9  8)
        ( 8  9 13 12)

        (16 17 21 20) // Tower (below)

        (20 24 28 32) //Tower
        (28 29 33 32)
        (25 21 33 29)
        (20 21 25 24)

        (32 33 37 36) //Tower (above)

        (17 40 42 21) // Post-block
        (21 42 44 33)
        (33 44 46 37)

    );
}

back_empty
{
    type empty;
```

```
        faces
        (
            ( 3  7  6  2) //pre-block
            ( 7 11 10  6)
            (11 15 14 10)

            (19 23 22 18) // Tower (below)

            (23 35 31 27) // Tower
            (31 35 34 30)
            (26 30 34 22)
            (23 27 26 22)

            (35 39 38 34) // Tower (above)

            (18 22 43 41) // Post-block
            (22 34 45 43)
            (34 38 47 45)
        );
    }
);

mergePatchPairs
(
);

// ************************************************************************* //
```

A.2. BlockMesh: Moving Part

```
/*--------------------------------*- C++ -*----------------------------------*\
```

```
| =========                 |                                                 |
| \\      /  F ield         | foam-extend: Open Source CFD                    |
|  \\    /   O peration     | Version:     4.0                                |
|   \\  /    A nd           | Web:         http://www.foam-extend.org         |
|    \\/     M anipulation  |                                                 |
\*---------------------------------------------------------------------------*/
FoamFile
{
    version     2.0;
    format      ascii;
    class       dictionary;
    location    "constant/polyMesh";
    object      blockMeshDict;
}
// * * * * * * * * * * * * * * * * * * * * * * * * * * * * * * * * * * * * //

 // Airfoil -moving mesh (Version - 5) at control points

scale 1; //meters

vertices
(
  //Airfoil inner part

     ( -8.37894171960202   2.250255197449192  -0.5) //0
     ( -8.37894171960202   0.250255197449192  -0.5) //1
     ( -8.35840891189491  -0.74988560120633   -0.5) //2
     ( -6.7045086         -2.1148204          -0.5) //3  ...
     ( -8.37894171960202   2.250255197449192   0.5) //4
     ( -8.37894171960202   0.250255197449192   0.5) //5
     ( -8.35840891189491  -0.74988560120633    0.5) //6
```

(-6.7045086 -2.1148204 0.5) //7 .....

(-8.37539298141910 -0.74988560120633 -0.5) //8

(-10.036464 -2.1121763 -0.5) //9

(-8.37539298141910 -0.74988560120633 0.5) //10

(-10.036464 -2.1121763 0.5) //11 ....,,

(-6.7045086 -2.1148204 -0.5) //12 ....

(-6.6081182 1.5252606 -0.5) //13

(-4.19 4.19 -0.5) //14

(-4.19 -4.19 -0.5) //15

(-6.7045086 -2.1148204 0.5) //16 .....

(-6.6081182 1.5252606 0.5) //17

(-4.19 4.19 0.5) //18

(-4.19 -4.19 0.5) //19

(-10.036464 -2.1121763 -0.5) //20

(-10.143752 1.5107425 -0.5) //21

(-12.57 4.19 -0.5) //22

(-12.57 -4.19 -0.5) //23

(-10.036464 -2.1121763 0.5) //24 ....,,

(-10.143752 1.5107425 0.5) //25

(-12.57 4.19 0.5) //26

(-12.57 -4.19 0.5) //27

// Above

(-12.57 4.19 -0.5) //28

(-4.19 4.19 -0.5) //29

(-4.19 73.19 -0.5) //30

(-12.57 73.19 -0.5) //31

(-12.57 4.19 0.5) //32

(-4.19 4.19 0.5) //33

(-4.19 73.19 0.5) //34

```
    (-12.57          73.19          0.5) //35
/*  ( -4.19          73.19          -0.5) //28
    (-12.57          73.19          -0.5) //29
    ( -4.19          73.19          0.5) //30
    (-12.57          73.19          0.5) //31 */


    // Below

    (-12.57          -73.19         -0.5) //36
    ( -4.19          -73.19         -0.5) //37
    ( -4.19          -4.19          -0.5) //38
    (-12.57          -4.19          -0.5) //39
    (-12.57          -73.19         0.5) //40
    ( -4.19          -73.19         0.5) //41
    ( -4.19          -4.19          0.5) //42
    (-12.57          -4.19          0.5) //43
    /*
    ( -4.19          -73.19         -0.5) //32
    (-12.57          -73.19         -0.5) //33
    (-12.57          -73.19         0.5) //34
    ( -4.19          -73.19         0.5) //35
    */
);

blocks
(

    hex ( 1  2  3  0  5  6  7  4) ( 180  340  1) simpleGrading (1    305                1) // Block
0 203600 points
```

```
    hex ( 2  8  9  3  6 10 11  7) (  90  340  1) simpleGrading (1    305              1) // Block
1
    hex ( 8  1  0  9 10  5  4 11) ( 180  340  1) simpleGrading (1    305              1) // Block
2
    hex (13 12 15 14 17 16 19 18) ( 125   42  1) simpleGrading (1     1.636363636      1)
// Block 3 //rightside 39
    hex (12 20 23 15 16 24 27 19) ( 125   42  1) simpleGrading (1     1.636363636      1)
// Block 4 //Down  42
    hex (20 21 22 23 24 25 26 27) ( 125   42  1) simpleGrading (1     1.636363636      1)
// Block 5 //leftside 40
    hex (21 13 14 22 25 17 18 26) ( 125   42  1) simpleGrading (1     1.636363636      1)
// Block 6 //Up  46
    hex (28 29 30 31 32 33 34 35) ( 125  150  1) //Above
    simpleGrading
    ( 1              //x Direction
    (                  //y Direction
    (0.6 0.90 16.67) //50% Geo, 50% Cell, 0.1 Expansion Ratio //(0.5 0.5 10)
    (0.4 0.10 3.424792525)
    )
       1 )    //z Direction
    hex (36 37 38 39 40 41 42 43) ( 125  150  1) //Below
    simpleGrading
    ( 1              //x Direction
    (                  //y Direction
    (0.4 0.10 0.29199)
    (0.6 0.90 0.06) //50% Geo, 50% Cell, 0.1 Expansion Ratio   //(0.5 0.5 10)
    )
       1 )    //z Direction
);

edges
```

```
(
    //internal
    arc  3   0  (-6.0345798   0.64598213    -0.5)
    arc  7   4  (-6.0345798   0.64598213     0.5)

    arc  9   3  ( -8.35841   -2.7498856     -0.5)
    arc 11   7  ( -8.35841   -2.7498856      0.5)

    arc  0   9  (-10.705727   0.63824464    -0.5)
    arc  4  11  (-10.705727   0.63824464     0.5)

    //external

    arc 13 12 (-5.8694536  -0.3157355    -0.5)
    arc 17 16 (-5.8694536  -0.3157355     0.5)

    arc 20 21 (-10.867673   -0.32376692  -0.5)
    arc 24 25 (-10.867673   -0.32376692   0.5)

    arc 21 13 (-8.37894171960202   2.250255197449192   -0.5)
    arc 25 17 (-8.37894171960202   2.250255197449192    0.5)

    arc 12 20 ( -8.35841    -2.7498856   -0.5)
    arc 16 24 ( -8.35841    -2.7498856    0.5)

   // Suction Side splines.
   spline 1 2
   (
        ( -8.37894171960202 0.250255197449192 -0.5 )  //-8.37874536          0.24994787
        ( -8.37884193993624 0.250248564489101 -0.5 )
        ( -8.37873932024441 0.250241205150188 -0.5 )
```

(-8.37863378414245 0.250233070692358 -0.5)

(-8.37852525330924 0.250224109726248 -0.5)

(-8.37841364917743 0.25021426825557 -0.5)

(-8.37829888817902 0.250203489153055 -0.5)

(-8.37818088888536 0.250191712691689 -0.5)

(-8.37805956551823 0.250178875846078 -0.5)

(-8.37793483221341 0.250164912597108 -0.5)

(-8.37780659977325 0.250149753482448 -0.5)

(-8.37767477781362 0.250133325715004 -0.5)

(-8.37753927648132 0.250115553327037 -0.5)

(-8.37740000072202 0.250096356335079 -0.5)

(-8.37725685518865 0.250075651251184 -0.5)

(-8.3771097429812 0.250053350840249 -0.5)

(-8.37695856674061 0.250029364212024 -0.5)

(-8.37680322360379 0.250003595925253 -0.5)

(-8.37664361399536 0.249975947323361 -0.5)

(-8.37647963215503 0.24994631489748 -0.5)

(-8.37631117251404 0.249914591275328 -0.5)

(-8.3761381289102 0.249880665075739 -0.5)

(-8.37596039086036 0.249844420126391 -0.5)

(-8.37577784841121 0.249805736365264 -0.5)

(-8.37559038943772 0.249764489292975 -0.5)

(-8.37539789755837 0.249720549449269 -0.5)

(-8.3752002586779 0.249673783873211 -0.5)

(-8.37499735343043 0.249624054390965 -0.5)

(-8.37478906183651 0.249571218683612 -0.5)

(-8.37457526236253 0.249515130115072 -0.5)

(-8.37435582981589 0.249455637206666 -0.5)

(-8.37413064001265 0.249392584942022 -0.5)

(-8.37389956280155 0.249325812921804 -0.5)

(-8.37366246930214 0.249255157459657 -0.5)

(-8.37341922583286 0.249180449940677 -0.5)

(-8.37316969755065 0.249101517982569 -0.5)

(-8.37291387922751 0.24901777906475 -0.5)

(-8.3726519065119 0.248928264570553 -0.5)

(-8.37238367744094 0.248832751275514 -0.5)

(-8.3721090819477 0.248731027917601 -0.5)

(-8.37182801055224 0.248622876525208 -0.5)

(-8.37154035290283 0.248508071487621 -0.5)

(-8.37124599578807 0.248386378233916 -0.5)

(-8.37094482699704 0.24825755423553 -0.5)

(-8.37063673419819 0.248121348048402 -0.5)

(-8.37032160460183 0.247977498560805 -0.5)

(-8.36999932540366 0.247825734516858 -0.5)

(-8.36966978594438 0.247665774846509 -0.5)

(-8.36933287418533 0.24749732621436 -0.5)

(-8.36898848137544 0.247320084437347 -0.5)

(-8.36863650019058 0.247133732699416 -0.5)

(-8.36827682715711 0.246937941841638 -0.5)

(-8.36790936035701 0.246732368054993 -0.5)

(-8.36753400272009 0.246516653458788 -0.5)

(-8.36715066180968 0.246290424703022 -0.5)

(-8.36675925093285 0.246053292158786 -0.5)

(-8.36635965165795 0.245804910473173 -0.5)

(-8.36595168426281 0.245545020653005 -0.5)

(-8.36553526527261 0.245273199082607 -0.5)

(-8.36511032295657 0.244988996064756 -0.5)

(-8.36467679552467 0.24469194503368 -0.5)

(-8.36423462921295 0.244381559953946 -0.5)

(-8.36378378237113 0.244057336718455 -0.5)

(-8.36332422384215 0.243718750523655 -0.5)

(-8.36285593544174 0.243365255997819 -0.5)

(-8.36237891438037 0.242996287324681 -0.5)

(-8.36189317314569 0.242611256359404 -0.5)

(-8.36139874154006 0.242209552237037 -0.5)

(-8.3608956681089 0.241790540415892 -0.5)

(-8.36038402408006 0.241353563747867 -0.5)

(-8.35986390232424 0.240897939296455 -0.5)

(-8.35933515189779 0.24042325728728 -0.5)

(-8.35879712536315 0.239929633469568 -0.5)

(-8.35824974298226 0.239416524455073 -0.5)

(-8.35769296047605 0.238883341297694 -0.5)

(-8.35712673234783 0.23832948185235 -0.5)

(-8.35655101796567 0.23775433664983 -0.5)

(-8.35596577597207 0.237157283508211 -0.5)

(-8.35537096778789 0.236537691009824 -0.5)

(-8.35476655508191 0.235894915949351 -0.5)

(-8.35415250080892 0.235228304367246 -0.5)

(-8.35352877063491 0.234537193154769 -0.5)

(-8.35289532886278 0.23382090557582 -0.5)

(-8.35225199186749 0.233078886317846 -0.5)

(-8.3515979095616 0.232311125081335 -0.5)

(-8.3509330366762 0.231516898195215 -0.5)

(-8.3502574861349 0.230695334559651 -0.5)

(-8.34957139543107 0.229845543590979 -0.5)

(-8.34887492554905 0.228966612633771 -0.5)

(-8.34816826174027 0.228057606516789 -0.5)

(-8.34745161537413 0.227117568516514 -0.5)

(-8.34672522714041 0.226145523304775 -0.5)

(-8.34598936467425 0.225140472610231 -0.5)

(-8.34524432652735 0.224101399313675 -0.5)

(-8.34448951548243 0.223027915010725 -0.5)

(-8.34372410439055 0.221919758533297 -0.5)

(-8.34294811163305 0.220776053157115 -0.5)

(-8.34216155891688 0.219595908030335 -0.5)

(-8.34136447436683 0.218378422955346 -0.5)

(-8.3405568887911 0.217122682875631 -0.5)

(-8.33973883879556 0.215827762687283 -0.5)

(-8.33891036552361 0.21449272546762 -0.5)

(-8.33807151529742 0.213116623645191 -0.5)

(-8.33722188786999 0.211698766268032 -0.5)

(-8.33636030676964 0.210238902206005 -0.5)

(-8.33548698987699 0.208735928482631 -0.5)

(-8.33460227817102 0.207188668105133 -0.5)

(-8.33370654369926 0.205595928134032 -0.5)

(-8.33280019123367 0.203956502692542 -0.5)

(-8.33188365689134 0.202269170764376 -0.5)

(-8.33095740970025 0.200532699423908 -0.5)

(-8.33002176488187 0.198745942457491 -0.5)

(-8.32907448964191 0.196909065889102 -0.5)

(-8.32811531742853 0.195021182309838 -0.5)

(-8.32714498403046 0.193080889411496 -0.5)

(-8.32616428825371 0.191086766675639 -0.5)

(-8.32517409510703 0.189037379369643 -0.5)

(-8.32417533703625 0.186931279059451 -0.5)

(-8.32316901646861 0.184767007281874 -0.5)

(-8.32215511343268 0.18254359161835 -0.5)

(-8.32113079995821 0.180261322578713 -0.5)

(-8.32009655358296 0.177918965505967 -0.5)

(-8.31905322243179 0.175515137388725 -0.5)

(-8.318001711958 0.173048449698074 -0.5)

(-8.31694298838536 0.170517517228423 -0.5)

(-8.31587807636151 0.167920954040239 -0.5)

(-8.31480708596963 0.165257770651901 -0.5)

(-8.3137270166866 0.162528218741038 -0.5)

(-8.31263876049253 0.159730980865559 -0.5)

(-8.31154379106021 0.156864548878325 -0.5)

(-8.31044367185863 0.153927419583013 -0.5)

(-8.30934005820645 0.150918104276425 -0.5)

(-8.3082346950342 0.147835131481216 -0.5)

(-8.30712573777093 0.144678345961504 -0.5)

(-8.30601132369836 0.141447573896836 -0.5)

(-8.30489295891146 0.138141486510053 -0.5)

(-8.30377223075211 0.134758777832898 -0.5)

(-8.30265080732378 0.13129816935612 -0.5)

(-8.30153043738259 0.127758417362579 -0.5)

(-8.30041007754564 0.124139199008656 -0.5)

(-8.29928668320743 0.120440813978904 -0.5)

(-8.29816214290474 0.116662063610883 -0.5)

(-8.29703852594748 0.112801764329395 -0.5)

(-8.29591799418477 0.108858780047134 -0.5)

(-8.29480279437829 0.104832030501874 -0.5)

(-8.29369029637324 0.10072183298728 -0.5)

(-8.29257855233693 0.096528322500426 -0.5)

(-8.29147014578854 0.092250464286427 -0.5)

(-8.29036777934694 0.087887286320535 -0.5)

(-8.28927427114551 0.083437885454612 -0.5)

(-8.28819115909364 0.078901765081718 -0.5)

(-8.28711304259629 0.074280128163177 -0.5)

(-8.28604174203963 0.069572492262551 -0.5)

(-8.28498066277136 0.064778111580373 -0.5)

(-8.28393335628564 0.059896327036389 -0.5)

(-8.28290325945484 0.054926634793971 -0.5)

(-8.28188587734081 0.049870244296914 -0.5)

(-8.28088066246903 0.044727581794152 -0.5)

(-8.2798910082084 0.039498382939787 -0.5)

(-8.27892042417306 0.034182487444717 -0.5)

(-8.27797243282059 0.028779864467819 -0.5)

(-8.27704258631212 0.023291971737783 -0.5)

(-8.27612967753648 0.017719731093775 -0.5)

(-8.27523795123985 0.012063251962118 -0.5)

(-8.27437179929034 0.00632277418458 -0.5)

(-8.27353544227298 0.000498719996655 -0.5)

(-8.27272337126682 -0.005406996505319 -0.5)

(-8.27193480843159 -0.011393101728529 -0.5)

(-8.27117377273149 -0.017458864450118 -0.5)

(-8.27044440978902 -0.023603416708864 -0.5)

(-8.26974972557521 -0.029825605442997 -0.5)

(-8.26908394699701 -0.036123215127075 -0.5)

(-8.26844917664733 -0.042494837180984 -0.5)

(-8.26784982152966 -0.048939164060407 -0.5)

(-8.26729043131231 -0.05545473749258 -0.5)

(-8.26677197240896 -0.06203964650733 -0.5)

(-8.26629088721275 -0.068691554777032 -0.5)

(-8.26585156226328 -0.075408641706717 -0.5)

(-8.26545882026694 -0.082188949745603 -0.5)

(-8.26511727532891 -0.089030332628715 -0.5)

(-8.26482213800712 -0.095930072347821 -0.5)

(-8.2645735656737 -0.102885652491451 -0.5)

(-8.26437609575679 -0.109894613684361 -0.5)

(-8.26423434159408 -0.116954332264779 -0.5)

(-8.2641476853814 -0.124061955239068 -0.5)

(-8.26410675544705 -0.13121452210155 -0.5)

(-8.26411462437253 -0.138409198122927 -0.5)

(-8.26417502751345 -0.145643023353534 -0.5)

(-8.26429066342091 -0.152912916067383 -0.5)

(-8.26444984968484 -0.160216016061192 -0.5)

(-8.26465227200007 -0.167549299616655 -0.5)

(-8.26490318618236 -0.174909520291241 -0.5)

(-8.26520787511298 -0.182293284131445 -0.5)

(-8.26556203348981 -0.18969752251072 -0.5)

(-8.26595663704862 -0.197119443311992 -0.5)

(-8.26639646764915 -0.204555573028795 -0.5)

(-8.26688641796762 -0.212002318919003 -0.5)

(-8.26742828017211 -0.219456194364033 -0.5)

(-8.26800832949898 -0.226914872744194 -0.5)

(-8.26862675683781 -0.234375079363255 -0.5)

(-8.26928655751843 -0.241833278310264 -0.5)

(-8.26999060022465 -0.249285889974513 -0.5)

(-8.27073006919609 -0.256730459012549 -0.5)

(-8.27150032401227 -0.264164208979256 -0.5)

(-8.27230448354912 -0.271583607025896 -0.5)

(-8.27314566322603 -0.278985090336253 -0.5)

(-8.27402377610015 -0.286365440664063 -0.5)

(-8.27493062253916 -0.293722468896846 -0.5)

(-8.27586480398837 -0.301053245856701 -0.5)

(-8.27682551906669 -0.308354818780594 -0.5)

(-8.27781201842484 -0.315624270969094 -0.5)

(-8.27882311944897 -0.322858797499693 -0.5)

(-8.27985618873505 -0.330055856535489 -0.5)

(-8.28090842971459 -0.337213009832765 -0.5)

(-8.28197713713456 -0.344327885306416 -0.5)

(-8.28306243041575 -0.351397763915451 -0.5)

(-8.28416790575332 -0.358419434797931 -0.5)

(-8.28528916424503 -0.365391000798442 -0.5)

(-8.28642149441264 -0.372310725450879 -0.5)

(-8.28756045083174 -0.379176936739828 -0.5)

(-8.28871160511404 -0.385986378664073 -0.5)

(-8.28987604864817 -0.392736597293529 -0.5)

(-8.29104865220605 -0.399426292406931 -0.5)

(-8.29222442348577 -0.406054263481563 -0.5)

(-8.29340035490011 -0.412619070211612 -0.5)

(-8.29458515297811 -0.419117238100513 -0.5)

(-8.29577615439171 -0.425547423207767 -0.5)

(-8.29696798124201 -0.431908891572311 -0.5)

(-8.29815541892713 -0.438201000429567 -0.5)

(-8.29933670041207 -0.444422560604163 -0.5)

(-8.30051896774343 -0.4505707796095 -0.5)

(-8.30169944473347 -0.456644830380976 -0.5)

(-8.30287446930194 -0.462644172027677 -0.5)

(-8.30404050323696 -0.468568341162293 -0.5)

(-8.30519719892442 -0.474416337773804 -0.5)

(-8.30635005366236 -0.480186100180949 -0.5)

(-8.30749602470744 -0.48587733774617 -0.5)

(-8.3086315995495 -0.491489958136445 -0.5)

(-8.30975340901819 -0.497023934945273 -0.5)

(-8.31085970982077 -0.502479001573097 -0.5)

(-8.31195459824692 -0.507853789491829 -0.5)

(-8.31303726441034 -0.513148006553243 -0.5)

(-8.31410621015582 -0.518361583435075 -0.5)

(-8.31516000702175 -0.523494517364185 -0.5)

(-8.31619748138972 -0.528546830811729 -0.5)

(-8.31722097117024 -0.533517899082479 -0.5)

(-8.31823038231832 -0.538407669336836 -0.5)

(-8.31922416814522 -0.543216457055275 -0.5)

(-8.32020086431733 -0.547944633021747 -0.5)

(-8.32115909533459 -0.552592612392487 -0.5)

(-8.32209839019163 -0.55716068662139 -0.5)

(-8.32302030791928 -0.561648790237609 -0.5)

(-8.3239247063258 -0.566057266398791 -0.5)

(-8.32481134078032 -0.570386535208757 -0.5)

(-8.3256799983252 -0.574637063375817 -0.5)

(-8.32653049836447 -0.578809361274756 -0.5)

(-8.32736298016573 -0.582903920756654 -0.5)

(-8.32817783060233 -0.586921232739602 -0.5)

(-8.32897501569388 -0.590861915400926 -0.5)

(-8.32975451671157 -0.594726622060978 -0.5)

(-8.33051633858377 -0.598516044939773 -0.5)

(-8.33126050853485 -0.602230906327025 -0.5)

(-8.33198700171007 -0.605871969096137 -0.5)

(-8.3326958396634 -0.60944002092734 -0.5)

(-8.33338743284589 -0.612935803446995 -0.5)

(-8.33406220945738 -0.616360080281457 -0.5)

(-8.33472059476797 -0.619713640504838 -0.5)

(-8.33536301071511 -0.622997300249265 -0.5)

(-8.33598986553464 -0.626211898929173 -0.5)

(-8.33660090354483 -0.629358422778789 -0.5)

(-8.33719614843875 -0.632437824448272 -0.5)

(-8.3377760491741 -0.635450984829825 -0.5)

(-8.33834104868621 -0.638398804601084 -0.5)

(-8.33889158165835 -0.641282194694885 -0.5)

(-8.33942807529918 -0.644102082160142 -0.5)

(-8.33995094362039 -0.646859403172383 -0.5)

(-8.34045979667206 -0.649555253339525 -0.5)

(-8.34095460188267 -0.652190670042036 -0.5)

(-8.34143598259905 -0.654766563820563 -0.5)

(-8.34190454253642 -0.657283857550228 -0.5)

(-8.34236086475295 -0.659743482939252 -0.5)

(-8.34280551030793 -0.662146374755519 -0.5)

(-8.34323901789763 -0.664493469800159 -0.5)

(-8.34366176427566 -0.666785736497103 -0.5)

(-8.3440731430129 -0.669024320332645 -0.5)

(-8.3444733743301 -0.671210212317602 -0.5)

(-8.3448628934395 -0.673344358408779 -0.5)

(-8.34524212068253 -0.675427700781195 -0.5)

(-8.34561146223077 -0.677461181224715 -0.5)

(-8.34597130944146 -0.679445736973627 -0.5)

(-8.34632203879017 -0.681382299503326 -0.5)

(-8.34666401029973 -0.683271796322231 -0.5)

(-8.34699711741459 -0.685115229250438 -0.5)

(-8.34732131068068 -0.686913581657188 -0.5)

(-8.34763686169934 -0.688667768588416 -0.5)

(-8.34794403470574 -0.690378695132433 -0.5)

(-8.34824308702058 -0.692047258457648 -0.5)

(-8.34853426864975 -0.693674345068136 -0.5)

(-8.34881782226518 -0.695260830132538 -0.5)

(-8.34909398429325 -0.696807582982994 -0.5)

(-8.3493629827125 -0.698315454156297 -0.5)

(-8.34962490905667 -0.699785312145255 -0.5)

(-8.34987970743368 -0.701218038887605 -0.5)

(-8.35012759224993 -0.702614452230581 -0.5)

(-8.35036878137521 -0.703975358578843 -0.5)

(-8.35060348629635 -0.705301551911216 -0.5)

(-8.35083191211014 -0.706593813282869 -0.5)

(-8.35105425787848 -0.707852912356693 -0.5)

(-8.35127071657292 -0.709079606593893 -0.5)

(-8.35148147475483 -0.710274638921269 -0.5)

(-8.35168671390562 -0.711438744735808 -0.5)

(-8.35188658696469 -0.71257264522035 -0.5)

(-8.35208100824213 -0.713677088926301 -0.5)

(-8.35227008555047 -0.714752785903386 -0.5)

(-8.35245399696919 -0.715800411043092 -0.5)

(-8.35263291542433 -0.716820630716096 -0.5)

(-8.35280700793118 -0.717814097703092 -0.5)

(-8.3529764361941 -0.718781453860883 -0.5)

(-8.35314135619808 -0.719723327050421 -0.5)

(-8.35330191889584 -0.720640334331169 -0.5)

(-8.35345826995332 -0.721533079794635 -0.5)

(-8.35361054996442 -0.722402155092405 -0.5)

(-8.35375889487283 -0.723248141161244 -0.5)

(-8.35390343189356 -0.724071607089565 -0.5)

(-8.35404423213731 -0.72487311815722 -0.5)

(-8.35418136040267 -0.725653231120878 -0.5)

(-8.3543148866421 -0.726412485915511 -0.5)

(-8.35444488091299 -0.727151414280863 -0.5)

(-8.35457141216242 -0.727870533179287 -0.5)

(-8.35469454894424 -0.728570349194787 -0.5)

(-8.35481435917091 -0.729251357437339 -0.5)

(-8.35493091001102 -0.729914041268224 -0.5)

(-8.35504426804094 -0.730558873463238 -0.5)

(-8.35515449907018 -0.731186315513334 -0.5)

(-8.35526166802767 -0.731796817262377 -0.5)

(-8.3553658395317 -0.732390820433547 -0.5)

(-8.35546707705349 -0.732968754136912 -0.5)

(-8.35556544010471 -0.733531038158546 -0.5)

(-8.35566097801937 -0.734078084629199 -0.5)

(-8.35575377795762 -0.734610288260487 -0.5)

(-8.35584393168631 -0.7351280342258 -0.5)

(-8.35593152839672 -0.735631697603557 -0.5)

(-8.35601665485374 -0.736121644783938 -0.5)

(-8.35609939530955 -0.736598233527198 -0.5)

(-8.35617983094819 -0.737061810302958 -0.5)

(-8.35625804154038 -0.737512720343602 -0.5)

(-8.35633410299124 -0.737951293984435 -0.5)

(-8.35640808876222 -0.738377855277996 -0.5)

(-8.35648006959045 -0.738792720731389 -0.5)

(-8.35655011338287 -0.739196198972782 -0.5)

(-8.35661828530552 -0.739588591456575 -0.5)

(-8.35668464764707 -0.739970191775979 -0.5)

(-8.35674926000906 -0.740341286761939 -0.5)

(-8.35681217942061 -0.740702157046518 -0.5)

(-8.35687346839102 -0.741053071165513 -0.5)

(-8.35693317510435 -0.741394298260069 -0.5)

(-8.35699132455196 -0.741726101429318 -0.5)

(-8.35704794456748 -0.742048736887733 -0.5)

(-8.35710306493045 -0.742362453944258 -0.5)

(-8.35715671662235 -0.742667495155667 -0.5)

(-8.35720893137052 -0.74296409691224 -0.5)

(-8.35725974094297 -0.743252487817828 -0.5)

(-8.35730917761629 -0.74353289320724 -0.5)

(-8.35735727286299 -0.743805529224274 -0.5)

(-8.35740405812318 -0.744070608545183 -0.5)

(-8.35744956412182 -0.744328337810302 -0.5)

(-8.35749382064761 -0.744578917809355 -0.5)

(-8.35753685644943 -0.744822544730908 -0.5)

(-8.35757869850627 -0.74505940876099 -0.5)

(-8.35761937145878 -0.7452896955803 -0.5)

(-8.35765889632797 -0.745513588574931 -0.5)

(-8.35769728567811 -0.745731264178422 -0.5)

(-8.3577345325556 -0.745942900362941 -0.5)

(-8.35777057590715 -0.74614867872699 -0.5)

(-8.35780570724381 -0.746348714220394 -0.5)

(-8.35784002834788 -0.746543151584032 -0.5)
(-8.3578734755788 -0.74673215921398 -0.5)
(-8.35790598836131 -0.746915901353046 -0.5)
(-8.35793751363057 -0.747094536671585 -0.5)
(-8.35796800967729 -0.747268218122699 -0.5)
(-8.35799744845614 -0.747437091921029 -0.5)
(-8.35802581646783 -0.747601297537403 -0.5)
(-8.35805311439012 -0.747760969041651 -0.5)
(-8.35807935449261 -0.747916229927685 -0.5)
(-8.35810466569758 -0.748067193148965 -0.5)
(-8.35812931595065 -0.748213928632773 -0.5)
(-8.35815331720457 -0.748356559945585 -0.5)
(-8.35817666988747 -0.748495199938529 -0.5)
(-8.35819937729405 -0.748629963066258 -0.5)
(-8.35822144405114 -0.748760957447563 -0.5)
(-8.35824287721762 -0.748888292598408 -0.5)
(-8.35826368429133 -0.749012068794738 -0.5)
(-8.35828387480015 -0.749132387695882 -0.5)
(-8.35830345874186 -0.749249344196394 -0.5)
(-8.35832244797978 -0.74936303583738 -0.5)
(-8.35834085411957 -0.749473551143853 -0.5)
(-8.35835869021854 -0.749580980807113 -0.5)
(-8.35837596938744 -0.749685410189008 -0.5)
(-8.35839270510961 -0.749786922034931 -0.5)
(-8.35840891189491 -0.74988560120633 -0.5)

)

spline 5 6
(
(-8.37894171960202 0.250255197449192 0.5)

(-8.37884193993624 0.250248564489101 0.5)

(-8.37873932024441 0.250241205150188 0.5)

(-8.37863378414245 0.250233070692358 0.5)

(-8.37852525330924 0.250224109726248 0.5)

(-8.37841364917743 0.25021426825557 0.5)

(-8.37829888817902 0.250203489153055 0.5)

(-8.37818088888536 0.250191712691689 0.5)

(-8.37805956551823 0.250178875846078 0.5)

(-8.37793483221341 0.250164912597108 0.5)

(-8.37780659977325 0.250149753482448 0.5)

(-8.37767477781362 0.250133325715004 0.5)

(-8.37753927648132 0.250115553327037 0.5)

(-8.37740000072202 0.250096356335079 0.5)

(-8.37725685518865 0.250075651251184 0.5)

(-8.3771097429812 0.250053350840249 0.5)

(-8.37695856674061 0.250029364212024 0.5)

(-8.37680322360379 0.250003595925253 0.5)

(-8.37664361399536 0.249975947323361 0.5)

(-8.37647963215503 0.24994631489748 0.5)

(-8.37631117251404 0.249914591275328 0.5)

(-8.3761381289102 0.249880665075739 0.5)

(-8.37596039086036 0.249844420126391 0.5)

(-8.37577784841121 0.249805736365264 0.5)

(-8.37559038943772 0.249764489292975 0.5)

(-8.37539789755837 0.249720549449269 0.5)

(-8.3752002586779 0.249673783873211 0.5)

(-8.37499735343043 0.249624054390965 0.5)

(-8.37478906183651 0.249571218683612 0.5)

(-8.37457526236253 0.249515130115072 0.5)

(-8.37435582981589 0.249455637206666 0.5)

(-8.37413064001265 0.249392584942022 0.5)

(-8.37389956280155 0.249325812921804 0.5)

(-8.37366246930214 0.249255157459657 0.5)

(-8.37341922583286 0.249180449940677 0.5)

(-8.37316969755065 0.249101517982569 0.5)

(-8.37291387922751 0.24901777906475 0.5)

(-8.3726519065119 0.248928264570553 0.5)

(-8.37238367744094 0.248832751275514 0.5)

(-8.3721090819477 0.248731027917601 0.5)

(-8.37182801055224 0.248622876525208 0.5)

(-8.37154035290283 0.248508071487621 0.5)

(-8.37124599578807 0.248386378233916 0.5)

(-8.37094482699704 0.24825755423553 0.5)

(-8.37063673419819 0.248121348048402 0.5)

(-8.37032160460183 0.247977498560805 0.5)

(-8.36999932540366 0.247825734516858 0.5)

(-8.36966978594438 0.247665774846509 0.5)

(-8.36933287418533 0.24749732621436 0.5)

(-8.36898848137544 0.247320084437347 0.5)

(-8.36863650019058 0.247133732699416 0.5)

(-8.36827682715711 0.246937941841638 0.5)

(-8.36790936035701 0.246732368054993 0.5)

(-8.36753400272009 0.246516653458788 0.5)

(-8.36715066180968 0.246290424703022 0.5)

(-8.36675925093285 0.246053292158786 0.5)

(-8.36635965165795 0.245804910473173 0.5)

(-8.36595168426281 0.245545020653005 0.5)

(-8.36553526527261 0.245273199082607 0.5)

(-8.36511032295657 0.244988996064756 0.5)

(-8.36467679552467 0.24469194503368 0.5)

(-8.36423462921295 0.244381559953946 0.5)

(-8.36378378237113 0.244057336718455 0.5)

(-8.36332422384215 0.243718750523655 0.5)
(-8.36285593544174 0.243365255997819 0.5)
(-8.36237891438037 0.242996287324681 0.5)
(-8.36189317314569 0.242611256359404 0.5)
(-8.36139874154006 0.242209552237037 0.5)
(-8.3608956681089 0.241790540415892 0.5)
(-8.36038402408006 0.241353563747867 0.5)
(-8.35986390232424 0.240897939296455 0.5)
(-8.35933515189779 0.24042325728728 0.5)
(-8.35879712536315 0.239929633469568 0.5)
(-8.35824974298226 0.239416524455073 0.5)
(-8.35769296047605 0.238883341297694 0.5)
(-8.35712673234783 0.23832948185235 0.5)
(-8.35655101796567 0.23775433664983 0.5)
(-8.35596577597207 0.237157283508211 0.5)
(-8.35537096778789 0.236537691009824 0.5)
(-8.35476655508191 0.235894915949351 0.5)
(-8.35415250080892 0.235228304367246 0.5)
(-8.35352877063491 0.234537193154769 0.5)
(-8.35289532886278 0.23382090557582 0.5)
(-8.35225199186749 0.233078886317846 0.5)
(-8.3515979095616 0.232311125081335 0.5)
(-8.3509330366762 0.231516898195215 0.5)
(-8.3502574861349 0.230695334559651 0.5)
(-8.34957139543107 0.229845543590979 0.5)
(-8.34887492554905 0.228966612633771 0.5)
(-8.34816826174027 0.228057606516789 0.5)
(-8.34745161537413 0.227117568516514 0.5)
(-8.34672522714041 0.226145523304775 0.5)
(-8.34598936467425 0.225140472610231 0.5)
(-8.34524432652735 0.224101399313675 0.5)

(-8.34448951548243 0.223027915010725 0.5)

(-8.34372410439055 0.221919758533297 0.5)

(-8.34294811163305 0.220776053157115 0.5)

(-8.34216155891688 0.219595908030335 0.5)

(-8.34136447436683 0.218378422955346 0.5)

(-8.3405568887911 0.217122682875631 0.5)

(-8.33973883879556 0.215827762687283 0.5)

(-8.33891036552361 0.21449272546762 0.5)

(-8.33807151529742 0.213116623645191 0.5)

(-8.33722188786999 0.211698766268032 0.5)

(-8.33636030676964 0.210238902206005 0.5)

(-8.33548698987699 0.208735928482631 0.5)

(-8.33460227817102 0.207188668105133 0.5)

(-8.33370654369926 0.205595928134032 0.5)

(-8.33280019123367 0.203956502692542 0.5)

(-8.33188365689134 0.202269170764376 0.5)

(-8.33095740970025 0.200532699423908 0.5)

(-8.33002176488187 0.198745942457491 0.5)

(-8.32907448964191 0.196909065889102 0.5)

(-8.32811531742853 0.195021182309838 0.5)

(-8.32714498403046 0.193080889411496 0.5)

(-8.32616428825371 0.191086766675639 0.5)

(-8.32517409510703 0.189037379369643 0.5)

(-8.32417533703625 0.186931279059451 0.5)

(-8.32316901646861 0.184767007281874 0.5)

(-8.32215511343268 0.18254359161835 0.5)

(-8.32113079995821 0.180261322578713 0.5)

(-8.32009655358296 0.177918965505967 0.5)

(-8.31905322243179 0.175515137388725 0.5)

(-8.318001711958 0.173048449698074 0.5)

(-8.31694298838536 0.170517517228423 0.5)

(-8.31587807636151 0.167920954040239 0.5)
(-8.31480708596963 0.165257770651901 0.5)
(-8.3137270166866 0.162528218741038 0.5)
(-8.31263876049253 0.159730980865559 0.5)
(-8.31154379106021 0.156864548878325 0.5)
(-8.31044367185863 0.153927419583013 0.5)
(-8.30934005820645 0.150918104276425 0.5)
(-8.3082346950342 0.147835131481216 0.5)
(-8.30712573777093 0.144678345961504 0.5)
(-8.30601132369836 0.141447573896836 0.5)
(-8.30489295891146 0.138141486510053 0.5)
(-8.30377223075211 0.134758777832898 0.5)
(-8.30265080732378 0.13129816935612 0.5)
(-8.30153043738259 0.127758417362579 0.5)
(-8.30041007754564 0.124139199008656 0.5)
(-8.29928668320743 0.120440813978904 0.5)
(-8.29816214290474 0.116662063610883 0.5)
(-8.29703852594748 0.112801764329395 0.5)
(-8.29591799418477 0.108858780047134 0.5)
(-8.29480279437829 0.104832030501874 0.5)
(-8.29369029637324 0.10072183298728 0.5)
(-8.29257855233693 0.096528322500426 0.5)
(-8.29147014578854 0.092250464286427 0.5)
(-8.29036777934694 0.087887286320535 0.5)
(-8.28927427114551 0.083437885454612 0.5)
(-8.28819115909364 0.078901765081718 0.5)
(-8.28711304259629 0.074280128163177 0.5)
(-8.28604174203963 0.069572492262551 0.5)
(-8.28498066277136 0.064778111580373 0.5)
(-8.28393335628564 0.059896327036389 0.5)
(-8.28290325945484 0.054926634793971 0.5)

(-8.28188587734081 0.049870244296914 0.5)

(-8.28088066246903 0.044727581794152 0.5)

(-8.2798910082084 0.039498382939787 0.5)

(-8.27892042417306 0.034182487444717 0.5)

(-8.27797243282059 0.028779864467819 0.5)

(-8.27704258631212 0.023291971737783 0.5)

(-8.27612967753648 0.017719731093775 0.5)

(-8.27523795123985 0.012063251962118 0.5)

(-8.27437179929034 0.00632277418458 0.5)

(-8.27353544227298 0.000498719996655 0.5)

(-8.27272337126682 -0.005406996505319 0.5)

(-8.27193480843159 -0.011393101728529 0.5)

(-8.27117377273149 -0.017458864450118 0.5)

(-8.27044440978902 -0.023603416708864 0.5)

(-8.26974972557521 -0.029825605442997 0.5)

(-8.26908394699701 -0.036123215127075 0.5)

(-8.26844917664733 -0.042494837180984 0.5)

(-8.26784982152966 -0.048939164060407 0.5)

(-8.26729043131231 -0.05545473749258 0.5)

(-8.26677197240896 -0.06203964650733 0.5)

(-8.26629088721275 -0.068691554777032 0.5)

(-8.26585156226328 -0.075408641706717 0.5)

(-8.26545882026694 -0.082188949745603 0.5)

(-8.26511727532891 -0.089030332628715 0.5)

(-8.26482213800712 -0.095930072347821 0.5)

(-8.2645735656737 -0.102885652491451 0.5)

(-8.26437609575679 -0.109894613684361 0.5)

(-8.26423434159408 -0.116954332264779 0.5)

(-8.2641476853814 -0.124061955239068 0.5)

(-8.26410675544705 -0.13121452210155 0.5)

(-8.26411462437253 -0.138409198122927 0.5)

(-8.26417502751345 -0.145643023353534 0.5)

(-8.26429066342091 -0.152912916067383 0.5)

(-8.26444984968484 -0.160216016061192 0.5)

(-8.26465227200007 -0.167549299616655 0.5)

(-8.26490318618236 -0.174909520291241 0.5)

(-8.26520787511298 -0.182293284131445 0.5)

(-8.26556203348981 -0.18969752251072 0.5)

(-8.26595663704862 -0.197119443311992 0.5)

(-8.26639646764915 -0.204555573028795 0.5)

(-8.26688641796762 -0.212002318919003 0.5)

(-8.26742828017211 -0.219456194364033 0.5)

(-8.26800832949898 -0.226914872744194 0.5)

(-8.26862675683781 -0.234375079363255 0.5)

(-8.26928655751843 -0.241833278310264 0.5)

(-8.26999060022465 -0.249285889974513 0.5)

(-8.27073006919609 -0.256730459012549 0.5)

(-8.27150032401227 -0.264164208979256 0.5)

(-8.27230448354912 -0.271583607025896 0.5)

(-8.27314566322603 -0.278985090336253 0.5)

(-8.27402377610015 -0.286365440664063 0.5)

(-8.27493062253916 -0.293722468896846 0.5)

(-8.27586480398837 -0.301053245856701 0.5)

(-8.27682551906669 -0.308354818780594 0.5)

(-8.27781201842484 -0.315624270969094 0.5)

(-8.27882311944897 -0.322858797499693 0.5)

(-8.27985618873505 -0.330055856535489 0.5)

(-8.28090842971459 -0.337213009832765 0.5)

(-8.28197713713456 -0.344327885306416 0.5)

(-8.28306243041575 -0.351397763915451 0.5)

(-8.28416790575332 -0.358419434797931 0.5)

(-8.28528916424503 -0.365391000798442 0.5)

(-8.28642149441264 -0.372310725450879 0.5)
(-8.28756045083174 -0.379176936739828 0.5)
(-8.28871160511404 -0.385986378664073 0.5)
(-8.28987604864817 -0.392736597293529 0.5)
(-8.29104865220605 -0.399426292406931 0.5)
(-8.29222442348577 -0.406054263481563 0.5)
(-8.29340035490011 -0.412619070211612 0.5)
(-8.29458515297811 -0.419117238100513 0.5)
(-8.29577615439171 -0.425547423207767 0.5)
(-8.29696798124201 -0.431908891572311 0.5)
(-8.29815541892713 -0.438201000429567 0.5)
(-8.29933670041207 -0.444422560604163 0.5)
(-8.30051896774343 -0.4505707796095 0.5)
(-8.30169944473347 -0.456644830380976 0.5)
(-8.30287446930194 -0.462644172027677 0.5)
(-8.30404050323696 -0.468568341162293 0.5)
(-8.30519719892442 -0.474416337773804 0.5)
(-8.30635005366236 -0.480186100180949 0.5)
(-8.30749602470744 -0.48587733774617 0.5)
(-8.3086315995495 -0.491489958136445 0.5)
(-8.30975340901819 -0.497023934945273 0.5)
(-8.31085970982077 -0.502479001573097 0.5)
(-8.31195459824692 -0.507853789491829 0.5)
(-8.31303726441034 -0.513148006553243 0.5)
(-8.31410621015582 -0.518361583435075 0.5)
(-8.31516000702175 -0.523494517364185 0.5)
(-8.31619748138972 -0.528546830811729 0.5)
(-8.31722097117024 -0.533517899082479 0.5)
(-8.31823038231832 -0.538407669336836 0.5)
(-8.31922416814522 -0.543216457055275 0.5)
(-8.32020086431733 -0.547944633021747 0.5)

(-8.32115909533459 -0.552592612392487 0.5)
(-8.32209839019163 -0.55716068662139 0.5)
(-8.32302030791928 -0.561648790237609 0.5)
(-8.3239247063258 -0.566057266398791 0.5)
(-8.32481134078032 -0.570386535208757 0.5)
(-8.3256799983252 -0.574637063375817 0.5)
(-8.32653049836447 -0.578809361274756 0.5)
(-8.32736298016573 -0.582903920756654 0.5)
(-8.32817783060233 -0.586921232739602 0.5)
(-8.32897501569388 -0.590861915400926 0.5)
(-8.32975451671157 -0.594726622060978 0.5)
(-8.33051633858377 -0.598516044939773 0.5)
(-8.33126050853485 -0.602230906327025 0.5)
(-8.33198700171007 -0.605871969096137 0.5)
(-8.3326958396634 -0.60944002092734 0.5)
(-8.33338743284589 -0.612935803446995 0.5)
(-8.33406220945738 -0.616360080281457 0.5)
(-8.33472059476797 -0.619713640504838 0.5)
(-8.33536301071511 -0.622997300249265 0.5)
(-8.33598986553464 -0.626211898929173 0.5)
(-8.33660090354483 -0.629358422778789 0.5)
(-8.33719614843875 -0.632437824448272 0.5)
(-8.3377760491741 -0.635450984829825 0.5)
(-8.33834104868621 -0.638398804601084 0.5)
(-8.33889158165835 -0.641282194694885 0.5)
(-8.33942807529918 -0.644102082160142 0.5)
(-8.33995094362039 -0.646859403172383 0.5)
(-8.34045979667206 -0.649555253339525 0.5)
(-8.34095460188267 -0.652190670042036 0.5)
(-8.34143598259905 -0.654766563820563 0.5)
(-8.34190454253642 -0.657283857550228 0.5)

(-8.34236086475295 -0.659743482939252 0.5)

(-8.34280551030793 -0.662146374755519 0.5)

(-8.34323901789763 -0.664493469800159 0.5)

(-8.34366176427566 -0.666785736497103 0.5)

(-8.3440731430129 -0.669024320332645 0.5)

(-8.3444733743301 -0.671210212317602 0.5)

(-8.3448628934395 -0.673344358408779 0.5)

(-8.34524212068253 -0.675427700781195 0.5)

(-8.34561146223077 -0.677461181224715 0.5)

(-8.34597130944146 -0.679445736973627 0.5)

(-8.34632203879017 -0.681382299503326 0.5)

(-8.34666401029973 -0.683271796322231 0.5)

(-8.34699711741459 -0.685115229250438 0.5)

(-8.34732131068068 -0.686913581657188 0.5)

(-8.34763686169934 -0.688667768588416 0.5)

(-8.34794403470574 -0.690378695132433 0.5)

(-8.34824308702058 -0.692047258457648 0.5)

(-8.34853426864975 -0.693674345068136 0.5)

(-8.34881782226518 -0.695260830132538 0.5)

(-8.34909398429325 -0.696807582982994 0.5)

(-8.3493629827125 -0.698315454156297 0.5)

(-8.34962490905667 -0.699785312145255 0.5)

(-8.34987970743368 -0.701218038887605 0.5)

(-8.35012759224993 -0.702614452230581 0.5)

(-8.35036878137521 -0.703975358578843 0.5)

(-8.35060348629635 -0.705301551911216 0.5)

(-8.35083191211014 -0.706593813282869 0.5)

(-8.35105425787848 -0.707852912356693 0.5)

(-8.35127071657292 -0.709079606593893 0.5)

(-8.35148147475483 -0.710274638921269 0.5)

(-8.35168671390562 -0.711438744735808 0.5)

(-8.35188658696469 -0.71257264522035 0.5)
(-8.35208100824213 -0.713677088926301 0.5)
(-8.35227008555047 -0.714752785903386 0.5)
(-8.35245399696919 -0.715800411043092 0.5)
(-8.35263291542433 -0.716820630716096 0.5)
(-8.35280700793118 -0.717814097703092 0.5)
(-8.3529764361941 -0.718781453860883 0.5)
(-8.35314135619808 -0.719723327050421 0.5)
(-8.35330191889584 -0.720640334331169 0.5)
(-8.35345826995332 -0.721533079794635 0.5)
(-8.35361054996442 -0.722402155092405 0.5)
(-8.35375889487283 -0.723248141161244 0.5)
(-8.35390343189356 -0.724071607089565 0.5)
(-8.35404423213731 -0.72487311815722 0.5)
(-8.35418136040267 -0.725653231120878 0.5)
(-8.3543148866421 -0.726412485915511 0.5)
(-8.35444488091299 -0.727151414280863 0.5)
(-8.35457141216242 -0.727870533179287 0.5)
(-8.35469454894424 -0.728570349194787 0.5)
(-8.35481435917091 -0.729251357437339 0.5)
(-8.35493091001102 -0.729914041268224 0.5)
(-8.35504426804094 -0.730558873463238 0.5)
(-8.35515449907018 -0.731186315513334 0.5)
(-8.35526166802767 -0.731796817262377 0.5)
(-8.3553658395317 -0.732390820433547 0.5)
(-8.35546707705349 -0.732968754136912 0.5)
(-8.35556544010471 -0.733531038158546 0.5)
(-8.35566097801937 -0.734078084629199 0.5)
(-8.35575377795762 -0.734610288260487 0.5)
(-8.35584393168631 -0.7351280342258 0.5)
(-8.35593152839672 -0.735631697603557 0.5)

(-8.35601665485374 -0.736121644783938 0.5)

(-8.35609939530955 -0.736598233527198 0.5)

(-8.35617983094819 -0.737061810302958 0.5)

(-8.35625804154038 -0.737512720343602 0.5)

(-8.35633410299124 -0.737951293984435 0.5)

(-8.35640808876222 -0.738377855277996 0.5)

(-8.35648006959045 -0.738792720731389 0.5)

(-8.35655011338287 -0.739196198972782 0.5)

(-8.35661828530552 -0.739588591456575 0.5)

(-8.35668464764707 -0.739970191775979 0.5)

(-8.35674926000906 -0.740341286761939 0.5)

(-8.35681217942061 -0.740702157046518 0.5)

(-8.35687346839102 -0.741053071165513 0.5)

(-8.35693317510435 -0.741394298260069 0.5)

(-8.35699132455196 -0.741726101429318 0.5)

(-8.35704794456748 -0.742048736887733 0.5)

(-8.35710306493045 -0.742362453944258 0.5)

(-8.35715671662235 -0.742667495155667 0.5)

(-8.35720893137052 -0.74296409691224 0.5)

(-8.35725974094297 -0.743252487817828 0.5)

(-8.35730917761629 -0.74353289320724 0.5)

(-8.35735727286299 -0.743805529224274 0.5)

(-8.35740405812318 -0.744070608545183 0.5)

(-8.35744956412182 -0.744328337810302 0.5)

(-8.35749382064761 -0.744578917809355 0.5)

(-8.35753685644943 -0.744822544730908 0.5)

(-8.35757869850627 -0.74505940876099 0.5)

(-8.35761937145878 -0.7452896955803 0.5)

(-8.35765889632797 -0.745513588574931 0.5)

(-8.35769728567811 -0.745731264178422 0.5)

(-8.3577345325556 -0.745942900362941 0.5)

(-8.35777057590715 -0.74614867872699 0.5)
(-8.35780570724381 -0.746348714220394 0.5)
(-8.35784002834788 -0.746543151584032 0.5)
(-8.3578734755788 -0.74673215921398 0.5)
(-8.35790598836131 -0.746915901353046 0.5)
(-8.35793751363057 -0.747094536671585 0.5)
(-8.35796800967729 -0.747268218122699 0.5)
(-8.35799744845614 -0.747437091921029 0.5)
(-8.35802581646783 -0.747601297537403 0.5)
(-8.35805311439012 -0.747760969041651 0.5)
(-8.35807935449261 -0.747916229927685 0.5)
(-8.35810466569758 -0.748067193148965 0.5)
(-8.35812931595065 -0.748213928632773 0.5)
(-8.35815331720457 -0.748356559945585 0.5)
(-8.35817666988747 -0.748495199938529 0.5)
(-8.35819937729405 -0.748629963066258 0.5)
(-8.35822144405114 -0.748760957447563 0.5)
(-8.35824287721762 -0.748888292598408 0.5)
(-8.35826368429133 -0.749012068794738 0.5)
(-8.35828387480015 -0.749132387695882 0.5)
(-8.35830345874186 -0.749249344196394 0.5)
(-8.35832244797978 -0.74936303583738 0.5)
(-8.35834085411957 -0.749473551143853 0.5)
(-8.35835869021854 -0.749580980807113 0.5)
(-8.35837596938744 -0.749685410189008 0.5)
(-8.35839270510961 -0.749786922034931 0.5)
(-8.35840891189491 -0.74988560120633 0.5)

)

// Pressure Side splines.

```
spline 1 8
(
    ( -8.37894171960202 0.250255197449192 -0.5 )
    ( -8.37904152308974 0.250261450830106 -0.5 )
    ( -8.37914421412417 0.250267622735631 -0.5 )
    ( -8.37924987360825 0.250273684937805 -0.5 )
    ( -8.37935858780945 0.250279606065593 -0.5 )
    ( -8.37947044360183 0.250285350971339 -0.5 )
    ( -8.37958553437967 0.250290880643862 -0.5 )
    ( -8.37970394885552 0.250296151227076 -0.5 )
    ( -8.37982578372649 0.250301114166131 -0.5 )
    ( -8.3799511362434  0.250305715318301 -0.5 )
    ( -8.38008010648178 0.250309894476334 -0.5 )
    ( -8.38021279597391 0.250313584679504 -0.5 )
    ( -8.38034930763761 0.25031671152019  -0.5 )
    ( -8.3804897517188  0.250319192468196 -0.5 )
    ( -8.38063423331904 0.250320935736951 -0.5 )
    ( -8.38078286562624 0.250321839559597 -0.5 )
    ( -8.38093575947653 0.25032179095893  -0.5 )
    ( -8.38109302957309 0.250320664615839 -0.5 )
    ( -8.38125479014613 0.250318321535566 -0.5 )
    ( -8.38142115947044 0.250314607513846 -0.5 )
    ( -8.38159225158028 0.250309351650886 -0.5 )
    ( -8.38176818266505 0.250302364444167 -0.5 )
    ( -8.38194906815415 0.250293435820051 -0.5 )
    ( -8.38213502091979 0.250282332998768 -0.5 )
    ( -8.38232614991771 0.250268798157836 -0.5 )
    ( -8.38252255976752 0.250252545796246 -0.5 )
    ( -8.38272434878413 0.250233259940668 -0.5 )
    ( -8.38293160960343 0.250210590815463 -0.5 )
```

(-8.38314441652525 0.250184152767448 -0.5)

(-8.38336284160036 0.250153518649716 -0.5)

(-8.38358692690054 0.250118219392034 -0.5)

(-8.38381670156718 0.250077737673882 -0.5)

(-8.38405216405726 0.250031506354649 -0.5)

(-8.38429328240747 0.249978904390299 -0.5)

(-8.384540052197 0.249919529544771 -0.5)

(-8.3847926541221 0.249853731491905 -0.5)

(-8.38505118295575 0.249781408657868 -0.5)

(-8.38531572755064 0.24970243838043 -0.5)

(-8.38558639796054 0.249616715773944 -0.5)

(-8.38586331671523 0.249524158967461 -0.5)

(-8.3861466288423 0.249424709231785 -0.5)

(-8.38643650038515 0.249318335283289 -0.5)

(-8.38673311731824 0.249205038660083 -0.5)

(-8.38703670179125 0.249084853506016 -0.5)

(-8.38734750425147 0.248957856712965 -0.5)

(-8.38766581024336 0.248824174526771 -0.5)

(-8.38799195151288 0.24868398941746 -0.5)

(-8.38832630873016 0.248537553414795 -0.5)

(-8.38866931415623 0.248385205734738 -0.5)

(-8.3890214644481 0.248227391329751 -0.5)

(-8.38938316790398 0.248064314332636 -0.5)

(-8.38975219535566 0.247890468749519 -0.5)

(-8.39012716261966 0.247702605594116 -0.5)

(-8.3905073913448 0.247499276837684 -0.5)

(-8.39089228897301 0.247279381912776 -0.5)

(-8.39128152525235 0.247042369902684 -0.5)

(-8.39167517438115 0.246788349994323 -0.5)

(-8.39207377646566 0.246518039133364 -0.5)

(-8.39247827729614 0.246232573222964 -0.5)

(-8.39288988277056 0.24593326589123 -0.5)

(-8.39330989336269 0.245621403563077 -0.5)

(-8.3937384329144 0.245296610416161 -0.5)

(-8.39417313642185 0.244955288728504 -0.5)

(-8.39461424573402 0.244597343316857 -0.5)

(-8.39506195596033 0.244222585947669 -0.5)

(-8.39551627992097 0.243830586664185 -0.5)

(-8.39597707297005 0.243420727848152 -0.5)

(-8.39644403376382 0.242992226054294 -0.5)

(-8.39691668704786 0.242544137040968 -0.5)

(-8.39739435626459 0.242075343852654 -0.5)

(-8.39787611268298 0.241584540591842 -0.5)

(-8.39836071006323 0.241070198407654 -0.5)

(-8.3988464804737 0.240530527568341 -0.5)

(-8.39933151502692 0.239963688336894 -0.5)

(-8.39982167713789 0.239374395632868 -0.5)

(-8.40031970789535 0.238764402819878 -0.5)

(-8.40082505194485 0.238132654206962 -0.5)

(-8.40133710147157 0.237478071997518 -0.5)

(-8.40185520048792 0.236799562568428 -0.5)

(-8.40237864836005 0.236096025615656 -0.5)

(-8.4029067074523 0.235366359483275 -0.5)

(-8.40343860799291 0.234609471385498 -0.5)

(-8.40397355566969 0.233824284868978 -0.5)

(-8.40451074127568 0.233009744433786 -0.5)

(-8.40504971249514 0.232165047849994 -0.5)

(-8.40559225414552 0.231290791657989 -0.5)

(-8.40613860631384 0.230386526576562 -0.5)

(-8.40668861195109 0.229451541915489 -0.5)

(-8.4072421168451 0.228485117193937 -0.5)

(-8.40779896672908 0.227486527305938 -0.5)

(-8.40835901046455 0.226455037183247 -0.5)

(-8.40892209835232 0.225389904871685 -0.5)

(-8.40948808444155 0.224290377236923 -0.5)

(-8.41005682298604 0.223155696776757 -0.5)

(-8.41062854366861 0.221985274555304 -0.5)

(-8.41120372591274 0.220778618245588 -0.5)

(-8.41178223642076 0.219534921087634 -0.5)

(-8.41236393013788 0.21825335879007 -0.5)

(-8.41294865880097 0.216933096159951 -0.5)

(-8.41353627095219 0.215573286939181 -0.5)

(-8.41412661092016 0.214173076102456 -0.5)

(-8.41471952077859 0.212731595179425 -0.5)

(-8.41531484455593 0.211247970211485 -0.5)

(-8.41591333996904 0.209721673202788 -0.5)

(-8.41651537473563 0.208151997604236 -0.5)

(-8.41712059980646 0.206537943956458 -0.5)

(-8.41772865333535 0.204878506125823 -0.5)

(-8.41833916170516 0.203172670023562 -0.5)

(-8.41895173881376 0.201419417162318 -0.5)

(-8.41956598762229 0.19961772200859 -0.5)

(-8.4201814991512 0.197766558200244 -0.5)

(-8.42079910133849 0.195865295604197 -0.5)

(-8.42141952887001 0.193913248123457 -0.5)

(-8.42204234856922 0.191909344614315 -0.5)

(-8.4226671099949 0.18985250779353 -0.5)

(-8.42329334409151 0.187741660153614 -0.5)

(-8.42392056465886 0.185575720931497 -0.5)

(-8.42454826873022 0.183353606553294 -0.5)

(-8.42517641307936 0.181074368572143 -0.5)

(-8.42580690533314 0.178737579958931 -0.5)

(-8.4264393906267 0.176342179685822 -0.5)

(-8.42707310954994 0.173887010405636 -0.5)

(-8.42770726976089 0.171370913041936 -0.5)

(-8.42834104371212 0.168792739550283 -0.5)

(-8.42897357090526 0.166151348820516 -0.5)

(-8.42960455703811 0.163445749131843 -0.5)

(-8.43023606699624 0.160675495668767 -0.5)

(-8.43086769501375 0.15783956526581 -0.5)

(-8.43149862173854 0.154936860410079 -0.5)

(-8.43212800228599 0.151966295667148 -0.5)

(-8.43275496640562 0.148926806587817 -0.5)

(-8.43337862135272 0.145817347215545 -0.5)

(-8.43400048363636 0.142637374324205 -0.5)

(-8.43462174670115 0.139386268221692 -0.5)

(-8.43524106418983 0.136062941699458 -0.5)

(-8.4358570330226 0.132666333636224 -0.5)

(-8.43646819533354 0.129195413660028 -0.5)

(-8.43707304074176 0.125649186973111 -0.5)

(-8.43767225896104 0.122027065220941 -0.5)

(-8.43826859388419 0.118328814268645 -0.5)

(-8.43886066124336 0.114553539690188 -0.5)

(-8.43944692335213 0.110700373197106 -0.5)

(-8.44002579275151 0.106768492715808 -0.5)

(-8.44059563623727 0.102757127278132 -0.5)

(-8.44115825388914 0.098666033431768 -0.5)

(-8.44171577222994 0.094495032589331 -0.5)

(-8.44226611869347 0.090243414442173 -0.5)

(-8.44280714106879 0.085910528567216 -0.5)

(-8.44333661910717 0.081495791461679 -0.5)

(-8.44385292198383 0.076998767470021 -0.5)

(-8.44436059079508 0.072419765480532 -0.5)

(-8.44485901206117 0.06775855875912 -0.5)

(-8.44534562856751 0.063014767802038 -0.5)

(-8.44581779905364 0.058188100053818 -0.5)

(-8.44627280762779 0.053278350365129 -0.5)

(-8.44671328619764 0.04828588376528 -0.5)

(-8.44714160368986 0.043211069197473 -0.5)

(-8.44755503592004 0.038053909731086 -0.5)

(-8.44795078721988 0.032814499422643 -0.5)

(-8.4483260002075 0.027493037583953 -0.5)

(-8.44868230395537 0.022090120878675 -0.5)

(-8.44902396422567 0.01660657408468 -0.5)

(-8.44934741302332 0.011042782068955 -0.5)

(-8.44964885498149 0.005399238182609 -0.5)

(-8.44992439880259 -0.000323437257529 -0.5)

(-8.45017580057809 -0.006124255218472 -0.5)

(-8.45040829509617 -0.012002015484082 -0.5)

(-8.45061799974821 -0.017955840426428 -0.5)

(-8.45080080357212 -0.023984723042135 -0.5)

(-8.45095250430219 -0.030087512517563 -0.5)

(-8.45107686454768 -0.036262769453487 -0.5)

(-8.45117686009814 -0.042509018638788 -0.5)

(-8.45124816762403 -0.048824832866615 -0.5)

(-8.45128636214998 -0.05520864224439 -0.5)

(-8.45128761901684 -0.061658727426222 -0.5)

(-8.4512582662485 -0.068173272262349 -0.5)

(-8.45119743688396 -0.074750406960544 -0.5)

(-8.45110041671497 -0.081388111080185 -0.5)

(-8.45096239658455 -0.088084211634794 -0.5)

(-8.4507822771747 -0.0948364713649 -0.5)

(-8.45056753495164 -0.101642833629397 -0.5)

(-8.45031452380994 -0.108500869166791 -0.5)

(-8.45001861999009 -0.11540797914591 -0.5)

(-8.44967527216395 -0.122361415099925 -0.5)

(-8.44929181135825 -0.12935893852098 -0.5)

(-8.44887162569791 -0.136398115458128 -0.5)

(-8.44841022704818 -0.14347599337223 -0.5)

(-8.44790314050378 -0.150589485510035 -0.5)

(-8.44735051441838 -0.15773573122161 -0.5)

(-8.4467660841955 -0.164912918675079 -0.5)

(-8.44614680748196 -0.172117939260753 -0.5)

(-8.44548770353677 -0.179347414625356 -0.5)

(-8.44478405046495 -0.186597868969619 -0.5)

(-8.44404767677528 -0.193867403354756 -0.5)

(-8.44328392609547 -0.201153538918642 -0.5)

(-8.44248801417556 -0.208452728678491 -0.5)

(-8.44165517819019 -0.215761339423609 -0.5)

(-8.44078645447288 -0.22307633862066 -0.5)

(-8.43989534407232 -0.230396204580226 -0.5)

(-8.43897909881973 -0.237717507833404 -0.5)

(-8.43803371974319 -0.245036621941759 -0.5)

(-8.43705569528811 -0.252349925594956 -0.5)

(-8.4360545211427 -0.259655552244022 -0.5)

(-8.43503454867187 -0.266950998358493 -0.5)

(-8.43399471891675 -0.274233049339601 -0.5)

(-8.43293396191726 -0.281498480207108 -0.5)

(-8.43185278489069 -0.288744318944746 -0.5)

(-8.43075569377892 -0.295968223278446 -0.5)

(-8.42964502982698 -0.303167582275687 -0.5)

(-8.42852294545505 -0.310339804723561 -0.5)

(-8.4273912386397 -0.317482293511252 -0.5)

(-8.42624537108368 -0.324591487245442 -0.5)

(-8.42508705794606 -0.331664858505844 -0.5)

(-8.42392136150551 -0.33870049699079 -0.5)

(-8.42275324504056 -0.345696558479917 -0.5)

(-8.42158344948055 -0.352650568477816 -0.5)

(-8.42040421009738 -0.359558668881022 -0.5)

(-8.41922020013152 -0.366419167269077 -0.5)

(-8.41803695941952 -0.373230615106672 -0.5)

(-8.41685989137645 -0.379991627907771 -0.5)

(-8.41568514867702 -0.386699292025262 -0.5)

(-8.41450980613848 -0.393350918799152 -0.5)

(-8.41333841896308 -0.399945218258106 -0.5)

(-8.41217543526973 -0.40648097535248 -0.5)

(-8.41102458221465 -0.412956933204722 -0.5)

(-8.40988145049089 -0.419370473224434 -0.5)

(-8.40874655454751 -0.425719937929633 -0.5)

(-8.40762295009642 -0.432004211837845 -0.5)

(-8.40651359453326 -0.438222250898623 -0.5)

(-8.40542067131239 -0.444372958931987 -0.5)

(-8.40434224538198 -0.450454595447086 -0.5)

(-8.40327903734077 -0.456465980989933 -0.5)

(-8.40223240022149 -0.462406137891858 -0.5)

(-8.40120361645788 -0.468274159283722 -0.5)

(-8.40019379221074 -0.47406919471383 -0.5)

(-8.39920318803996 -0.479790331096338 -0.5)

(-8.39823199038646 -0.48543672843049 -0.5)

(-8.39728039698846 -0.491007633858581 -0.5)

(-8.39634856312963 -0.496502371035949 -0.5)

(-8.39543670632166 -0.501920356618303 -0.5)

(-8.39454596773891 -0.507261242072485 -0.5)

(-8.39367667626852 -0.512524619563944 -0.5)

(-8.39282884469689 -0.517710105863504 -0.5)

(-8.39200244507857 -0.522817387167816 -0.5)

(-8.39119741373461 -0.527846218166841 -0.5)

(-8.39041502113535 -0.532796636510476 -0.5)

(-8.38965582470254 -0.537668631474529 -0.5)

(-8.38891908395343 -0.542462055994094 -0.5)

(-8.38820404609677 -0.547176830866006 -0.5)

(-8.38750995050494 -0.55181294304859 -0.5)

(-8.38683653154116 -0.556370517238686 -0.5)

(-8.38618580890125 -0.560850070718597 -0.5)

(-8.3855571887746 -0.565251788585118 -0.5)

(-8.38494960394169 -0.5695758460715 -0.5)

(-8.38436200069331 -0.57382247814558 -0.5)

(-8.38379334309309 -0.577991977079108 -0.5)

(-8.38324357375306 -0.582084818232937 -0.5)

(-8.38271457508542 -0.586101777851046 -0.5)

(-8.38220551301052 -0.590043307628347 -0.5)

(-8.38171536980138 -0.59390987893941 -0.5)

(-8.38124314687687 -0.597702011040798 -0.5)

(-8.38078786824781 -0.601420265025239 -0.5)

(-8.38034927136209 -0.605065325700533 -0.5)

(-8.37992967167827 -0.608638213531499 -0.5)

(-8.37952802990951 -0.612139572343415 -0.5)

(-8.37914284267525 -0.615570026213268 -0.5)

(-8.3787726603949 -0.618930240010112 -0.5)

(-8.3784160908289 -0.622220912940329 -0.5)

(-8.37807180149416 -0.625442780279531 -0.5)

(-8.37774063845572 -0.628596829116446 -0.5)

(-8.37742371941956 -0.631684086757353 -0.5)

(-8.37712029250361 -0.634705398552821 -0.5)

(-8.37682962565109 -0.637661628800927 -0.5)

(-8.37655100784526 -0.640553658303286 -0.5)

(-8.37628374982017 -0.643382386001915 -0.5)

(-8.37602718565639 -0.646148720208981 -0.5)

(-8.37578099569451 -0.648853613324727 -0.5)

(-8.37554544341526 -0.651498075713109 -0.5)

(-8.37532073856772 -0.654083114944115 -0.5)

(-8.37510705792318 -0.656609736179517 -0.5)

(-8.37490454499434 -0.65907894167463 -0.5)

(-8.37471331006502 -0.661491728546239 -0.5)

(-8.37453343022383 -0.663849088478667 -0.5)

(-8.37436487105963 -0.666152001052767 -0.5)

(-8.3742070177137 -0.668401400935848 -0.5)

(-8.37405965827176 -0.670598249969054 -0.5)

(-8.37392268662922 -0.672743512400791 -0.5)

(-8.37379598279254 -0.674838146231887 -0.5)

(-8.3736794133407 -0.676883100995892 -0.5)

(-8.37357283173919 -0.678879318559577 -0.5)

(-8.37347607881378 -0.680827732057672 -0.5)

(-8.37338900726629 -0.682729267197023 -0.5)

(-8.37331227155259 -0.684584871072202 -0.5)

(-8.37324567618498 -0.686395443181601 -0.5)

(-8.37318848059483 -0.688161852956339 -0.5)

(-8.37313997599925 -0.689884967861718 -0.5)

(-8.37309948490151 -0.691565650361856 -0.5)

(-8.37306636034076 -0.693204763567984 -0.5)

(-8.37303998549332 -0.694803160339032 -0.5)

(-8.37301977282704 -0.696361689481635 -0.5)

(-8.37300516826648 -0.697881195001583 -0.5)

(-8.37299775015069 -0.699362519021738 -0.5)

(-8.37299830040718 -0.70080647601169 -0.5)

(-8.37300570949288 -0.702213856746364 -0.5)

(-8.37301893144168 -0.703585459375468 -0.5)

(-8.37303698166436 -0.704922073947462 -0.5)

(-8.37305893473621 -0.706224487209663 -0.5)

(-8.37308392222643 -0.707493484858147 -0.5)

(-8.37311113022568 -0.708729840188047 -0.5)

(-8.37313979713334 -0.709934319020166 -0.5)

(-8.37316921133937 -0.711107677249684 -0.5)

(-8.37320018427414 -0.71225061993442 -0.5)

(-8.37323480019642 -0.713363794506748 -0.5)

(-8.37327246697452 -0.714447905585185 -0.5)

(-8.37331257076652 -0.715503651038892 -0.5)

(-8.37335453652021 -0.716531720697129 -0.5)

(-8.37339782596011 -0.717532792054252 -0.5)

(-8.37344193583408 -0.718507531943894 -0.5)

(-8.37348639620388 -0.719456597665717 -0.5)

(-8.37353076856383 -0.720380633508225 -0.5)

(-8.37357464413937 -0.721280270430585 -0.5)

(-8.37361764230723 -0.722156127052012 -0.5)

(-8.37365945861607 -0.723008806872161 -0.5)

(-8.37370137128197 -0.723838820459887 -0.5)

(-8.37374390169188 -0.724646703851037 -0.5)

(-8.37378683153711 -0.725433015996134 -0.5)

(-8.37382995549015 -0.726198306260303 -0.5)

(-8.3738730805 -0.726943110405824 -0.5)

(-8.37391602554739 -0.72766795475729 -0.5)

(-8.37395862100369 -0.728373353211308 -0.5)

(-8.37400070827964 -0.729059809162807 -0.5)

(-8.37404213918936 -0.729727812563103 -0.5)

(-8.37408277590238 -0.730377846366747 -0.5)

(-8.3741224900152 -0.73101037860144 -0.5)

(-8.37416116245298 -0.731625867671311 -0.5)

(-8.3741986829741 -0.732224761073114 -0.5)

(-8.37423529295544 -0.732807473042647 -0.5)

(-8.37427157639668 -0.733374387770746 -0.5)

(-8.37430748121158 -0.733925917405552 -0.5)

(-8.37434294288694 -0.734462467509859 -0.5)

(-8.37437790096014 -0.734984431145688 -0.5)

(-8.37441229919718 -0.735492195070232 -0.5)

(-8.37444608500997 -0.735986134376335 -0.5)

(-8.3744792094529 -0.73646661572835 -0.5)

(-8.37451162701058 -0.736933997349768 -0.5)

(-8.37454329538384 -0.737388628924866 -0.5)

(-8.3745741752741 -0.737830851412437 -0.5)

(-8.37460423004039 -0.73826099496611 -0.5)

(-8.37463342593108 -0.738679384996158 -0.5)

(-8.37466173150261 -0.739086336526767 -0.5)

(-8.37468911764829 -0.739482157222287 -0.5)

(-8.37471556668918 -0.739867146246192 -0.5)

(-8.37474125360063 -0.740241582024873 -0.5)

(-8.37476626910312 -0.740605741541733 -0.5)

(-8.37479063374474 -0.740959899686443 -0.5)

(-8.37481436749683 -0.741304323463331 -0.5)

(-8.37483748994989 -0.741639274535262 -0.5)

(-8.37486002018754 -0.741965007075524 -0.5)

(-8.37488197679183 -0.742281767521876 -0.5)

(-8.37490337816608 -0.742589798876455 -0.5)

(-8.37492424221676 -0.742889335718317 -0.5)

(-8.37494458658645 -0.743180607124934 -0.5)

(-8.37496442863361 -0.743463835880681 -0.5)

(-8.37498378558407 -0.743739240059342 -0.5)

(-8.37500267446887 -0.744007031449959 -0.5)

(-8.37502111215238 -0.744267415155238 -0.5)

(-8.37503911564826 -0.744520593066184 -0.5)

(-8.37505670189537 -0.744766759472172 -0.5)

(-8.37507388818042 -0.745006105465247 -0.5)

(-8.37509072933132 -0.745238813329846 -0.5)

(-8.37510737690532 -0.745465053503249 -0.5)

(-8.37512381799814 -0.745685003345639 -0.5)

(-8.37514002219496 -0.745898837666356 -0.5)

(-8.37515595946528 -0.746106724815189 -0.5)

(-8.37517160029828 -0.746308831589232 -0.5)

(-8.37518691505384 -0.746505318211737 -0.5)

(-8.37520187392959 -0.746696341815764 -0.5)

(-8.37521644653634 -0.746882055406998 -0.5)

(-8.37523060149724 -0.747062607901452 -0.5)

(-8.37524430599506 -0.74723814446855 -0.5)

(-8.37525752518935 -0.747408806494217 -0.5)

(-8.37527022152343 -0.747574731847044 -0.5)

(-8.37528235384569 -0.74773605509005 -0.5)

(-8.37529387622089 -0.747892906853825 -0.5)

(-8.37530473652078 -0.748045414848366 -0.5)

(-8.37531487442247 -0.748193703526264 -0.5)

(-8.37532422486485 -0.748337893516381 -0.5)

(-8.37533299016143 -0.748478084797022 -0.5)

(-8.37534129871405 -0.748614381045019 -0.5)

(-8.37534914357508 -0.748746889389604 -0.5)

(-8.37535651401864 -0.748875716307637 -0.5)

(-8.37536339406089 -0.749000964481302 -0.5)

(-8.37536976061712 -0.74912273412118 -0.5)

(-8.37537558051089 -0.749241122875773 -0.5)

(-8.37538080563551 -0.74935622643664 -0.5)

(-8.37538536447534 -0.749468137574472 -0.5)

(-8.37538914633365 -0.749576946992193 -0.5)

(-8.37539196826732 -0.749682742235023 -0.5)

(-8.37539349438618 -0.749785605102076 -0.5)

(-8.3753929814191 -0.74988560120633 -0.5)

)

spline 5 10
(
(-8.37894171960202 0.250255197449192 0.5)
(-8.37904152308974 0.250261450830106 0.5)
(-8.37914421412417 0.250267622735631 0.5)
(-8.37924987360825 0.250273684937805 0.5)
(-8.37935858780945 0.250279606065593 0.5)
(-8.37947044360183 0.250285350971339 0.5)
(-8.37958553437967 0.250290880643862 0.5)
(-8.37970394885552 0.250296151227076 0.5)
(-8.37982578372649 0.250301114166131 0.5)
(-8.3799511362434 0.250305715318301 0.5)
(-8.38008010648178 0.250309894476334 0.5)
(-8.38021279597391 0.250313584679504 0.5)
(-8.38034930763761 0.25031671152019 0.5)
(-8.3804897517188 0.250319192468196 0.5)
(-8.38063423331904 0.250320935736951 0.5)
(-8.38078286562624 0.250321839559597 0.5)
(-8.38093575947653 0.25032179095893 0.5)
(-8.38109302957309 0.250320664615839 0.5)
(-8.38125479014613 0.250318321535566 0.5)
(-8.38142115947044 0.250314607513846 0.5)
(-8.38159225158028 0.250309351650886 0.5)
(-8.38176818266505 0.250302364444167 0.5)
(-8.38194906815415 0.250293435820051 0.5)
(-8.38213502091979 0.250282332998768 0.5)
(-8.38232614991771 0.250268798157836 0.5)
(-8.38252255976752 0.250252545796246 0.5)
(-8.38272434878413 0.250233259940668 0.5)

(-8.38293160960343 0.250210590815463 0.5)

(-8.38314441652525 0.250184152767448 0.5)

(-8.38336284160036 0.250153518649716 0.5)

(-8.38358692690054 0.250118219392034 0.5)

(-8.38381670156718 0.250077737673882 0.5)

(-8.38405216405726 0.250031506354649 0.5)

(-8.38429328240747 0.249978904390299 0.5)

(-8.384540052197 0.249919529544771 0.5)

(-8.3847926541221 0.249853731491905 0.5)

(-8.38505118295575 0.249781408657868 0.5)

(-8.38531572755064 0.24970243838043 0.5)

(-8.38558639796054 0.249616715773944 0.5)

(-8.38586331671523 0.249524158967461 0.5)

(-8.3861466288423 0.249424709231785 0.5)

(-8.38643650038515 0.249318335283289 0.5)

(-8.38673311731824 0.249205038660083 0.5)

(-8.38703670179125 0.249084853506016 0.5)

(-8.38734750425147 0.248957856712965 0.5)

(-8.38766581024336 0.248824174526771 0.5)

(-8.38799195151288 0.24868398941746 0.5)

(-8.38832630873016 0.248537553414795 0.5)

(-8.38866931415623 0.248385205734738 0.5)

(-8.3890214644481 0.248227391329751 0.5)

(-8.38938316790398 0.248064314332636 0.5)

(-8.38975219535566 0.247890468749519 0.5)

(-8.39012716261966 0.247702605594116 0.5)

(-8.3905073913448 0.247499276837684 0.5)

(-8.39089228897301 0.247279381912776 0.5)

(-8.39128152525235 0.247042369902684 0.5)

(-8.39167517438115 0.246788349994323 0.5)

(-8.39207377646566 0.246518039133364 0.5)

(-8.39247827729614 0.246232573222964 0.5)
(-8.39288988277056 0.24593326589123 0.5)
(-8.39330989336269 0.245621403563077 0.5)
(-8.3937384329144 0.245296610416161 0.5)
(-8.39417313642185 0.244955288728504 0.5)
(-8.39461424573402 0.244597343316857 0.5)
(-8.39506195596033 0.244222585947669 0.5)
(-8.39551627992097 0.243830586664185 0.5)
(-8.39597707297005 0.243420727848152 0.5)
(-8.39644403376382 0.242992226054294 0.5)
(-8.39691668704786 0.242544137040968 0.5)
(-8.39739435626459 0.242075343852654 0.5)
(-8.39787611268298 0.241584540591842 0.5)
(-8.39836071006323 0.241070198407654 0.5)
(-8.3988464804737 0.240530527568341 0.5)
(-8.39933151502692 0.239963688336894 0.5)
(-8.39982167713789 0.239374395632868 0.5)
(-8.40031970789535 0.238764402819878 0.5)
(-8.40082505194485 0.238132654206962 0.5)
(-8.40133710147157 0.237478071997518 0.5)
(-8.40185520048792 0.236799562568428 0.5)
(-8.40237864836005 0.236096025615656 0.5)
(-8.4029067074523 0.235366359483275 0.5)
(-8.40343860799291 0.234609471385498 0.5)
(-8.40397355566969 0.233824284868978 0.5)
(-8.40451074127568 0.233009744433786 0.5)
(-8.40504971249514 0.232165047849994 0.5)
(-8.40559225414552 0.231290791657989 0.5)
(-8.40613860631384 0.230386526576562 0.5)
(-8.40668861195109 0.229451541915489 0.5)
(-8.4072421168451 0.228485117193937 0.5)

(-8.40779896672908 0.227486527305938 0.5)
(-8.40835901046455 0.226455037183247 0.5)
(-8.40892209835232 0.225389904871685 0.5)
(-8.40948808444155 0.224290377236923 0.5)
(-8.41005682298604 0.223155696776757 0.5)
(-8.41062854366861 0.221985274555304 0.5)
(-8.41120372591274 0.220778618245588 0.5)
(-8.41178223642076 0.219534921087634 0.5)
(-8.41236393013788 0.21825335879007 0.5)
(-8.41294865880097 0.216933096159951 0.5)
(-8.41353627095219 0.215573286939181 0.5)
(-8.41412661092016 0.214173076102456 0.5)
(-8.41471952077859 0.212731595179425 0.5)
(-8.41531484455593 0.211247970211485 0.5)
(-8.41591333996904 0.209721673202788 0.5)
(-8.41651537473563 0.208151997604236 0.5)
(-8.41712059980646 0.206537943956458 0.5)
(-8.41772865333535 0.204878506125823 0.5)
(-8.41833916170516 0.203172670023562 0.5)
(-8.41895173881376 0.201419417162318 0.5)
(-8.41956598762229 0.19961772200859 0.5)
(-8.4201814991512 0.197766558200244 0.5)
(-8.42079910133849 0.195865295604197 0.5)
(-8.42141952887001 0.193913248123457 0.5)
(-8.42204234856922 0.191909344614315 0.5)
(-8.4226671099949 0.18985250779353 0.5)
(-8.42329334409151 0.187741660153614 0.5)
(-8.42392056465886 0.185575720931497 0.5)
(-8.42454826873022 0.183353606553294 0.5)
(-8.42517641307936 0.181074368572143 0.5)
(-8.42580690533314 0.178737579958931 0.5)

(-8.4264393906267 0.176342179685822 0.5)
(-8.42707310954994 0.173887010405636 0.5)
(-8.42770726976089 0.171370913041936 0.5)
(-8.42834104371212 0.168792739550283 0.5)
(-8.42897357090526 0.166151348820516 0.5)
(-8.42960455703811 0.163445749131843 0.5)
(-8.43023606699624 0.160675495668767 0.5)
(-8.43086769501375 0.15783956526581 0.5)
(-8.43149862173854 0.154936860410079 0.5)
(-8.43212800228599 0.151966295667148 0.5)
(-8.43275496640562 0.148926806587817 0.5)
(-8.43337862135272 0.145817347215545 0.5)
(-8.43400048363636 0.142637374324205 0.5)
(-8.43462174670115 0.139386268221692 0.5)
(-8.43524106418983 0.136062941699458 0.5)
(-8.4358570330226 0.132666333636224 0.5)
(-8.43646819533354 0.129195413660028 0.5)
(-8.43707304074176 0.125649186973111 0.5)
(-8.43767225896104 0.122027065220941 0.5)
(-8.43826859388419 0.118328814268645 0.5)
(-8.43886066124336 0.114553539690188 0.5)
(-8.43944692335213 0.110700373197106 0.5)
(-8.44002579275151 0.106768492715808 0.5)
(-8.44059563623727 0.102757127278132 0.5)
(-8.44115825388914 0.098666033431768 0.5)
(-8.44171577222994 0.094495032589331 0.5)
(-8.44226611869347 0.090243414442173 0.5)
(-8.44280714106879 0.085910528567216 0.5)
(-8.44333661910717 0.081495791461679 0.5)
(-8.44385292198383 0.076998767470021 0.5)
(-8.44436059079508 0.072419765480532 0.5)

(-8.44485901206117 0.06775855875912 0.5)

(-8.44534562856751 0.063014767802038 0.5)

(-8.44581779905364 0.058188100053818 0.5)

(-8.44627280762779 0.053278350365129 0.5)

(-8.44671328619764 0.04828588376528 0.5)

(-8.44714160368986 0.043211069197473 0.5)

(-8.44755503592004 0.038053909731086 0.5)

(-8.44795078721988 0.032814499422643 0.5)

(-8.4483260002075 0.027493037583953 0.5)

(-8.44868230395537 0.022090120878675 0.5)

(-8.44902396422567 0.01660657408468 0.5)

(-8.44934741302332 0.011042782068955 0.5)

(-8.44964885498149 0.005399238182609 0.5)

(-8.44992439880259 -0.000323437257529 0.5)

(-8.45017580057809 -0.006124255218472 0.5)

(-8.45040829509617 -0.012002015484082 0.5)

(-8.45061799974821 -0.017955840426428 0.5)

(-8.45080080357212 -0.023984723042135 0.5)

(-8.45095250430219 -0.030087512517563 0.5)

(-8.45107686454768 -0.036262769453487 0.5)

(-8.45117686009814 -0.042509018638788 0.5)

(-8.45124816762403 -0.048824832866615 0.5)

(-8.45128636214998 -0.05520864224439 0.5)

(-8.45128761901684 -0.061658727426222 0.5)

(-8.4512582662485 -0.068173272262349 0.5)

(-8.45119743688396 -0.074750406960544 0.5)

(-8.45110041671497 -0.081388111080185 0.5)

(-8.45096239658455 -0.088084211634794 0.5)

(-8.4507822771747 -0.0948364713649 0.5)

(-8.45056753495164 -0.101642833629397 0.5)

(-8.45031452380994 -0.108500869166791 0.5)

(-8.45001861999009 -0.11540797914591 0.5)

(-8.44967527216395 -0.122361415099925 0.5)

(-8.44929181135825 -0.12935893852098 0.5)

(-8.44887162569791 -0.136398115458128 0.5)

(-8.44841022704818 -0.14347599337223 0.5)

(-8.44790314050378 -0.150589485510035 0.5)

(-8.44735051441838 -0.15773573122161 0.5)

(-8.4467660841955 -0.164912918675079 0.5)

(-8.44614680748196 -0.172117939260753 0.5)

(-8.44548770353677 -0.179347414625356 0.5)

(-8.44478405046495 -0.186597868969619 0.5)

(-8.44404767677528 -0.193867403354756 0.5)

(-8.44328392609547 -0.201153538918642 0.5)

(-8.44248801417556 -0.208452728678491 0.5)

(-8.44165517819019 -0.215761339423609 0.5)

(-8.44078645447288 -0.22307633862066 0.5)

(-8.43989534407232 -0.230396204580226 0.5)

(-8.43897909881973 -0.237717507833404 0.5)

(-8.43803371974319 -0.245036621941759 0.5)

(-8.43705569528811 -0.252349925594956 0.5)

(-8.4360545211427 -0.259655552244022 0.5)

(-8.43503454867187 -0.266950998358493 0.5)

(-8.43399471891675 -0.274233049339601 0.5)

(-8.43293396191726 -0.281498480207108 0.5)

(-8.43185278489069 -0.288744318944746 0.5)

(-8.43075569377892 -0.295968223278446 0.5)

(-8.42964502982698 -0.303167582275687 0.5)

(-8.42852294545505 -0.310339804723561 0.5)

(-8.4273912386397 -0.317482293511252 0.5)

(-8.42624537108368 -0.324591487245442 0.5)

(-8.42508705794606 -0.331664858505844 0.5)

(-8.42392136150551 -0.33870049699079 0.5)

(-8.42275324504056 -0.345696558479917 0.5)

(-8.42158344948055 -0.352650568477816 0.5)

(-8.42040421009738 -0.359558668881022 0.5)

(-8.41922020013152 -0.366419167269077 0.5)

(-8.41803695941952 -0.373230615106672 0.5)

(-8.41685989137645 -0.379991627907771 0.5)

(-8.41568514867702 -0.386699292025262 0.5)

(-8.41450980613848 -0.393350918799152 0.5)

(-8.41333841896308 -0.399945218258106 0.5)

(-8.41217543526973 -0.40648097535248 0.5)

(-8.41102458221465 -0.412956933204722 0.5)

(-8.40988145049089 -0.419370473224434 0.5)

(-8.40874655454751 -0.425719937929633 0.5)

(-8.40762295009642 -0.432004211837845 0.5)

(-8.40651359453326 -0.438222250898623 0.5)

(-8.40542067131239 -0.444372958931987 0.5)

(-8.40434224538198 -0.450454595447086 0.5)

(-8.40327903734077 -0.456465980989933 0.5)

(-8.40223240022149 -0.462406137891858 0.5)

(-8.40120361645788 -0.468274159283722 0.5)

(-8.40019379221074 -0.47406919471383 0.5)

(-8.39920318803996 -0.479790331096338 0.5)

(-8.39823199038646 -0.48543672843049 0.5)

(-8.39728039698846 -0.491007633858581 0.5)

(-8.39634856312963 -0.496502371035949 0.5)

(-8.39543670632166 -0.501920356618303 0.5)

(-8.39454596773891 -0.507261242072485 0.5)

(-8.39367667626852 -0.512524619563944 0.5)

(-8.39282884469689 -0.517710105863504 0.5)

(-8.39200244507857 -0.522817387167816 0.5)

(-8.39119741373461 -0.527846218166841 0.5)

(-8.39041502113535 -0.532796636510476 0.5)

(-8.38965582470254 -0.537668631474529 0.5)

(-8.38891908395343 -0.542462055994094 0.5)

(-8.38820404609677 -0.547176830866006 0.5)

(-8.38750995050494 -0.55181294304859 0.5)

(-8.38683653154116 -0.556370517238686 0.5)

(-8.38618580890125 -0.560850070718597 0.5)

(-8.3855571887746 -0.565251788585118 0.5)

(-8.38494960394169 -0.5695758460715 0.5)

(-8.38436200069331 -0.57382247814558 0.5)

(-8.38379334309309 -0.577991977079108 0.5)

(-8.38324357375306 -0.582084818232937 0.5)

(-8.38271457508542 -0.586101777851046 0.5)

(-8.38220551301052 -0.590043307628347 0.5)

(-8.38171536980138 -0.59390987893941 0.5)

(-8.38124314687687 -0.597702011040798 0.5)

(-8.38078786824781 -0.601420265025239 0.5)

(-8.38034927136209 -0.605065325700533 0.5)

(-8.37992967167827 -0.608638213531499 0.5)

(-8.37952802990951 -0.612139572343415 0.5)

(-8.37914284267525 -0.615570026213268 0.5)

(-8.3787726603949 -0.618930240010112 0.5)

(-8.3784160908289 -0.622220912940329 0.5)

(-8.37807180149416 -0.625442780279531 0.5)

(-8.37774063845572 -0.628596829116446 0.5)

(-8.37742371941956 -0.631684086757353 0.5)

(-8.37712029250361 -0.634705398552821 0.5)

(-8.37682962565109 -0.637661628800927 0.5)

(-8.37655100784526 -0.640553658303286 0.5)

(-8.37628374982017 -0.643382386001915 0.5)

(-8.37602718565639 -0.646148720208981 0.5)

(-8.37578099569451 -0.648853613324727 0.5)

(-8.37554544341526 -0.651498075713109 0.5)

(-8.37532073856772 -0.654083114944115 0.5)

(-8.37510705792318 -0.656609736179517 0.5)

(-8.37490454499434 -0.65907894167463 0.5)

(-8.37471331006502 -0.661491728546239 0.5)

(-8.37453343022383 -0.663849088478667 0.5)

(-8.37436487105963 -0.666152001052767 0.5)

(-8.3742070177137 -0.668401400935848 0.5)

(-8.37405965827176 -0.670598249969054 0.5)

(-8.37392268662922 -0.672743512400791 0.5)

(-8.37379598279254 -0.674838146231887 0.5)

(-8.3736794133407 -0.676883100995892 0.5)

(-8.37357283173919 -0.678879318559577 0.5)

(-8.37347607881378 -0.680827732057672 0.5)

(-8.37338900726629 -0.682729267197023 0.5)

(-8.37331227155259 -0.684584871072202 0.5)

(-8.37324567618498 -0.686395443181601 0.5)

(-8.37318848059483 -0.688161852956339 0.5)

(-8.37313997599925 -0.689884967861718 0.5)

(-8.37309948490151 -0.691565650361856 0.5)

(-8.37306636034076 -0.693204763567984 0.5)

(-8.37303998549332 -0.694803160339032 0.5)

(-8.37301977282704 -0.696361689481635 0.5)

(-8.37300516826648 -0.697881195001583 0.5)

(-8.37299775015069 -0.699362519021738 0.5)

(-8.37299830040718 -0.70080647601169 0.5)

(-8.37300570949288 -0.702213856746364 0.5)

(-8.37301893144168 -0.703585459375468 0.5)

(-8.37303698166436 -0.704922073947462 0.5)

(-8.37305893473621 -0.706224487209663 0.5)

(-8.37308392222643 -0.707493484858147 0.5)

(-8.37311113022568 -0.708729840188047 0.5)

(-8.37313979713334 -0.709934319020166 0.5)

(-8.37316921133937 -0.711107677249684 0.5)

(-8.37320018427414 -0.71225061993442 0.5)

(-8.37323480019642 -0.713363794506748 0.5)

(-8.37327246697452 -0.714447905585185 0.5)

(-8.37331257076652 -0.715503651038892 0.5)

(-8.37335453652021 -0.716531720697129 0.5)

(-8.37339782596011 -0.717532792054252 0.5)

(-8.37344193583408 -0.718507531943894 0.5)

(-8.37348639620388 -0.719456597665717 0.5)

(-8.37353076856383 -0.720380633508225 0.5)

(-8.37357464413937 -0.721280270430585 0.5)

(-8.37361764230723 -0.722156127052012 0.5)

(-8.37365945861607 -0.723008806872161 0.5)

(-8.37370137128197 -0.723838820459887 0.5)

(-8.37374390169188 -0.724646703851037 0.5)

(-8.37378683153711 -0.725433015996134 0.5)

(-8.37382995549015 -0.726198306260303 0.5)

(-8.3738730805 -0.726943110405824 0.5)

(-8.37391602554739 -0.72766795475729 0.5)

(-8.37395862100369 -0.728373353211308 0.5)

(-8.37400070827964 -0.729059809162807 0.5)

(-8.37404213918936 -0.729727812563103 0.5)

(-8.37408277590238 -0.730377846366747 0.5)

(-8.3741224900152 -0.73101037860144 0.5)

(-8.37416116245298 -0.731625867671311 0.5)

(-8.3741986829741 -0.732224761073114 0.5)

(-8.37423529295544 -0.732807473042647 0.5)

(-8.37427157639668 -0.733374387770746 0.5)

(-8.37430748121158 -0.733925917405552 0.5)

(-8.37434294288694 -0.734462467509859 0.5)

(-8.37437790096014 -0.734984431145688 0.5)

(-8.37441229919718 -0.735492195070232 0.5)

(-8.37444608500997 -0.735986134376335 0.5)

(-8.3744792094529 -0.73646661572835 0.5)

(-8.37451162701058 -0.736933997349768 0.5)

(-8.37454329538384 -0.737388628924866 0.5)

(-8.3745741752741 -0.737830851412437 0.5)

(-8.37460423004039 -0.73826099496611 0.5)

(-8.37463342593108 -0.738679384996158 0.5)

(-8.37466173150261 -0.739086336526767 0.5)

(-8.37468911764829 -0.739482157222287 0.5)

(-8.37471556668918 -0.739867146246192 0.5)

(-8.37474125360063 -0.740241582024873 0.5)

(-8.37476626910312 -0.740605741541733 0.5)

(-8.37479063374474 -0.740959899686443 0.5)

(-8.37481436749683 -0.741304323463331 0.5)

(-8.37483748994989 -0.741639274535262 0.5)

(-8.37486002018754 -0.741965007075524 0.5)

(-8.37488197679183 -0.742281767521876 0.5)

(-8.37490337816608 -0.742589798876455 0.5)

(-8.37492424221676 -0.742889335718317 0.5)

(-8.37494458658645 -0.743180607124934 0.5)

(-8.37496442863361 -0.743463835880681 0.5)

(-8.37498378558407 -0.743739240059342 0.5)

(-8.37500267446887 -0.744007031449959 0.5)

(-8.37502111215238 -0.744267415155238 0.5)

(-8.37503911564826 -0.744520593066184 0.5)

(-8.37505670189537 -0.744766759472172 0.5)

(-8.37507388818042 -0.745006105465247 0.5)
(-8.37509072933132 -0.745238813329846 0.5)
(-8.37510737690532 -0.745465053503249 0.5)
(-8.37512381799814 -0.745685003345639 0.5)
(-8.37514002219496 -0.745898837666356 0.5)
(-8.37515595946528 -0.746106724815189 0.5)
(-8.37517160029828 -0.746308831589232 0.5)
(-8.37518691505384 -0.746505318211737 0.5)
(-8.37520187392959 -0.746696341815764 0.5)
(-8.37521644653634 -0.746882055406998 0.5)
(-8.37523060149724 -0.747062607901452 0.5)
(-8.37524430599506 -0.74723814446855 0.5)
(-8.37525752518935 -0.747408806494217 0.5)
(-8.37527022152343 -0.747574731847044 0.5)
(-8.37528235384569 -0.74773605509005 0.5)
(-8.37529387622089 -0.747892906853825 0.5)
(-8.37530473652078 -0.748045414848366 0.5)
(-8.37531487442247 -0.748193703526264 0.5)
(-8.37532422486485 -0.748337893516381 0.5)
(-8.37533299016143 -0.748478084797022 0.5)
(-8.37534129871405 -0.748614381045019 0.5)
(-8.37534914357508 -0.748746889389604 0.5)
(-8.37535651401864 -0.748875716307637 0.5)
(-8.37536339406089 -0.749000964481302 0.5)
(-8.37536976061712 -0.74912273412118 0.5)
(-8.37537558051089 -0.749241122875773 0.5)
(-8.37538080563551 -0.74935622643664 0.5)
(-8.37538536447534 -0.749468137574472 0.5)
(-8.37538914633365 -0.749576946992193 0.5)
(-8.37539196826732 -0.749682742235023 0.5)
(-8.37539349438618 -0.749785605102076 0.5)

```
        ( -8.3753929814191 -0.74988560120633 0.5 )
 )

/*  spline  3  0
 (
   ( -6.6982955  -2.1199479          -0.5)
 //( -6.5907455  -2.017695           -0.5)
   ( -6.0488451  -1.2066837          -0.5)
   ( -5.858555   -0.25003056         -0.5)
   ( -6.0488451   0.70662255         -0.5)
   ( -6.5907455   1.5176339          -0.5)
   ( -7.4017569   2.0595343          -0.5)
   ( -8.35841     2.24982447799      -0.5)
 )

spline  7  4
 (
   (-6.6982955  -2.1199479          0.5)
 //(-6.5907455  -2.017695           0.5)
   (-6.0488451  -1.2066837          0.5)
   (-5.858555   -0.25003056         0.5)
   (-6.0488451   0.70662255         0.5)
   (-6.5907455   1.5176339          0.5)
   (-7.4017569   2.0595343          0.5)
   (-8.35841     2.24982447799      0.5)
 )

spline 0 9
(
  (-8.35841      2.24982447    -0.5)
  (-9.3150631  2.0595343      -0.5)
```

```
    (-10.126074  1.5176339      -0.5)
    (-10.667975  0.70662255     -0.5)
    (-10.858265 -0.25003056     -0.5)
    (-10.667975 -1.2066837      -0.5)
    (-10.034855 -2.1108567      -0.5)
  )

  spline 4 11
  (
    ( -8.35841    2.24982447       0.5)
    ( -9.3150631  2.0595343        0.5)
    (-10.126074   1.5176339        0.5)
    (-10.667975   0.70662255       0.5)
    (-10.858265  -0.25003056       0.5)
    (-10.667975  -1.2066837        0.5)
  //(-10.126074  -2.017695         0.5) //Extra
    (-10.034855  -2.1108567        0.5)
  )  */
);

boundary
(

  patch_1  //top-mid-A
  {
    type patch;
    faces
    (
      //(  32 33 29 28 )
      (  28 29 33 32 )
    );
```

```
}

patch_2  //top-mid-B
{
    type patch;
    faces
    (
        ( 26 18 14 22 )
    );
}

patch_3  //mid-bottom-A
{
    type patch;
    faces
    (
        ( 27 19 15 23 )
    );
}

patch_4  //mid-bottom-B
{
    type patch;
    faces
    (
        (  43 42 38 39 )
    );
}

patch_5 //Exterior-A
{
```

```
    type patch;
    faces
    (
        ( 25 17 13 21 )
        ( 17 16 12 13 )
        ( 16 24 20 12 )
        ( 24 25 21 20 )

    );
}

patch_6  //Aifoil-B
{
    type patch;
    faces
    (
        (  4  7 3 0 )
        (  7 11 9 3 )
        ( 11  4 0 9 )
    );
}

//Regular
airfoilSS_wall
{
    type wall;
    faces
    (
        ( 1  2  6  5 )
    );
}
```

```
airfoilPS_wall
{
    type wall;
    faces
    (
        ( 8 1 5 10 )
    );
}
airfoilTE_wall
{
    type wall;
    faces
    (
        ( 8 2 10 6 )
    );
}

mvTop_freestream_free
{
    type patch;
    faces
    (
        (30 31 35 34)
    );
}

mvBottom_freestream_free
{
    type patch;
    faces
    (
```

```
        (37  36  40  41)
    );
}

mvFront_empty
{
    type empty;
    faces
    (
        (32  33  34  35) //Above

        (40  41  42  43) // Below

        (5  6  7  4) //Airfoil
        (6 10 11  7)
        (10  5  4 11)

        (17 16 19 18) //Airfoil Exterior
        (16 24 27 19)
        (24 25 26 27)
        (25 17 18 26)

    );
}

mvBack_empty
{
    type empty;
    faces
    (
        (28 29 30 31) //Above
```

```
        (36 37 38 39) // Below

        (1  2  3  0 ) //Airfoil
        (2  8  9  3 )
        (8  1  0  9 )

        (13 12 15 14 ) //Airfoil Exterior
        (12 20 23 15 )
        (20 21 22 23 )
        (21 13 14 22 )
    );
  }

  int_foilIn_ami
  {
    type patch;
    faces
    (
      (32  35  31  28) //Above

      (40  43  39  36) // Below

      (27  26  22  23) //Airfoil Exterior
    );
  }
int_foilOut_ami
  {
    type patch;
    faces
    (
```

```
            (29  30  34  33) //Above

            (37  38  42  41) // Below

            (15  14  18  19) //Airfoil Exterior
        );
    }
);
mergePatchPairs
(
 (patch_1 patch_2)
  (patch_3 patch_4)
 (patch_5 patch_6)
);
// ************************************************************************* //
```

List of Figures

List if Tables

List of symbols

Variable	Description	SI unit
$\boldsymbol{A}$	wing area	m^2
$\boldsymbol{C_f}$	coefficient of friction	-
$\boldsymbol{Cp}$	specific heat capacity at constant pressure	J/(kg.K)
$\boldsymbol{Cp}$	pressure coefficient	-
c	speed of sound	m/s
$\boldsymbol{c}$	inflow velocity	m/s
$\boldsymbol{c_\tau}$	shear stress velocity	m/s
$\boldsymbol{c_w}$	two-dimensional Resistance coefficient	-
$\boldsymbol{D}$	tower diameter	m
$\boldsymbol{E}$	Mass-specific energy	J/kg
$\boldsymbol{e}$	Mass-specific internal energy	J/kg
$\boldsymbol{F}$	force	N
f	mass-specific force	N/kg
$\boldsymbol{f}$	frequency	Hz
f_i	frequency of the i-th harmonics	Hz
g	Influencing factor	-
H	enthalpy	J
$\boldsymbol{H}$	Height	m
h	Tower-profile distance	m
h	Mass-specific enthalpy	J/kg
I	pulse	kg m/s
I	current	$kg\ m/s^2$
i, j, k	Cell indices	-
k	Turbulent kinetic energy	Turbulent kinetic energy
k	Radial cell growth rate	Radial cell growth rate
k	Thermal conductivity	W/(m K)
L	Characteristic length	m
l_{grid}	Characteristic length of a rake grid	m
Ma	Mach number	-

m	mass	kg
n	speed	min^{-1}
p	Pressure	Pa
$\dot{Q}$	Low current	J/s
q	flux density	$J/(m^2 s)$
R	Specific gas constant	J/(kg K)
R_ρ	Poetesiduum	-
r	Radial distance to the axis of rotation	m
r_b	vector of the viewer's place	m
R_{eL}	Reynolds number based on size L	-
S	Sensitivity	-
S	Cell aspect ratio	-
S_{rL}	Strouhal number oriented on the Size L	-
t	time	s
T	Temperature	m
T	Period duration	K
TIMESTEP	Input parameters of the time step for OpenFOAM	-
Tu	degree of turbulence	-
u, v, w	speeds in x−, y− and zdirection	m/s
U	solid displacement	m
$\boldsymbol{u}_f$	fluid displacement	m
V	Volume flow	m^3/s
V	amount of speed	m/s
v	velocity vector	m/s
x, y, z	Cartesian coordinates	m
x	Dimension of a connector	-
$y+$	Dimensionless wall spacing	-
z	cell count	-
α °	Angle of attack	-
β°	pitch angle	-
Δ ca	Variation of the buoyancy coefficient	-
$\Delta p_{Amplitude}$	Amplitude measurement of pressure fluctuation	*Pa*
$\Delta p_{Deflection}$	Deflection measurement of pressure fluctuation	*Pa*
Δs_1	height of the first cell in the boundary layer	m
Δ t	time step	s

$\Delta\tau$	Dimensionless Time step	-
η	Dynamic viscosity	kg/(ms)
Γ m	Circulation of the bound vortex	^{2}/s
ι	Number of internal iterations per time step	-
κ	Adiabatic coefficient	-
ρ	kg/m^3	density
σ	Normal Voltage	*Pa*
τ	Shear stress	*Pa*
θ	Azimuth angle	°
ξ	Dimensionless profile coordinate	-

Acknowledgments

Completing this thesis was far from an individual accomplishment. For helping me reach the finish line, I would like to thank the following people:

My supervisor, Luca Cortelezzi, for taking me under his supervision and helping me achieve my research objectives. Also, for caring for administrative matters.

Gabriel Axtmann, my co-supervisor, for introducing me to this project and for the continuous stream of ideas to explore. His expertise in aerodynamics and aeroacoustics has been invaluable in completing this thesis.

Muhammad Ali, my friend, played a vital role in my relocation and supported my thesis completion.

Lastly, my parents and siblings; without their love and support, I would not have been able to achieve this.